EXECUTIVE SUMMARY

Tire-pavement interaction noise is one of the significant environmental problem in highly populated urban areas situated near busy highways. Though the use of sound barriers, as well as texturing methods are adopted to minimize this problem, they have their own limitations. The understanding that methodologies to reduce the sound at the source itself is necessary, has led to the development of porous paving materials. This report outlines the systematic research effort conducted in order to develop and characterize Enhanced Porosity Concrete (EPC) to mitigate the problem of tire-road interaction noise. The basic tenet of this research is that carefully introduced porosity of about 15% - 25% in the material structure of concrete will allow sound waves to pass through and dissipate its energy.

EPC mixtures were proportioned with three different aggregate sizes, and the binary blends of these sizes. The physical and mechanical properties of these mixtures were studied in detail. Methods to determine the porosity of EPC were developed. One method involved the use of image analysis on an epoxy filled specimen to distinguish between the accessible and inaccessible pores. A water saturation method was also used to determine the porosity. Flexural strengths of EPC specimens were studied in detail, and the influence of sand content, and silica fume were ascertained.

The acoustic absorption coefficients of EPC were determined using an impedance tube. It was found that the pore volume and pore sizes have a significant influence on acoustic absorption. The tortuosity of the pore network, which forces the waves to travel

longer, and the frictional losses in the pore walls are the main mechanisms that are responsible for energy loss. The influence of specimen thickness on the acoustic absorption coefficient is also brought out. Using a simple shape specific model, and incorporating the principle of acoustic wave propagation through semi-open cells, the acoustic absorption in EPC has been modeled. The model agrees with the experimental values quite well.

EPC has been characterized by using electrical impedance spectroscopy. Using a multi-phase conducting model, a pore connectivity factor has been developed, that correlates well with the acoustic absorption coefficient. This factor takes into effect the features of the pore structure in addition to porosity, in determining the material performance. A falling head permeameter has been developed to ascertain the water permeability of EPC mixtures. Permeability depends on parameters other than porosity, which are hard to experimentally measure. Therefore, a hydraulic connectivity factor has been developed, the variation of which with intrinsic permeability is linear. This factor could be used to classify EPC mixtures based on their permeability. The intrinsic permeability also could be predicted using electrical conductivity. Thus, electrical conductivity is a single measurable quantity that can vastly help in the prediction of properties of EPC.

Selected EPC specimens were tested in the Tire Pavement Test Apparatus (TPTA) to evaluate their noise reduction. It was observed that EPC specimens reduce the noise at greater than 1000 Hz frequency whereas at frequencies less than 1000 Hz, they are not very beneficial.

TABLE OF CONTENTS

LIST OF TABLES

LIST OF FIGURES

CHAPTER 1: INTRODUCTION

1.1 General

Noise pollution affects more people than any other kind of pollution in the modern industrialized world [Sandberg and Ejsmont 2002]. Among the many sources of noise, the one that clearly dominates is the road traffic noise. In the United States, more people are exposed to highway noise than from any other single noise source [AASHTO 1974]. Noise pollution is especially problematic in densely congested urban settings where residents live near highways and main transportation thoroughfares. Road traffic noise has traditionally been associated with engine and exhaust noise of vehicles. However, of late, while the emission and propagation noise from these sources are greatly reduced, the emission from tire-road interaction has become more prominent. This effect has been reported to be more significant in Portland Cement Concrete (PCC) pavements [Onstenk et al 1993, BE 3415 1994].

Currently, the most commonly adopted solution to reduce the noise generated by traffic is the installation of sound barriers. While the construction of sound barriers impedes the sound transmission path between vehicles and the neighboring development alongside the highways resulting in noise abatement, they tend to be extremely costly, unsightly, and not practical for bridges and/or urban highways. This, coupled with the understanding that the pavement surface has a significant effect on noise generation mechanisms, has led to the development of techniques to achieve quieter PCC riding

surfaces. Some of the most commonly used techniques include special surface texturing like tines, use of exposed aggregates, chip sealing with small aggregates, grinding etc [BE 3415 1994, Descornet et al. 2000].

The extension of the concept of porous materials being used for sound absorption has led to the use of porous concrete as a means to reduce tire-pavement interaction noise. Though this material is being used in some parts of the world in very small amounts, there is not enough understanding of the mechanism of noise reduction, and its various physical and mechanical properties. This research is a step in that direction. Though the main emphasis of this research study is to develop porous Portland cement concrete to absorb sound and evaluate its properties and performance, there are other potential advantages of this material like storm water replenishment, and increased safety due to reduced hydroplaning and wet weather spray.

1.2 Porous Concrete (Enhanced Porosity Concrete – EPC) as a Low-Noise Road Surface

The early history of porous surfaces dates back to the days of unbound macadam surfaces, which were open-graded and porous [Sandberg and Ejsmont 2002]. To reduce the risks of hydroplaning, porous surfaces were used for military airport runways in UK and USA during the 1960s.

Based on the results of several European studies [Onstenk et al. 1993, Francois and Michel 1993, Nelson 1994, Nelson and Philips 1994], the most promising noise-reduction technique for pavements appears to be the use of a porous concrete surface layer (Enhanced Porosity Concrete – EPC). Porosity is introduced in the non-aggregate component of the mixture by gap-grading the aggregates. Noise-reduction in this case is

reported to be the result of a combination of reduced noise generation and sound absorption. The porous concrete surface has a reduced contact area with the tire and minimizes the air pumping by permitting the air that is trapped under the tire to escape into the pores of concrete [Bernhard 2002]. This is the mechanism by which porous concrete reduce the noise generation. The propagation of noise is altered by the porous surface since this will affect the surface impedance and phase interactions that occur between the direct and reflected waves.

Though porous pavements were used for pedestrian areas and parking lots since 1983 in Japan, these have been tried in several European countries of late, and have been shown to be a promising technique to reduce pavement noise [Descornet et al. 1993, Iwase 2000]. Experimental sections of porous concrete pavements in Europe have shown that altering the pavement surface can reduce the noise level by as much as 10dB (A) as well as minimize wet weather spray and reduce glare [Gerharz 1999]. Research undertaken in France [Christory et al. 1993] has examined the capability of thick porous cement concrete pavements to reduce noise. An experimental porous concrete section showed significant improvements in noise reduction. However, preventive anti-clogging measures were required. The key factors that dictate the efficiency of EPC for absorbing sound are the accessible porosity (accessible to sound waves), pore size, pore aperture size, and the porous layer thickness.

1.3 Enhanced Porosity Concrete as a Storm Water Drainage Medium

In recent years, there has been a growing concern towards protecting water supplies and environments. It was realized long back that runoff from developed real

estate had the potential to pollute surface and groundwater supplies [ACI 522 – Draft document]. Further, as land is developed, runoff leaves the site in higher rates and volumes, leading to downstream flooding and bank erosion. In winter climates, runoff is replaced by snow, which necessitates the use of chemical agents to melt ice, thereby adding more contaminants to the drainage. The porous nature of EPC allows water to percolate quickly through the pavement layer to an underlying designed filter fabric layer. A pervious pavement could be considered as either a retention or infiltration system, as its behavior would be similar in runoff control and treatment efficiency. Pollutant removal would occur through filtration, absorption, and adsorption by the underlying soils. Pollutant sources for urban parking lots include atmospheric fallout, vegetation, fertilizers, pesticides, litter, spills and vehicle pollutants such as heavy metals, greases and oils. Conceptually, a pervious pavement should provide significant removal for all of these pollutants.

1.5 Enhanced Porosity Concrete as a Safer Riding Surface

Hydroplaning and visibility are concerns in wet weather conditions. EPC pavements remove splashing and the danger of hydroplaning since they contain about 20-25% voids. Tires are in contact with the pavement even in wet weather, thereby improving traction. The reflection from pools of water on the pavement surface is eliminated, thereby reducing the spray.

1.4 Organization of this Report

This section gives an outline on the organization of this report. Chapter 2 provides a review of existing literature on the mechanisms of tire-pavement interaction noise. The major mechanisms responsible for generation and propagation of noise have been dealt with in this chapter. In addition, a literature review on Enhanced Porosity Concrete is provided in Chapter2. Details from literature including the materials and construction procedure of EPC, advantages of EPC, and its physical, mechanical, and acoustic properties are explained.

The research needs, and the objectives are listed in Chapter 3. The objectives were arrived at after a critical review of existing literature. The underlying goal was to develop EPC mixtures that performed efficiently in reducing the tire-pavement interaction noise, at the same time maintaining necessary mechanical and durability characteristics.

Chapter 4 elucidates the materials used in the production of EPC, the mixture proportions, and test methods used to evaluate the properties and performance of EPC. Certain test methods that are described in various standards are used, where as for certain other tests, procedures are developed.

The relationship between the aggregate size and gradation, and the pore structure features like pore size and porosity are presented in Chapter 5. The influence of mixture proportions, and pore structure features on the properties (flexural strength, permeability) is also brought out in this chapter.

Chapter 6 provides the detailed results of acoustic absorption studies on EPC carried out using the impedance tube. The acoustic absorption spectra (plot of acoustic

absorption coefficient against frequency) for EPC made using both single sized aggregates as well as aggregate blends are provided. The influence of aggregate size and proportion on the acoustic absorption coefficient is explained.

Modeling the acoustic absorption phenomena in EPC is described in Chapter 7. The physical features of the simulated pore network, the concept of the physical model adopted, and its validity are discussed. Parametric studies described later on in the chapter isolates the influence of various pore structure features on acoustic absorption.

Characterizing EPC using electrical impedance to predict the acoustic and hydraulic performance forms the core of Chapter 8. Multi-phase conducting models are used to predict the electrical conductivity of EPC system. The determination of hydraulic conductivity using a falling head permeameter designed specifically for EPC is discussed. The need for a pore connectivity factor, in addition to porosity, to accurately model the electrical and hydraulic conductivities is brought out. A hydraulic connectivity factor is defined, which allows to relate the hydraulic conductivity to electrical conductivity.

Response of EPC to alternate cycles of freezing and thawing is described in Chapter 9. The influence of aggregate size in relative dynamic modulus after freeze and thaw is brought out. The influence of freezing rate, and the impact of air entrainment are also discussed.

Chapter 10 discusses the testing carried out in the Tire Pavement Testing Apparatus. The specimens tested, testing procedure, and the analysis of results are covered in this chapter

Chapter 11 summarizes the research and lists the pertinent conclusions.

CHAPTER 2: REVIEW OF LITERATURE ON TIRE-PAVEMENT NOISE AND ENHANCED POROSITY CONCRETE

2.1 General

This chapter provides an introduction to the various aspects of tire-pavement interaction noise, as described in literature. The mechanisms of tire-pavement noise generation and propagation are explained, followed by the pavement characteristics that have a bearing on these mechanisms. Different methods adopted to reduce noise including texture modification are described. A detailed treatment on porous concrete or Enhanced Porosity Concrete (EPC) is provided in the latter part of this chapter.

2.2 Mechanisms of Noise Generation

The mechanisms of tire-road noise generation are stated to be extremely complex. They are commonly divided into two main groups according to the media in which they occur and their effects. The first one is related to the mechanical vibrations of the tire, and the second, related to the aerodynamic phenomena. The first category can further be classified into impacts and shocks, and adhesion mechanisms [Nelson and Phillips 1994]. The relative contributions of these mechanisms vary with the type of tire, road surface, and vehicle speed [Sandberg and Ejsmont 2002, Nelson 1994]. Figure 2.1 shows these mechanisms, and they are described in the following sections.

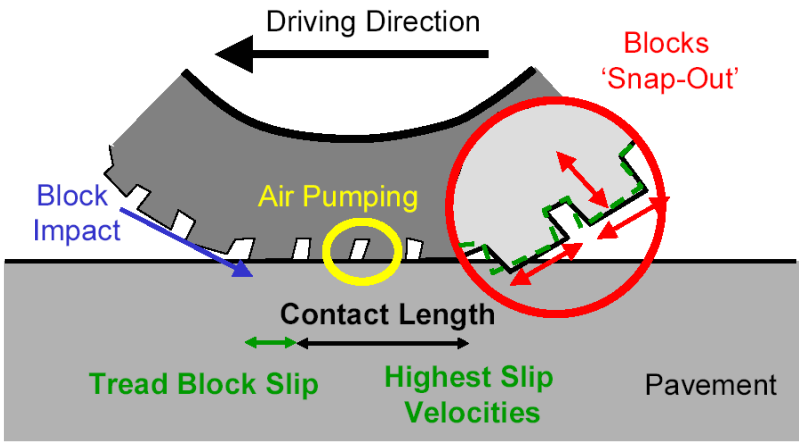

Figure 2.1 Overview of noise generation mechanisms (After Nelson 1994)

2.2.1 Impacts and Shocks

Vibrations are generated in the tires due to the impacts and deflections which occur as the tread blocks enter and leave the contact with the road surface and as a result of movement of tread elements in contact with the pavement. Vibrations in the tread and sidewall of the tire excite the air surrounding the tire, generating sound pressure waves that propagate away from the tire.

Figure 2.2 is a concise representation of the mechanisms of tire-road noise generation, depicting the mechanisms as the tire rolls. As the tread block impacts the road surface, vibrations are driven radially into the tire. While the tread block moves through the contact patch, it is subjected to tension, whereas the tension is released when the block leaves the contact patch. This sudden release of tension returns the tire back to its undeflected rolling radius. This phenomenon is known as block snap-out, which excites both the radial and tangential vibration modes [Nelson and Phillips 1994]. The tread compression, as shown in Figure 2.2, also induces radial vibration of the tire carcass.

Both these phenomena occur at the lower end of the frequency range (<1 KHz). Another impact phenomenon that results in tangential vibration is the tread oscillation. It is attributed to the tangential strain on the tread blocks and impact of the pavement, and is a process dominated at the high frequency range (>1 KHz) [Bernhard 2002, BE 3415 1994].

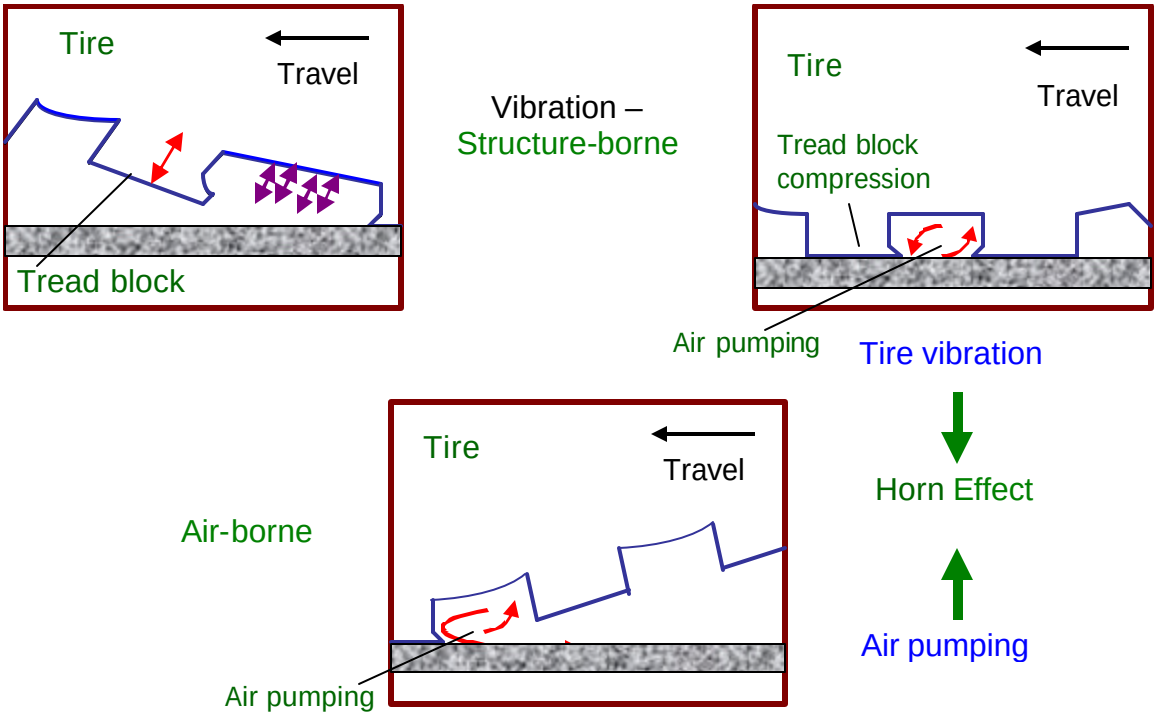

Figure 2.2 Different mechanisms of tire-road noise generation

2.2.2 Adhesion Mechanisms

Adhesion mechanisms are set up by the tire vibrations associated with the frictional losses created in the contact patch between the tire and the pavement [Sandberg and Ejsmont 2002]. These are predominantly tangential forces, produced by the changing radial deflection when the tire flattens in the contact patch. These forces are

resisted by friction and tire stiffness. The friction mechanism is governed by the small scale roughness characteristics or microtexture of the pavement surface [Nelson 1994].

2.2.3 Aerodynamic Mechanisms

Tire-pavement noise is also generated by several mechanisms which are related to the movement of air in the cavities of the tread pattern. The most common of these is air pumping, shown in Figure 2.2. When the tread block enters the contact patch, air is sucked in between the grooves of the tread pattern, and when it leaves the contact patch, air is pumped out. The pressure modulations caused by this process is responsible for high frequency noise. Additional aerodynamic mechanisms include:

(i) Air turbulence, which is the turbulence around the tire due to the tire displacing air when rolling,

(ii) Pipe resonance, which is the air displacement in the grooves in the tire tread, and

(iii) Helmholtz resonance, which is the air displacement into or out of the connected air cavities in the tread pattern and pavement surface.

The latter two mechanisms are often considered as special cases of air pumping [Sandberg and Ejsmont 2002, Bernhard 2002].

2.2.4 Amplification or Reduction Mechanisms

Though not strictly generation mechanisms, several other mechanisms in addition to the primary ones described earlier also have been found to augment or reduce the tire-pavement interaction noise. The most important of them is the horn effect. Noise

generated at or near the contact patch can be amplified due to the shape of the region between the tire and the pavement surface, immediately to the rear of the contact patch. Multiple reflections between the tire and pavement surface tend to occur, amplifying the sound [Descornet et al. 2000, Sandberg 2000, Nelson 1994, Bernhard 2002]. The acoustic and mechanical impedance effects of the pavement surface are suggested as noise reducing mechanisms. The acoustic impedance depends on the communicating voids in the pavement whereas the mechanical impedance depends on the relative stiffnesses of the tire and the pavement.

2.3 Mechanisms of Noise Propagation

Noise propagating from a sound source into free space attenuates with distance from the source, the rate of attenuation depending on the shape of the wavefront [Nelson 1994, Nelson and Phillips 1994].

Figure 2.3 shows a simple geometry of a source and receiver above a flat surface. If the source and receiver are close to the ground, reflections from the ground plane will occur. For a normal dense concrete pavement surface, the path difference between the directed and reflected wave is small and no destructive interference occurs between these waves at practical frequencies. Under these conditions, the sound waves arriving from both these paths add together to give a 6 dB increase over the free field amplitude. The frequencies and amplitudes of these interference effects depend greatly on the acoustic properties of the surface layer and the angle of incidence of the surface wave.

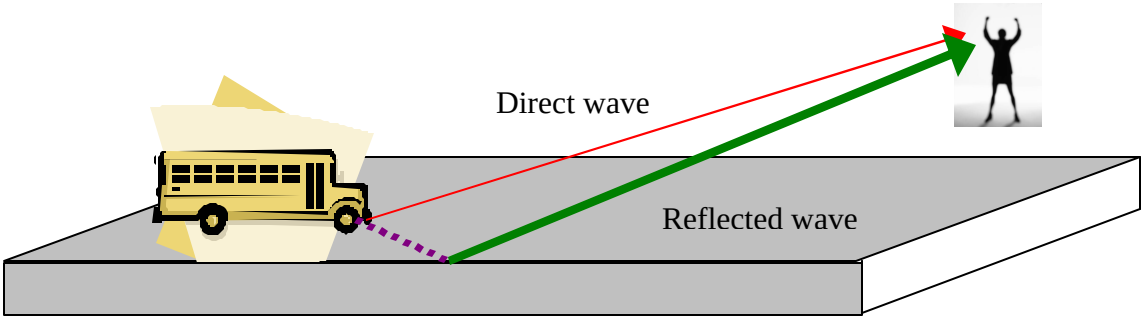

Figure 2.3 Reflection of noise from a dense surface

2.3.1 Effect of Surface Porosity on Noise Propagation

When the surface layer is porous, the difference in path lengths between the direct and the reflected waves is large (Figure 2.4), and destructive interference occurs in the frequency range of 250 – 1000 Hz. The noise, as it reaches the observer, is of lower intensity in this case. This is one of the main advantages in using a porous pavement for noise abatement purposes.

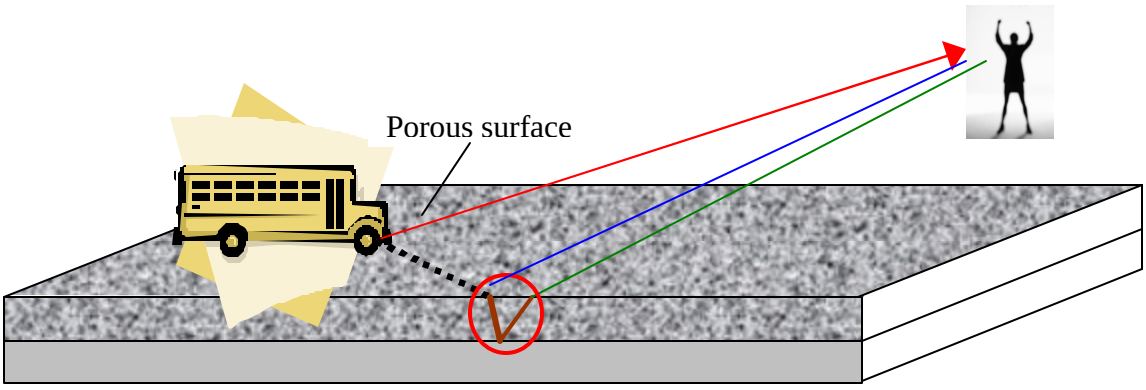

Figure 2.4 Reflection of noise from a porous surface

2.4 Pavement Characteristics that Influence Noise

It is widely recognized that the pavement surface has a very significant effect on the traffic noise. There are several pavement characteristics that are reported to influence the noise generated by tire-pavement interaction [Descornet et al. 2000, Sandberg and Ejsmont 2002]. This section deals with those characteristics that are described in literature.

2.4.1 Macrotexture

This is defined as the deviation of a road surface from a true planar surface with the characteristic dimensions along the surface ranging from 0.5 mm to 50 mm. It is most often thought of as determined by the aggregate prominent on the surface. Macrotexture should have high amplitudes in the 0.5 to 10 mm wavelength and low amplitudes in the 10 to 50 mm wavelength to reduce tire noise [BE 3415 1994]. Treatments like grooving and grinding also create macrotexture [Descornet and Fuchs

1992, Descornet et al. 2000]. Surfaces are designed with sufficient macrotexture to obtain suitable water drainage also, resulting in enhanced wet skid resistance. Mixture proportioning and surface finishing influence the macrotexture. Macrotexture is stated to have a very high influence on the noise generated [Sandberg and Ejsmont 2002, Nelson and Phillips 1994].

2.4.2 Megatexture

Megatexture is defined as the deviation of a road surface from a true planar surface with the characteristic dimensions of 50 mm to 500 mm along the surface. It can be a defect in the pavement surface, resulting from the wear and fatigue of the surface material. An inhomogeneity in macrotexture can also result in megatexture. Megatexture exerts considerable influence on the noise generated, and should be minimized to reduce noise. Further, characteristic dimensions along the surface of 0.5 m to 50 m are sometimes termed as roughness, or unevenness.

2.4.3 Microtexture

Microtexture is defined as the deviation of a road surface from a true planar surface with the characteristic dimensions along the surface of less than 5 mm. The influence of microtexture on noise is not as high as either macrotexture or megatexture.

The ranges of texture and their most significant anticipated results are shown in Figure 2.5 [Wayson 1998].

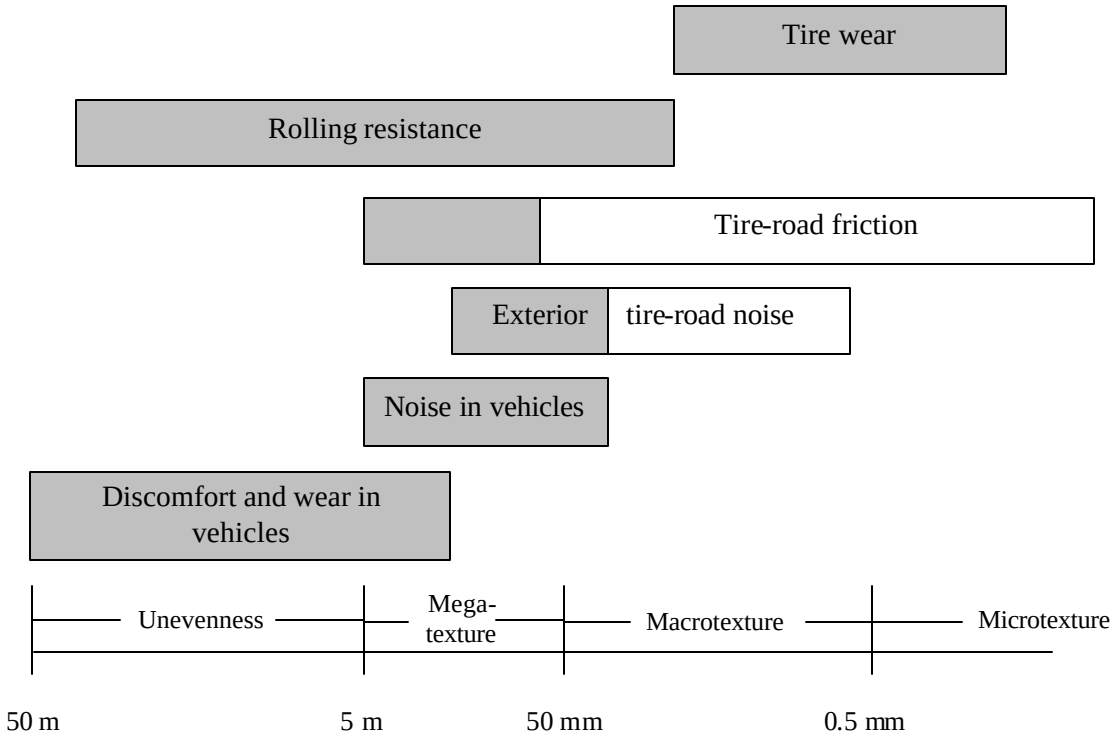

Figure 2.5 Ranges of texture and their most significant anticipated results (after Wayson 1998). Unfavorable effects are shown in the shaded boxes

2.4.4 Porosity

The significance of surface porosity in the noise propagation mechanism has been explained in Section 2.3.1. Porosity effectively reduces the air pumping effect, thereby reducing the tire noise [Bernhard 2002, Sandberg and Ejsmont 2002, BE 3415 1994]. The amplifying effect of the acoustic horn is also reduced when the sound waves are allowed to attenuate through the pores in the surface layer of the material, though there is no unified opinion about this mechanism [Bernhard, Personal communication 2003].

Acoustic absorption occurs when sound waves pass through the series of pores in the material. Details of the effect of porosity will be given later in this chapter.

2.4.5 Friction and Noise

Friction is a property of the tire-road interaction that is derived from a number of tire and road surface characteristics. Due to friction, the tire may transmit longitudinal and lateral forces between the road and the vehicle. Friction constitutes a key factor for safety and drivability. It was believed that coarse (and hence noisy) surfaces were necessary in order to ensure good skid resistance. But it is now accepted that high friction and low noise are not conflicting requirements [PIARC 1991]. The road surface characteristics that determine friction are megatexture, macrotexture, microtexture, and the pavement interacting with the rubber of the tire. Megatexture and macrotexture can be measured directly but microtexture measurements are indirect, mainly from tire-road friction, using British Pendulum method [Sandberg and Ejsmont 2002].

The skid resistance of various types of road surfaces were calculated using sensor-measured texture depth (SMTD), obtained from laser profile devices [Phillips et al. 1994]. It was concluded from this study that high levels of SMTD implying good skid resistance are associated with high levels of megatexture, and therefore high levels of tire-road noise. For porous surfaces, which retain the texture in the form of pores, the skid resistance was found to be higher, even without high levels of megatexture.

2.5 Low Noise Concrete Pavements

A “low noise” pavement is defined as one, which, when interacting with a rolling tire, influences vehicle noise in such a way as to cause at least 3 dB lower vehicle noise than obtained on conventional and most common road surfaces [Sandberg and Ejsmont 2002].

Descornet et al (2000) has stated three basic rules for designing a low noise pavement:

(i) Sufficiently deep macrotexture (minimum 0.5 mm texture depth), using small to medium sized aggregates (< 10 mm),

(ii) Alternatively, the role of macrotexture can be played by porosity. Pores should be connected to the surface and should be interconnected (around 15% connected voids), and

(iii) Minimize megatexture by ensuring that macrotexture is homogeneous.

Sandberg and Ejsmont (2002) also recommend the above three methods to design low noise pavements, but add the following points:

(i) Avoid very smooth macrotextures, instead maximize macrotexture at wavelengths around 2-8 mm, and

(ii) Construct the wearing course with as high a porosity that is viable from a durability standpoint and have wide channels to avoid pore clogging.

Several methods of making low noise concrete pavements are discussed in this section. Only non porous low noise concrete pavements are discussed in this section. Porous concrete is dealt with in detail under a separate heading.

2.5.1 Exposed Aggregate Concrete

This technique consists of removing the top layer of paste / mortar either by mechanical means or chemical means (spraying retarding agent on fresh concrete surface), and exposing the aggregates to create a certain surface texture [Descornet et al. 2000, Descornet and Fuchs 1992, Descornet et al. 1993, Nelson and Phillips 1994, BE 3415 1994]. It has been found that exposing the aggregates can reduce noise levels only if the aggregate sizes are relatively small. The lower noise properties of these surfaces can be related to the relatively low levels of megatexture found for this surface. This is accomplished by using a longitudinal smoothing beam. Exposing the aggregates ensures adequate levels of macrotexture, and hence skid resistance and durability. Exposed aggregate concrete is sometimes called “whisper concrete”.

2.5.2 Chip Sprinkling

The sprinkling treatment consists of spreading highly polish resistant aggregate chippings of a given size on the pavement surface under construction, and partly embedding them so as to create a rough surface macrotexture. The chippings used are in the size range of 10-15 mm. Due to the difficulty in uniformly embedding the chippings, this technique never went beyond the experimental stages [Descornet et al. 1993].

2.5.3 Tining or Grooving

A rake with a number of tines is pulled on a fresh concrete surface to create grooves on the surface. This process is called tining. Three major types of tining are

identified by the main direction of the surface texture – longitudinal, transverse, and random. The spacing of the tines can be uniform or random. Tines are typically 2-5 mm wide, 3-5 mm deep, and the spacing ranges from 10 to 40 mm. Grooving the hardened concrete also produces such texture. Random surface textures are generated either by grooving the surface at an angle, or by using different de-mortaring techniques. Grooves typically are deeper and wider than the tines. It has been reported that road surfaces with longitudinal and random textures are less noisy than transversely textured surfaces [Wayson 1998, Kuemmel 2000]. The degree of noise reduction is determined by the characteristic distribution of macro- and megatexture on the surface. A pure longitudinal texture is often advisable since the tread will then ride on smooth and flat longitudinal ridges and not push down the parts of tire rubber into the groove each time a new groove is impacted. This reduces tire radial vibration, as well as air pumping. The potential disadvantages are that there are no escape channels for water during heavy rain, and trouble with steering of motorcycles.

2.5.4 Grinding

Grinding is a special case of longitudinal texturing in which the concrete surface is ground using densely spaced diamond saw wheels. This process removes ridges and other uneven features and leaves a track of fine and densely spaced grooves in the treatment direction. Grinding is often used as a rehabilitation technique to pavement surfaces that have become rough and uneven, though it can be used for new surfaces as well. The level of smoothness that is obtained can be comparable to a new surface.

2.6 Porous Concrete (Enhanced Porosity Concrete - EPC)

Concretes with higher than normal porosity and pore sizes, which enable water to drain through them quickly, are known as porous concretes, pervious concretes or Enhanced Porosity Concretes (EPC). The latter term will be used throughout this study. They are typically produced by gap grading aggregates, eliminating / minimizing the use of sand, and using low binder contents. It has been reported that an EPC layer over a conventional concrete base is one of the efficient means of reducing pavement noise [BE 3415 1994, Christory et al. 1993, Descornet et al. 2000, Sandberg and Ejsmont 2002].

Though EPC was used in pedestrian areas and parking lots in Japan as early as 1983, its use in United States and Europe was not popular till the 1990s when the tire-pavement interaction noise became a prominent issue. It was reported that EPC resulted in a 6 dB(A) (A-weighted average – Sandberg and Ejsmont 2002, Nelson 1994) reduction in noise level compared to the conventional pavement in a study in Belgium [Descornet et al. 2000]. A 5-6 dB(A) reduction was also reported by Nissoux et al. (1993).

2.6.1 Requirements for an Effective EPC Pavement

For EPC to perform effectively with respect to its acoustic behavior, it has been recommended that 15-25% interconnected porosity is required [Christory et al. 1993, Nelson and Phillips 1994, Onstenk et al. 1993, BE 3415 1994, Descornet et al. 2000]. But it is also necessary that the material has adequate mechanical resistance and durability. A listing of the desirable properties has been given by Onstenk et al. (1993).

(i) Significant noise reduction and drainage properties,

(ii) Acceptable strength and stiffness,

(iii) Adequate surface properties with respect to traffic safety – skid resistance, evenness,

(iv) Sufficient service life – bonding to underlying dense concrete, freeze-thaw resistance,

(v) Construction by means of available techniques, and

(vi) Costs comparable to conventional pavements.

2.6.2 Advantages of EPC Pavements

The advantages of using an EPC pavement in place of a conventional pavement are three-fold, as shown in Figure 2.6 – (i) Ground water recharging, (ii) Reduced hydroplaning, and (iii) Noise reduction. The first two were the prominent reasons for using EPC before the tire-pavement noise issues took center stage, and its efficiency in acoustic absorption ascertained. EPC were used in the design of foundations for pavement structures to provide continuous drainage necessary for extending the service life of these structures. EPC was also reported to be used on the runway of airports, primarily for its better drainage capacities. EPC pavements also exhibited reduced hydroplaning [Christory et al. 1993].

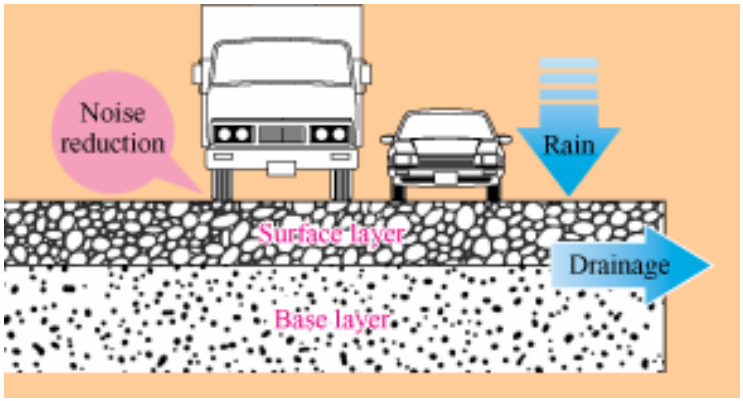

Figure 2.6 Three-fold advantage of EPC (from www.hepc.go.jp)

2.7 Materials, Mixture Proportioning, and Construction Procedure of EPC Pavements

In order to achieve such desirable properties with high porosity, materials and mixture proportioning method should be chosen taking into account a host of factors. Those parameters are described as follows.

2.7.1 Aggregate Sizes and Gradation

To ensure that EPC contains about 15-25% open porosity, careful selection and gradation of aggregates are necessary. Gap-graded aggregates, resulting in lack of material to fill out the space between the larger aggregates, are the most favored choice. The accessible porosity and strength are reported to be a function of the grain size of the fine aggregate in relation to that of the coarse aggregate [BE 3415 1994]. The maximum grain size of coarse aggregate has to be limited to 10 mm as per another study [Onstenk et al. 1993]. This study also reports that the grain size of fine aggregate has a major effect on accessible porosity and strength, while the grain size of coarse aggregate does

not have a major effect. Gerharz (1999) recommends that the aggregate size for EPC lie between 4 and 8 mm. A 6-10 mm aggregate size range has been used for a demonstration project [Nissoux et al.]. The use of coarse aggregates of size up to 30 mm and sand of size less than 2.5 mm has been reported [Jing and Guoliang 2002]. The use of larger aggregate sizes (20 mm maximum size) has been recommended for EPC since they result in large sized pathways in the material, thereby preventing clogging [Nelson 1994].

2.7.2 Cement Content

EPC is proportioned with just enough cement content required to bind the aggregates together. This is to minimize the occurrence of excess cement paste seeping through the material structure, reducing its openness. The water-binder ratio also is kept low for the same reasons. It is recommended to conduct binder drainage tests to ascertain the optimum binder content for the aggregate gradation chosen [Nelson 1994]. This procedure is expected to ensure high residual porosity, with acceptable strength characteristics.

2.7.3 Additives

The use of silica fume (10% by weight of cement), and a superplasticizer were reported not to increase the strength of EPC [Onstenk et al. 1993]. Polymer additives were reported to result in an increase in strength as well as freeze-thaw resistance of EPC. Since the cement content of EPC is low, fine mineral admixtures and organic intensifier

(polymer) were incorporated in concrete to improve the microstructure and strength of EPC [Jing and Guoliang 2002].

2.7.4 Construction Procedure

From a construction point of view, two alternatives are stated in literature for EPC – (i) wet on wet, and (ii) wet on dry [BE 3415 1994].

The "wet-on-wet" process consists of laying the conventional concrete base layer and the EPC top layer within a short time so that the base layer has not begun to set when laying the top layer. The benefit of this system is that no additional products are required to bond the two layers. In some cases, a retarding admixture is applied to the base layer so that it does not set before the EPC layer is placed. This process requires careful planning of the construction process – either two pavers, or modified pavers which can simultaneously lay two layers of different materials, are needed. It also necessitates the use of two mixing plants with different capacities, due to the different thicknesses used in both layers.

The "wet-on-dry" process consists of laying the EPC layer once the conventional concrete in the base layer has hardened enough to sustain a roller on it. The bond between the two layers is obtained through the use of an adherent material which can be cement based or polymer based. This may result in an increased cost. Moreover, the joints in the lower layer need to be sawed, and sealed to avoid cement paste from the top layer penetrating into it.

2.8 Mechanical Properties and Durability Characteristics

This section describes the different mechanical properties and durability characteristics of EPC as described by various authors.

2.8.1 Compressive and Flexural Strengths

The strength of EPC depends on the grain size distribution, accessible porosity, and the type and amount of additive used. A maximum compressive strength of about 18 MPa, at an accessible porosity of 25% has been reported. The maximum flexural tensile strength at this porosity was found to be about 4 MPa. Increase in tensile strength was observed when a polymer additive was used [Onstenk et al. 1993]. Flexural tensile strength of about 3 MPa was achieved for a total porosity of 25%, using 6-10 mm aggregates [Nissoux et al.]. A 28-day compressive strength of 20 MPa, and flexural strength of 3 MPa has been reported for an EPC with 25% porosity in another study [BE 3415 1994]. Increase in aggregate size resulted in a reduced compressive strength, where as the addition of polymer and mineral admixture resulted in an increased strength [Jing and Guoliang 2002].

2.8.2 Water Permeation

The water permeation capacity or the drainage properties are closely related to the accessible porosity. For an accessible porosity of 20-29%, the coefficient of permeability is about 0.01 m/s [BE 3415 1994]. It has also been found from this study that the fine

aggregate determines the permeability. A permeability of around 36 l/s/m^2 has been reported for EPC in another study [Nissoux et al. 1993].

2.8.3 Durability Characteristics

Since EPC forms the top layer of the pavement, it is exposed to the most severe conditions. Some studies have suggested that a polymer additive is required to develop sufficient freeze-thaw resistance in EPC [BE 3415 1994, Gerharz 1999, Onstenk et al. 1993], whereas results of field implementation of EPC in low volume pavements show that EPC proportioned with gap graded aggregates and with a porosity of around 20% sustained freeze-thaw cycles without any additives [GCPA 2003]. Freeze-thaw tests have also been conducted by submerging the lower part of EPC in 3% NaCl solution. This type of testing is reported to be more severe than the conventional freeze and thaw tests [Onstenk et al. 1993].

2.9 Acoustic Absorption of EPC

Several studies on the acoustic absorption of EPC have concluded that the porosity accessible to the sound waves, and the thickness of the porous layer are the significant factors that determine the acoustic absorption of EPC [Nelson 1994, Francois and Michel 1993, Onstenk et al. 1993, BE 3415 1994, Descornet et al. 1993]. The frequencies and amplitudes of the maxima and minima of the absorption coefficients are related to the porosity of the surface layer, air flow resistance, tortuosity of the pore network, and the thickness of the porous layer [Descornet et al. 2000]. Varying the

thickness affects the frequency at which the maximum acoustic absorption occurs while increasing the porosity is said to be beneficial in increasing the absorption at any frequency. The first absorption peak determines the effectiveness of the material in terms of noise reduction. The optimization of acoustic properties of EPC therefore depends on the efficiency in obtaining the maximum amplitude and width of the first peak, which in turn depends on the four above-mentioned parameters. However, from a practical standpoint, only the porosity and thickness can be designed and achieved by proper mixture proportioning whereas the tortuosity and flow resistivity can be determined later only. Normal variations in air flow resistivity and tortuosity of the pore channels are reported to have only a marginal effect in the acoustic absorption of EPC [Nelson 1994]. A layer thickness of between 0.05 m and 0.08 mm was arrived at as the optimum thickness to reduce tire-pavement noise, from this study. To ensure significant acoustical effectiveness (3 dB(A) reduction as compared to a dense surface), porous surfaces are reported to require a minimum voids content of 20%, and a minimum thickness of 40 mm [Descornet et al. 2000]. It has been stated in this study that the maximum acoustic absorption coefficient (α) measured using a standing wave tube on cores of 100 mm diameter should satisfy those given in Table 2.1. In a German study, an EPC pavement of 80 mm thickness and 25% porosity exhibited an average noise reduction of about 6 dB(A) [Descornet et al. 2000].

Table 2.1 Maximum acoustic absorption coefficient measured from cores, for different frequencies (Italian specifications, Descornet et al. 2000)

Frequency (Hz)	Acoustic absorption coefficient (α)
400-630	≥ 0.15
800-1600	≥ 0.30
2000-2500	≥ 0.30

2.10 Noise Reduction Mechanisms in EPC

The primary mechanism with which EPC reduces the tire-pavement interaction noise is acoustic absorption. The component of noise that is eliminated by absorption is mainly the air-borne ones. However, there are several other mechanisms by which EPC reduce noise [Sandberg and Ejsmont 2002, Nelson and Phillips 1994, Descornet et al. 2000]. They are briefly described in this section.

(i) The open porosity prevents the development of high pressure gradients at the edges of the tire-road contact patch, and also within the contact patch. This is responsible for the reduction or even elimination of all air displacement noise generation mechanisms

(ii) Small chippings in the surface results in the impact mechanism being not a very dominant effect

(iii) The porosity in the EPC results in acoustic absorption so that sound waves are dissipated into heat in the small pores inside the material. The acoustic absorption effect will influence not only the tire-pavement noise but also other types of vehicle noise

(iv) If sound is reflected between the pavement surface and the underbody of the vehicle a number of times, each reflection causes loss of acoustic energy

(v) The acoustically "soft" EPC surface will affect the acoustical impedance in and around the tire-road contact patch, as well as between the source and receiver. This is similar to the explanation of Section 2.3.1. The absence of a reflecting plane eliminates the horn effect.

2.11 Maintenance of EPC Pavements

Concrete pavements are fairly durable and needs little maintenance as long as it is well designed and built. But the high amounts of porosity in EPC gives rise to certain special problems such as clogging of voids, bond between EPC and dense concrete, and freezing and thawing damages in cold climates [BE 3415 1994]. Studies have shown that a well designed and constructed EPC may not undergo freezing and thawing damage provided it is well draining. Clogging of pores is a serious issue which limits the draining capacity of EPC pavements and thus affects its freeze-thaw resistance. Clogging can occur because of depositions of dirt or dust from the surroundings, and wear products from the pavement and tire, in the voids of EPC. Also, the surface becomes somewhat compacted, and compaction occurs at the expense of the voids. Many cleaning methodologies have been recommended in the literature [Sandberg and Ejsmont 2002], but the most efficient one has been a combination of water jet blasting, dirt water suction, and vibrations transmitted by a "plane of water" between the water blasting and suction.

An interesting method of "self cleaning" of porous pavements has been reported by the above authors. It is postulated that the most effective cleaning process is one that

takes place during heavy rainfall and when vehicles travel at high speed on the pavement. The removal of water at the leading edge of the tire-road interface, and the suction of dirt water from the trailing edge may occur with very high pressure gradients, giving an efficient self-cleaning effect. For instance, at a vehicle speed of 90 km/h, the tire moves at 25 mm per millisecond. This indicates that the pressure at a particular spot changes from atmospheric pressure to a large value in just a millisecond. This is equivalent to shooting a "water-bomb" on the surface.

2.12 The Concept of Double Layers (Twin lay)

Acoustically efficient EPC can be prepared either with small maximum size aggregates (4-6 mm) or large maximum size aggregates (16-20mm). A method that combines the above two principles, using smaller sized aggregates in top layer and larger sized aggregates in the bottom layer has been tried in France and Netherlands [Sandberg and Ejsmont 2002]. This concept is especially intended to avoid the clogging effect of EPC. The idea is that the upper layer of small aggregates acts as a filter in which most of the dirt gets accumulated. The aggregate sizes being small, a smooth megatexture is easier to obtain, resulting in reduced noise. When a cleaning machine sprays water, the dirt can escape and can be sucked up. It is reported that the top layer can be easily cleaned, and that does not result in filling the bottom layer since the particles are small enough to be drained off. The acoustic absorption behavior of double layered EPC is reported to be better in a wide frequency range of 800 Hz to 3 kHz. A 1-2 dB reduction in noise in the near field and 3-4 dB in the far field has been reported in comparison with ordinary porous concrete. In addition to these reduction effects, the smoother

megatexture may effectively suppress the striking tire noise caused by the roughness of the pavement surface [Iwase 2000].

CHAPTER 3: RESEARCH NEEDS AND OBJECTIVES

3.1 Research Needs

Based on the results of previous studies [BE 3415 1994, Descornet et al. 2000], one promising noise-reduction technique appears to be the use of a porous concrete surface layer, where noise-reduction occurs due to the combination of reduced noise generation and sound absorption. The generation of noise is altered by the effect of porous surface minimizing the air pumping. In addition, the pores act to absorb sound through internal friction. Although porous pavements have been used for pedestrian areas and parking lots since 1983 in Japan, they have only been recently tried in European countries and have been shown to be a promising technique to reduce pavement noise. Experimental sections of porous concrete pavements in Europe have shown that altering the pavement surface can reduce the noise level by as much as 10dB. While the pavement surfaces have been optimized primarily based on trial and error, research is needed to systematically identify characteristics of the surface that can be explored to reduce sound generation.

While the concept of EPC is a promising approach that may lead to quieter PCC pavements, little work has been reported on how to optimize the performance of EPC mixtures. In order to ensure that EPC achieves the maximum possible sound attenuation, it is necessary to develop a fundamental understanding of the parameters that influence sound absorption. The determination of how concrete mixture characteristics (i.e., the

size and distribution of aggregates, binder etc.) and structural design parameters (layer thickness) influence the performance is essential in the development of design procedures to tailor the material to satisfy both functional requirements and noise mitigation. The development of a material with "designed" porosity and pore structure is the key to achieving this objective.

3.2 Objectives of this Study

EPC mixtures can be useful for sound attenuation; however the mixture compositions and the pore properties need to be carefully optimized so that the methods used to maximize noise-reduction do not have a negative impact on mechanical performance and durability. This research aims at identifying EPC mixtures that may have significant potential for acoustic absorption and characterizing their mechanical properties, porosity, and durability.

The objectives of this research are listed as follows:

1. To study the influence of aggregate size and gradation on the pore structure features (porosity, and pore size), hydraulic conductivity, and mechanical properties of EPC.
2. To study the influence of pore structure characteristics on the acoustic absorption behavior of EPC.
3. To model the acoustic absorption behavior of EPC using physical concepts of acoustic wave propagation in porous materials.

4. To characterize the pore structure of EPC using Electrical Impedance Spectroscopy, and predict the acoustic and hydraulic performance from electrical property measurements.
5. To ascertain the resistance of EPC mixtures to cycles of freezing and thawing.
6. To test EPC slabs in the TPTA and obtain the noise spectra under different tire speeds.

CHAPTER 4: MATERIALS, MIXTURE PROPORTIONING, AND TEST METHODS

4.1 Introduction

This chapter explains the materials used in this study, mixture proportions adopted, and the test methods employed to study the various properties of Enhanced Porosity Concrete (EPC). Existing testing methodologies reported in standards were adopted to study some of the properties of EPC, whereas custom test equipment and procedures were developed to ascertain some other properties. Detailed descriptions of the experimental set up developed, and the testing method are provided.

4.2 Materials

This section gives an outline about the various materials used in the experimental investigations. The materials are kept constant throughout the study so as to nullify the influence of change in materials on the physical, mechanical, and durability characteristics of EPC.

4.2.1 Cement

Commercially available Type I Ordinary Portland Cement manufactured by Lonestar Industries was used for the entire study. Table 4.1 summarizes the chemical properties of the cement.

Table 4.1 Chemical properties of cement

C_3S (%)	C_3A (%)	Total Alkali (%)	Insoluble Residue (%)	Loss on Ignition (%)	MgO (%)	SO_3 (%)
--	15.0 (max)	--	0.8 (max)	3.0 (max)	6.0 (max)	4.5 (max)
62.0	9.0	0.5	1.94	0.58	1.82	2.67

4.2.2 Fine Aggregate

The fine aggregate used for the study was a locally available river sand, with an absorption of 2.3%. The sand conforms to ASTM C 128-94.

4.2.3 Coarse Aggregate

Limestone aggregates were used as coarse aggregates in this study. Aggregates were sieved into different size fractions to create gap grading used in this study. The aggregate sizes used were: # 8 (passing 4.75 mm and retained on 2.36 mm sieve), # 4 (passing 9.5 mm and retained on 4.75 mm sieve), and 3/8” (passing 12.5 mm and retained on 9.75 mm sieve).

4.2.4 Silica Fume

A commercially available silica fume was used in some of the mixtures investigated to ascertain its impact on the mechanical and acoustical properties. Addition of silica fume was carried out at 6% and 12% by weight of cement.

4.3 Mixture Proportioning and Specimen Preparation

This section describes the mixture proportions used in this study, mixing procedure and the method of preparing specimens for the various testing that are described later.

4.3.1 Mixture Proportions

The water-cement (w/c) ratio used for all the mixtures investigated in this study was kept constant at 0.33. The cement content was established by providing just enough paste to coat the aggregates since an excessive amount of paste may drain through the pores of the material. It was found out from a trial and error process that the aggregate-cement ratio could be kept around 5.6 at the selected w/c to achieve this. The mixtures were prepared with either the single sized aggregates alone as explained in Section 4.2.3, or binary blends of these mixtures. Blends were prepared by replacing 25, 50, and 75% by weight of the larger sized aggregates successively by smaller sized aggregates. To study the influence of sand, # 4 aggregates were replaced by 2.5, 5.0, and 7.5% by weight of natural sand. Silica fume was added to the mixtures at 6% and 12% by weight of

cement to study its influence on the properties of EPC. Table 4.2 shows the mixture proportions used in this study.

Table 4.2 Proportions of EPC mixtures used in this study

Mixture I.D.	3/8" Aggregate (9.5-12.5mm)	#4 Aggregate (4.75-9.5mm)	#8 Aggregate (2.36-4.75mm)	Fine Aggregate (Sand)	Water-to-Cement Ratio	Silica Fume Addition by Cement Weight
	%	%	%	%		%
Gap grading and Single Sized Aggregate Size						
PC-100-3/8	100	0	0	0	0.33	0
PC-100-#4	0	100	0	0	0.33	0
PC-100-#8	0	0	100	0	0.33	0
Blending # 8 and # 4 Aggregates						
PC-100-#8	0	0	100	0	0.33	0
PC-75-#8, 25-#4	0	25	75	0	0.33	0
PC-50-#8, 50 #4	0	50	50	0	0.33	0
PC-25-#8, 75-#4	0	75	25	0	0.33	0
PC-100-#4	0	100	0	0	0.33	0
Blending # 8 and # 3/8" Aggregates						
PC-100-#8	0	0	100	0	0.33	0
PC-75-#8, 25-3/8	25	0	75	0	0.33	0
PC-50-#8, 50-3/8	50	0	50	0	0.33	0
PC-25-#8, 75-3/8	75	0	25	0	0.33	0
PC-100-3/8	100	0	0	0	0.33	0
Blending # 4 and # 3/8" Aggregates						
PC-100-#4	0	100	0	0	0.33	0
PC-50-#4, 50-3/8	50	50	0	0	0.33	0
PC-100-3/8	100	0	0	0	0.33	0
Addition of Sand						
PC-100-#4	0	100	0	0	0.33	0
PC-95-#4, 5-Sand	0	97	0	2.5	0.33	0
PC-97.5-#4, 2.5-Sand	0	95	0	5.0	0.33	0
PC-92.5-#4, 7.5-Sand	0	92	0	7.5	0.33	0
Addition of Silica Fume						
PC-100-#4	0	100	0	0	0.33	0
PC-100-#4, 6-SF	0	100	0	0	0.33	6
PC-100-#4-12-SF	0	100	0	0	0.33	12

4.3.2 Mixing and Placing Procedure

The constituent materials were batched immediately prior to mixing. The weighed quantity of aggregates was added to the mixer, followed by cement, and silica fume, if desired. Water was slowly added while the dry materials were being mixed in a pan mixer. The mixer was allowed to run for three minutes. At the end of three minutes, the bottom and sides of the mixer were scrapped, and the mixer was allowed to rest for three minutes. A final two minutes of mixing followed this step.

The contents of the mixer were then discharged from the mixing pan into the molds using scoops. The concrete was placed in the forms in two equal lifts. The forms were vibrated on a table vibrator while the concrete was being placed. In addition, the sides of the forms were struck with rubber mallet so as to ensure that the molds are properly filled. No needle vibrator was used since the workability of EPC is low because of gap graded aggregates and low cement content. The forms were finished and were kept under wet burlap for the first 24 hours. After this period, the specimens were removed from the molds, and were kept in the curing chamber at a relative humidity of greater than 98% till further testing.

4.4 Test Procedures

The following section gives an outline of the various test procedures employed in this study to obtain the material properties of EPC.

4.4.1 Flexural Strength Determination

Flexural strength was determined in accordance with ASTM C 78-02. Two tests were conducted on each mixture from a single beam (150 mm x 150 mm x 700 mm), and the average strength reported. Figure 4.1 shows the loading arrangement for flexural strength testing. The first flexural strength test was conducted on 450 mm span of the beam and the second test on the longer remaining portion of the beam after the first flexural failure.

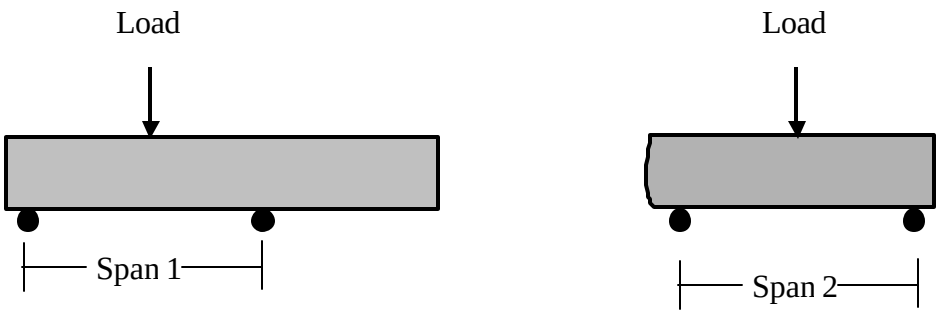

Figure 4.1 Flexural strength determination

4.4.2 Porosity Determination using Image Analysis

Porosity was determined using cores of 95 mm diameter and 150 mm length, drilled from the 150 mm x 150 mm x 700 mm beam specimens. The sides and the bottom of the core was sealed using a tape, leaving the top surface open. The core was then placed in a 100 mm x 200 mm plastic cylindrical mold and flooded with a low viscosity epoxy. Approximately 25 mm of excess epoxy was left above the top of the specimen. The mold and the specimen was then externally vibrated using a vibrating

table for eight to ten minutes to allow the epoxy to permeate into all accessible pores. The specimen was left undisturbed for 24 hours allowing the epoxy to harden. After the epoxy hardened, the mold was stripped and the specimen was cut at depths of 12.5 mm, 37.5 mm, 62.5 mm, 87.5 mm, and 112.5 mm from the top surface, as shown in Figure 4.2. The epoxy impregnated slices were allowed to cure for twenty-four hours. No measurements were conducted on the bottom most slice. The bottom sides of each slice were then brushed clean to remove any debris left from the sawing.

Figure 4.2 Sectioning the core for image analysis

The slices were then placed directly on a flatbed scanner over a clear plastic film, scanned in the grayscale mode, and a bitmap image created. Figure 4.3 shows the image processing procedure. After capture, the images of each slice were cropped using Microsoft Photo Editor® to create a smooth outer circumference with no edge effects and a uniform diameter of 69 mm (Figure 4.3 (a)). The light gray areas of this image correspond to the aggregates and paste whereas the dark areas correspond to both epoxy-filled and unfilled pores. The cropped images were then analyzed using ImagePro®

software. A filter was used to “clean” the image by comparing each pixel to the surrounding pixels, thereby removing miscellaneous marks that may otherwise interfere in the calculation of porosity. A mask was then applied to each image to darken the aggregates and paste, leaving the open and epoxy filled pores as bright objects (Figure 4.3 (b)). The area of the “bright objects” was computed in pixels (72641 white pixels), and the total porosity was calculated based on the known area of the pores and the known total area of the image (237463 pixels).

After the initial grayscale image was obtained, the same specimen surface (scanned as a grayscale image) was then stained black using a fat-tip marker and scanned in the true color mode. This created a second image where the epoxy, aggregate, and paste could be segmented from unfilled pores (inaccessible pores), as shown in Figure 4.3 (c). The same image analysis procedure that was used on the initial grayscale images was applied to the true color bitmap of the stained slices; however, for the second image, the pore areas were masked dark and the flat surfaces of the plane bright (Figure 4.3 (d)). Again, the filter was used to clean the image and the area of the bright objects was computed in pixels. This allowed the area of the aggregate, paste, and epoxy filled pores to be determined (225087 pixels). The inaccessible porosity was then calculated by subtracting this value from the known total area of the image. Once the image analyses has been completed for each grayscale image and each true color image, the accessible porosities of each slice could be approximated by subtracting the inaccessible porosity (obtained from the stained slices) from the total porosity (obtained from the unstained slices). The averages of the values obtained from the slices were reported.

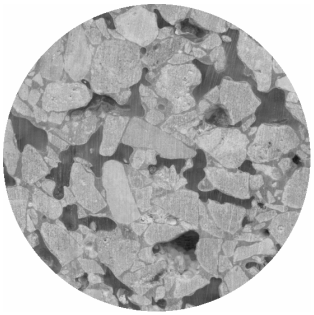

(a) Scanned image cropped to a diameter of 69 mm

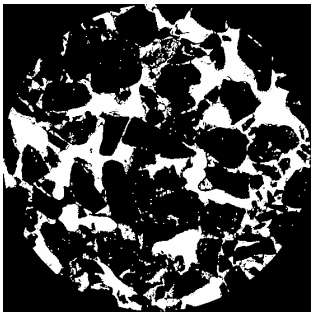

(b) Image threshold established and cleaned white pixels (total porosity) counted

(c) Surface colored and rescanned, cropped to a diameter of 69 mm

(d) Image threshold established and cleaned black pixels (inaccessible porosity) counted

Figure 4.3 Image processing procedure

4.4.3 Porosity Determination using Volume Method

Because of the presence of large interconnected pores in the EPC system, the following procedure was adopted to determine the volume porosity. The cylindrical specimens (95 mm in diameter and 150 mm long) that were cored from beams were

immersed in water for 24 hours to saturate the pores in the matrix. After this period, the sample was removed from water and allowed to achieve SSD condition. The sample was then enclosed in a latex membrane and the bottom of the cylinder was sealed using a stainless steel plate with silicone sealant. The mass of the sample, latex membrane, and the steel plate (M_1) was measured. Water was added to the top of the sample until it was filled, which indicated that all the interconnected pores were saturated. The mass of the system filled with water was taken (M_2). The difference in the mass $\Delta M = (M_2-M_1)$ represents the water in the pores. This mass was converted into a volume, expressed as a percentage of the total volume of the specimen to provide an indication of the total porosity.

4.4.4 Pore Size Determination

The pore size was estimated using the grayscale images from the porosity measurements. Measurements were conducted on middle three slices from each specimen (Figure 4.2). As was done for porosity determination, the images were masked and filtered, leaving the pores as bright objects. The maximum and minimum diameters of the each of the selected pores were recorded. Since the pores are of varying sizes, and the process of establishing threshold intensity is likely to merge two very small bright features into one big feature and identify it as a pore, the average pore size thus obtained was not thought to be an adequate indicator of the representative pore sizes in the specimen. The median of all the pore sizes greater than 1mm was chosen as an approximation of the representative pore size of the sample, and is termed as the

"characteristic" pore size. The 1mm threshold was adopted to account for the fact that the imaging process records a large number of features of size less than 1mm and considering them in the analysis will always result in a median size that does not correlate to the physical sizes present in the system. However, pore sizes determined by this method are only estimates to provide an indicator of the sizes of the pores in the system and provide a useful method of comparison of different systems with varying aggregate sizes and blends.

4.4.5 Determination of Hydraulic Conductivity

Since the EPC has a large interconnected pore network, the conventional methods that are used to evaluate the hydraulic conductivity of normal concrete are not directly applicable. To estimate the hydraulic conductivity of EPC, a falling head permeability cell has been designed, as shown in Figure 4.4.

The permeability cell consists of a 250 mm long acrylic tube with an inner diameter of 92 mm. The top 150 mm of the tube was machined to an inner diameter of 95 mm so that the specimen can be seated on an O-ring at a distance of 100 mm from the bottom. A 50 mm diameter valve connects the bottom part of the tube to a vertical pipe through which water can drain out. The top of this pipe is positioned 10 mm above the top of the specimen so that no unsaturated flow occurs during the test. A graduated acrylic cylinder of 300 mm length was attached to the top of the specimen assembly and clamped tightly using a rubber sleeve. This was used to monitor the water level during the test.

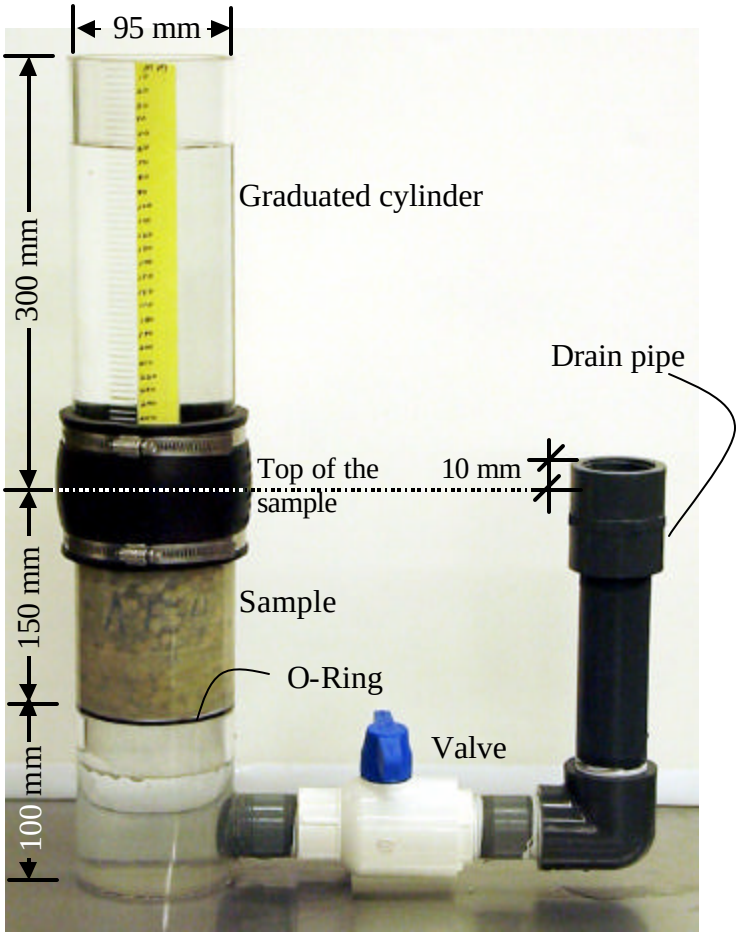

Figure 4.4 Test Set up to measure hydraulic conductivity

The specimen was enclosed in a latex membrane (as was done for the electrical property measurements), and was inserted into the test set up. Water was added to the graduated cylinder to fill the specimen cell and the draining pipe. The specimen was pre-conditioned by allowing water to drain out through the pipe until the level in the graduated cylinder was the same as the top of the drain pipe. This eliminated any air pockets in the specimen and ensured that the specimen was completely saturated. With the valve closed, the graduated cylinder was filled with water. The valve was then open, and the time in seconds (t) required for water to fall from an initial head of 290 mm (h_1)

to a final head of 70 mm (h_2) noted. This procedure was repeated three times, and the average value of t was used.

The coefficient of permeability (K) was calculated according to Darcy's law as:

$$K = \frac{A_1 l}{A_2 t} \log\left(\frac{h_2}{h_1}\right) \qquad 4.1$$

where A_1 and A_2 are the areas of the cross-section of the sample and the tube respectively and l is the length of the specimen. For a given specimen geometry, and same initial and final heads, the coefficient of permeability is given as:

$$K = \frac{A}{t} \qquad 4.2$$

where A is a constant, which in this study was 0.084 m.

4.5.6 Measurement of Acoustic Absorption

To evaluate the acoustic absorption characteristics of EPC, a Brüel & Kjær™ impedance tube was employed, as shown in Figure 4.5. Cylindrical specimens with a diameter of 95 mm were cored from beams after they were tested in flexure. Three specimen lengths – 150 mm, 75 mm and 37.5 mm were tested using the impedance tube. The sample was placed inside a thin cylindrical Teflon sleeve, into which it fits snuggly. The sample assembly was placed against a rigid backing at one end of the impedance tube which is equipped with a sound source. A plane acoustic wave generated by the sound source was propagated along the axis of the tube. Microphones placed along the axis of the tube were used to detect the sound wave pressure transmitted to the sample and the portion of the wave that is reflected (ASTM E-1050). The pressure reflection

coefficient (R) is the ratio of the pressure of reflected wave to that of incoming wave, at a particular frequency, expressed as:

$$R = \frac{e^{jkd_1} - e^{jkd_2} P}{e^{-jkd_2} P - e^{-jkd_1}} \qquad 4.3$$

where d_1 and d_2 are the distances from the specimen surface to the closest and farthest active microphones respectively, j is an imaginary number ($\sqrt{-1}$), k is the wave number (ratio of angular frequency to the wave speed in the medium) and P is the ratio of acoustic pressures at the two active microphone locations.

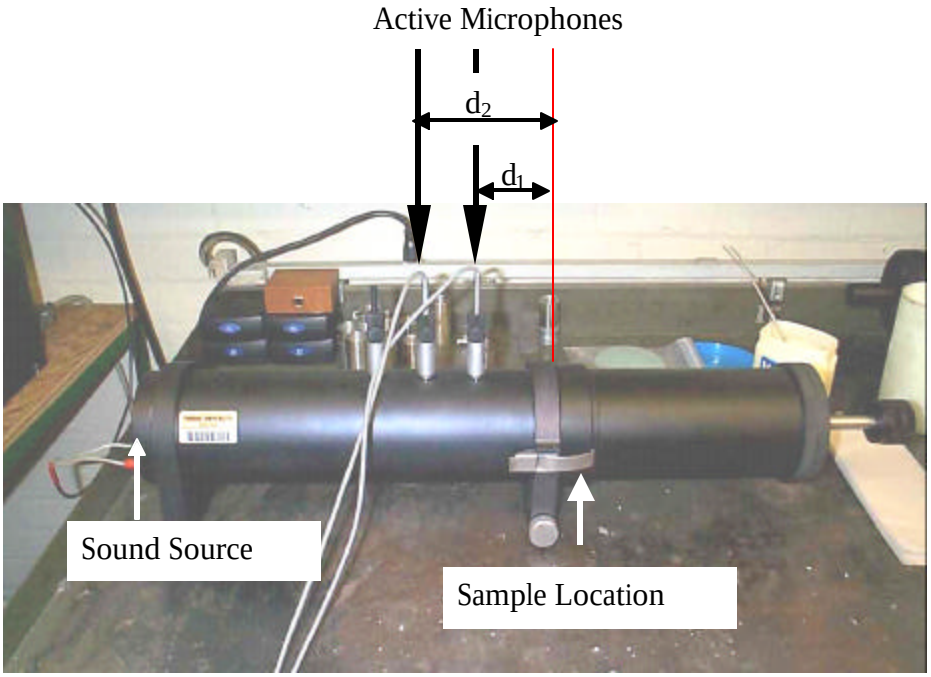

Figure 4.5 Impedance tube set up

A data acquisition system (PULSE ™) is attached to the impedance tube, which converts the signals in the time domain to one in the frequency domain. A software program written in Matlab™ allows graphic display of the real and imaginary components of the impedance with respect to the frequency. The program has also been

tailored to output the variation of acoustic absorption coefficient with frequency. The software code is given in Appendix A.

The absorption coefficient (α) is commonly reported as a measure of a material's ability to absorb sound. A material with an absorption coefficient of 1.0 indicates a purely absorbing material whereas a material with an absorption coefficient of 0 indicates that it is purely reflective. The absorption coefficient at each frequency can be calculated from the pressure reflection coefficient (R) as given in Equation 4.4.

$$\alpha = 1-|R|^2 \qquad 4.4$$

In this work the frequency range of interest was limited from 100 Hz to 1600 Hz. A threshold of 100 Hz was established because at very low frequencies, the acoustic pressures were difficult to stabilize. Frequencies higher than 1600 Hz could be measured accurately only when the impedance tube has a small diameter. (To achieve acoustic measurements over the widest range of frequencies, and to ensure that a "standing wave" is generated inside the impedance tube, its diameter should be as small as possible). Preparation of homogeneous concrete samples of such small sizes tends to be difficult due to the size of the aggregates.

4.5.7 Electrical Impedance Spectroscopy

Electrical Impedance Spectroscopy (EIS) was used to determine the bulk resistance of EPC samples, in order to estimate the conductivities. EIS measurements were conducted in this study using a Solartron 1260 ™ Impedance / Gain-Phase analyzer that was interfaced with a personal computer for data acquisition. A typical Nyquist plot

(plot of real versus imaginary impedance) obtained from EIS measurements consists of two arcs – the bulk arc and the electrode arc. The two arcs meet at a point where the imaginary component of the impedance is minimum, and the corresponding real impedance is the bulk resistance (R_b) of the sample.

Figure 4.6 shows the specimen set up that was used for the EIS experiments. The cylindrical EPC specimen, 95 mm in diameter, and 150 mm long was enclosed in a latex membrane to contain the electrolyte. The bottom of the specimen was sealed to a stainless steel plate using silicone sealant. The specimen was saturated with the electrolyte and another stainless steel plate with a small acrylic dyke was placed at the top of the specimen, with a piece of porous foam in between. The entire set up was firmly gripped with adjustable clamping mechanism. The stainless steel plates served as the electrodes and alligator plugs from the impedance analyzer were attached to the electrodes. The impedance measurements were made over the frequency range of 1 MHz to 10 Hz using a 250 mV AC signal.

Using the bulk resistance (R_b) obtained from the Nyquist plots, the effective electrical conductivity (σ_{eff}) of the sample was calculated as:

$$s_{eff} = \frac{l}{R_b A} \qquad 4.5$$

where l is the specimen length and A is the cross sectional area of the specimen.

The electrolytes used in this study were sodium chloride (NaCl) solutions of varying concentrations (1%, 3%, and 10%). The conductivity of 1% NaCl solution was 1.56 S/m whereas the conductivities of 3% and 10% solutions were 4.40 S/m and 12.40 S/m respectively.

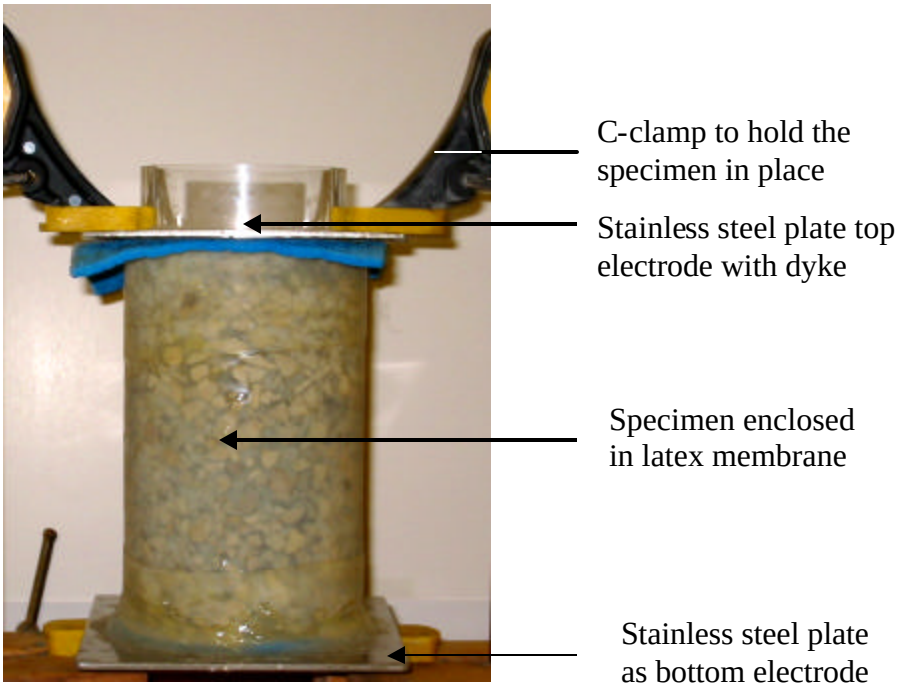

Figure 4.5 Specimen set up for EIS experiments

4.5.8 Dynamic Modulus of Elasticity

The dynamic modulus of elasticity was determined using Grindosonic ™ equipment, as per ASTM E 1876-01. The specimen was supported on rollers at a distance of 0.224L from the edges (L is the specimen length). The pick up of the Grindosonic equipment was positioned on the center of the side face of the specimen and a light impact was given on the center of the top face of the specimen to transmit flexural waves through the specimen. The instrument indicated the fundamental flexural frequency. The procedure was repeated for 5 times (a very consistent reading was obtained in this case) and the average was taken as the fundamental flexural frequency of the specimen. The dynamic modulus of elasticity is given by:

$$E = 0.9465 m f_f^2 \frac{L^3}{t^3 b} T_1 \qquad 4.6$$

where E is the dynamic modulus of elasticity in Pa, m is the mass of the specimen in g, f_f is the fundamental flexural frequency of the specimen in Hz, L is the specimen length in mm, t and b are the specimen thickness and width respectively in mm, and T_1 is a correction factor to account for the finite length of the bar, Poisson's ratio and so forth. The equation for calculation of T_1 is given in ASTM E 1876.

4.5.9 Freezing and Thawing

Freezing and thawing studies on EPC were carried out using two methods: (i) rapid freezing and thawing in water, as per ASTM C 666 Procedure A, and (ii) slow freezing and thawing in water, in a controlled temperature chamber where the specimens are subjected to one freeze-thaw cycle per day. The temperature of the slow freezing and thawing chamber cycled from -16 ^{0}C to 22 ^{0}C. The fundamental flexural resonant frequencies of the specimens were determined prior to freezing, and then periodically during the test. A waveform spectrum analyzer was used to determine the frequencies. The relative dynamic modulus (P_c) was calculated according to Equation 4.7 periodically during the test.

$$P_c = \left(\frac{n_1^2}{n^2} \right) \times 100\% \qquad 4.7$$

where n_1 is the fundamental frequency after a certain specified number of cycles, and n is the fundamental frequency before freezing and thawing cycles were started.

CHAPTER 5: PROPERTIES AND PORE STRUCTURE FEATURES OF EPC

5.1 General

This chapter deals with the fundamental mechanical properties (flexural strength), and pore structure features (porosity, pore size, and permeability) of EPC. The influence of aggregate size and gradation on the pore structure features and the mechanical properties are presented. In addition, the variation in mechanical properties with pore structure features also is explained. The central idea of this chapter therefore is to bring out the significant features of the pore structure of EPC and develop an understanding of how it affects the other properties.

5.2 Aggregate Sizes and Pore Sizes

The three sizes of aggregates used to produce gap graded EPC mixtures in this study were # 8 (passing 4.75 mm and retained on 2.36 mm sieve), # 4 (passing 9.5 mm and retained on 4.75 mm sieve), and 3/8" (passing 12.5 mm and retained on 9.75 mm sieve). Moreover, binary blends of these aggregate sizes were also used as given in Table 4.2. The pore sizes are significantly influenced by the aggregate sizes and their gradation. This section discusses the influence of single sized aggregates as well as aggregate blends on the pore sizes of various EPC mixtures.

5.2.1 Influence of Single Sized Aggregates on Pore Size

The plot of aggregate size versus characteristic pore size shown in Figure 5.1 for EPC mixtures with single sized aggregates.

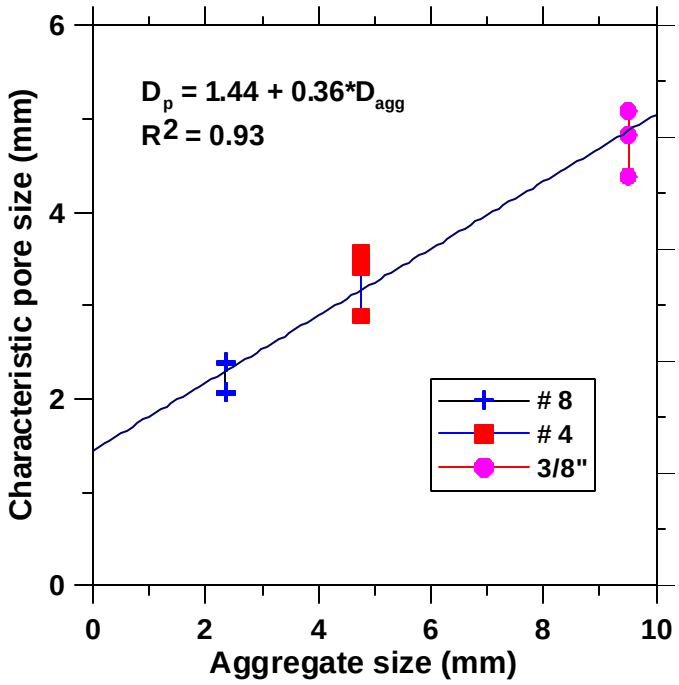

Figure 5.1 Variation of characteristic pore size with aggregate size for single sized aggregate EPC mixtures

The mixture made using only 3/8" aggregates has the largest characteristic pore size (4.76 mm) among all the mixtures investigated whereas the mixture with only # 8 aggregates has the smallest pore size (2.17 mm). An increase in aggregate size therefore is found to result in an increase in characteristic pore size. The relationship between the aggregate size and the characteristic pore size for a single sized aggregate EPC mixture can be described using the linear equation given below:

$$D_p = 1.44 + 0.36\, D_{agg} \qquad 5.1$$

where D_p is the characteristic pore size, and D_{agg} is the aggregate size, both in mm.

5.2.2 Influence of Aggregate Blends on Pore Size

The variations in characteristic pore size with aggregate blends are shown in Figures 5.2 and 5.3. The characteristic pore size is plotted against the percentage of larger aggregates replacing the smaller ones. Figure 5.2 shows the relationship between the aggregate size and pore size for an aggregate size ratio of 2.0 in the blend (i.e, 3/8" aggregates replacing #4, and # 4 replacing # 8), where as Figure 5.3 depicts the relationship for an aggregate size ratio of 4.0 (i.e, 3/8" replacing # 8).

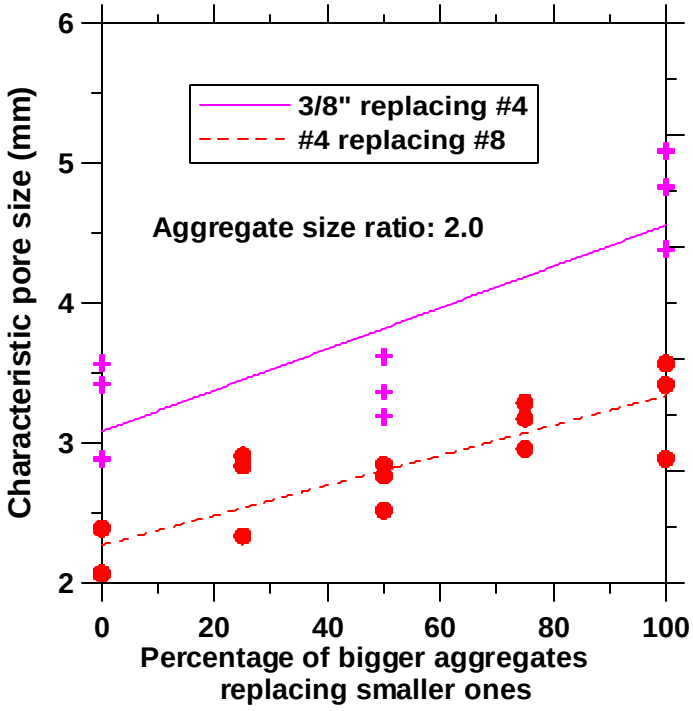

Figure 5.2 Variation of characteristic pore size with aggregate size for binary blends with aggregate size ratio of 2.0

It can be readily noticed that replacing the smaller sized aggregates with an increasing percentage of larger sized ones increases the characteristic pore size. This happens because the introduced coarser particle may not be able to fit in the void left

behind by the removed finer particle. Also, according to the theory of particle packing, when fewer coarser particles are introduced in a mixture of finer particles, there is a further amount of voids introduced in the packing of finer particles at the interface, called the wall effect.

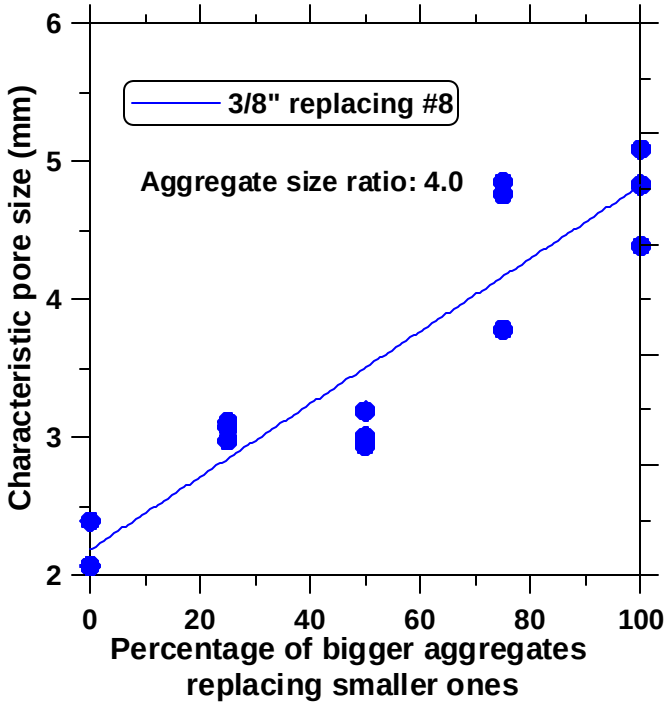

Figure 5.3 Variation of characteristic pore size with aggregate size for binary blends with aggregate size ratio of 4.0

The plots are essentially parallel when the aggregate size ratio is 2.0, (combination of either # 4 and # 8 or # 4 and 3/8”), as seen in Figure 5.2. The variation is steepest when the smallest size is replaced by the largest size (i.e., # 8 by 3/8” aggregates, giving an aggregate size ratio of 4.0), as depicted in Figure 5.3. Figures 5.2 and 5.3 show the dependence of pore size on the ratio of aggregate sizes. The trends indicate that an increase in aggregate size, be it in single sized, or blended system, increases the characteristic pore size of the system.

The characteristic pore size is an important parameter in the design of EPC for optimal acoustic characteristics as well as hydraulic permeability, as will be explained later. Figures 5.1, 5.2 and 5.3 can also be used as design aids in such circumstances. Based on the required characteristic pore size, which is dictated by the requirements of acoustics or permeability, the optimal aggregate size (in the case of single sized aggregates) or the proportion of different aggregate sizes (in the case of blends) can be obtained from these figures.

5.3 Aggregate Sizes and Porosity

The aggregate sizes and gradation have a significant effect on porosity of EPC mixtures. This section explains how the aggregate sizes and gradation influences the porosity of EPC mixtures. As explained earlier, porosity was determined using an image analysis procedure as well as a volumetric procedure. The figures in this section uses data from the image analysis procedure, and as a means of comparison between porosities obtained from both the methods, a Table is included later in this section.

Figure 5.4 illustrates the variation in accessible porosity with percentage of # 8 aggregates, the remaining percentage made up of either # 4 or 3/8" aggregates, i.e., 50% # 8 aggregates indicate that the remaining 50% is made up of either # 4 or 3/8" aggregates. There is no significant difference in the total pore volume between mixtures consisting of single sized (# 4, # 8, or 3/8") aggregates; with an accessible porosity between 21 and 24% for all of these mixtures. For mixtures made using blends of # 4 and # 8 aggregates, the accessible porosity is found to be higher than those for mixtures

with single sized aggregates. This is again attributable to the increased volume of voids in the interface in a mixture of coarse and fine particles. When 3/8" aggregates are blended with # 8 aggregates, the accessible porosity is higher than or at least roughly similar to that of single sized aggregate mixtures. The only exception was for the case of 50% 3/8" aggregates replacing # 8. This may be attributed to the fact that the # 8 aggregates (2.36 mm) appear to fill the pore spaces that develop between the 3/8" aggregates because they are smaller than the characteristic pore sizes in a system with 3/8" aggregates alone. An increase in either the 3/8" or the # 8 fraction tends to approach a single sized aggregate system, thereby increasing the accessible porosity.

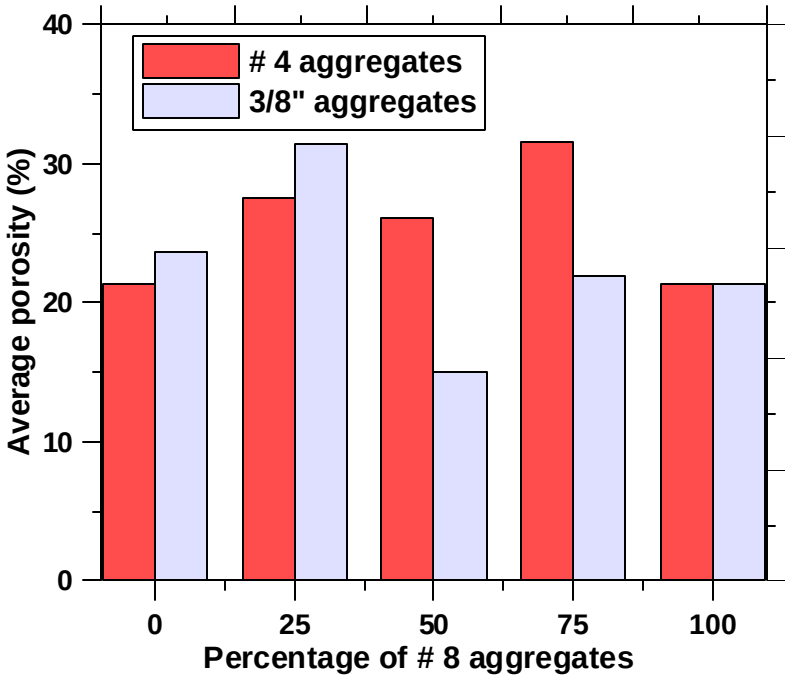

Figure 5.4 Variation in porosity with aggregate blends (# 8 and either # 4 or 3/8")

Similarly, Figure 5.5 shows the variation in average accessible porosity with the amount of # 4 aggregates, the remaining portion being made up of either # 8 or 3/8"

aggregates. The accessible porosity is the highest for a blend of # 4 and 3/8” aggregates. The # 4 aggregates (4.75 mm) cannot fit into the pore space of a mixture with 3/8” aggregates alone, and thus it is not surprising that the accessible porosity of a blend of # 4 and 3/8” aggregates is the highest.

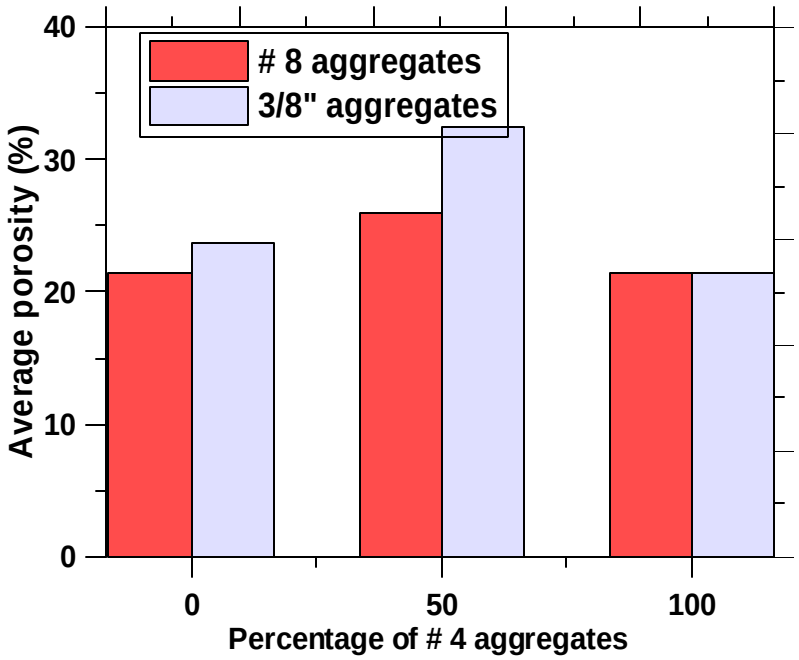

Figure 5.5 Variation in porosity with aggregate blends (# 4 and either # 8 or 3/8”)

Table 5.1 gives a comparison between the porosities obtained from the image analysis procedure and the volumetric method. The general trend of the values is the same but there are certain variations induced due to the methodology of testing.

Table 5.1 Comparison between porosities obtained from both methods

Mixture ID	Porosity (volume method)	Porosity (image analysis method)
100 - #8	0.207	0.214
75-#8 - 25-#4	0.208	0.305
50-#8 - 50-#4	0.247	0.260
25-#8 - 75-#4	0.225	0.276
100 - #4	0.206	0.203
75-#8 - 25-3/8	0.225	0.219
50-#8 - 50-3/8	0.190	0.151
25-#8 - 75-3/8	0.174	0.244
100 - 3/8	0.193	0.237
50-#4 - 50-3/8	0.264	0.303
97.5-#4 - 2.5 sand	0.187	0.189
95-#4 - 5sand	0.176	0.212
92.5-#4 - 7.5sand	0.160	0.231

5.4 Flexural Strengths

The flexural strengths of EPC specimens were determined according to the procedure described in Section 4.4.1. The influence of aggregate size, pore size, and porosity as well as the addition of sand and silica fume on flexural strength is dealt with in detail in this section.

5.4.1 Influence of Aggregate Size

For single sized aggregates, Figure 5.6 depicts the influence of aggregate size on the flexural strength. It can be seen that the flexural strength is reduced as the aggregate size is increased. This trend has been found true for the blended systems also.

Substituting the smaller size aggregate fraction with larger size results in a reduced strength. This occurs since an increase in aggregate size results in an increase in pore size and overall porosity of the mixture.

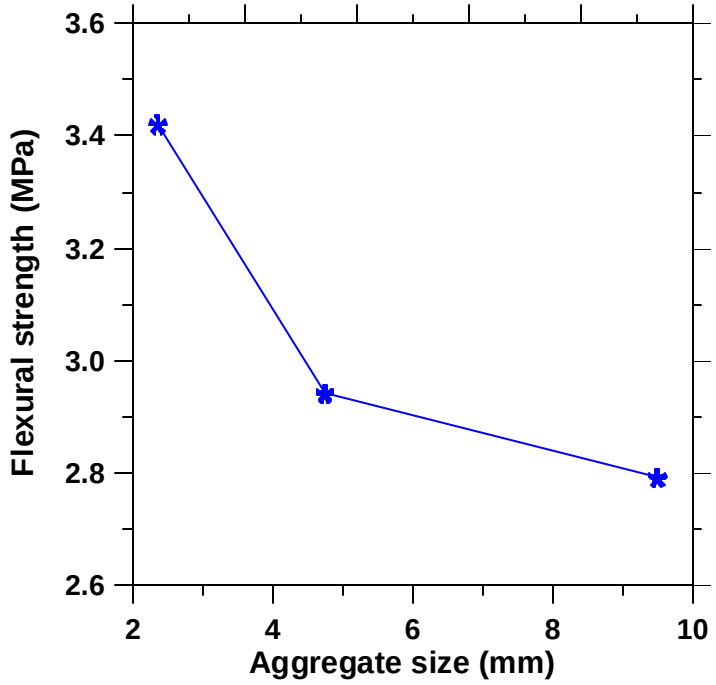

Figure 5.6 Influence of aggregate size on flexural strength

5.4.2 Influence of Pore Size and Porosity

Figure 5.7 illustrates the relationship between pore size and flexural strength for all the EPC mixtures chosen for this study (excluding the mixtures with sand and silica fume). Increase in the pore size results in a reduction in the flexural strength, and the relationship is fairly linear. As expected, the flexural strength also reduces with increasing porosity, and the relationship is roughly linear; however there is considerable scatter in the results. The plot is shown in Figure 5.8.

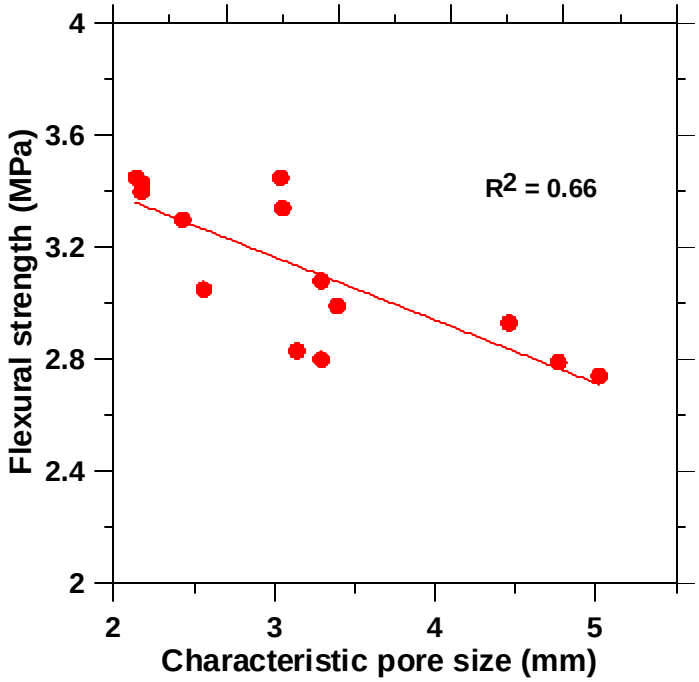

Figure 5.7 Influence of pore size on flexural strength

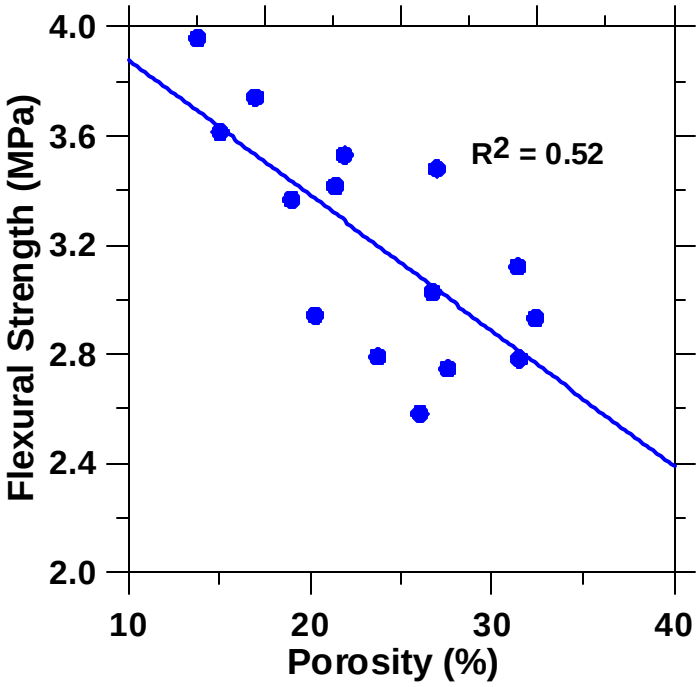

Figure 5.8 Influence of porosity on flexural strength

5.4.3 Influence of Addition of Sand and Silica Fume

In single sized aggregate EPC mixtures made using # 4 aggregates, natural sand was successively added, replacing 2.5, 5, and 7.5% of the coarse aggregates. It was found that addition of sand increases the flexural strength, as shown in Figure 5.9. This effect is not too surprising since sand fills up some of the pores in the EPC system.

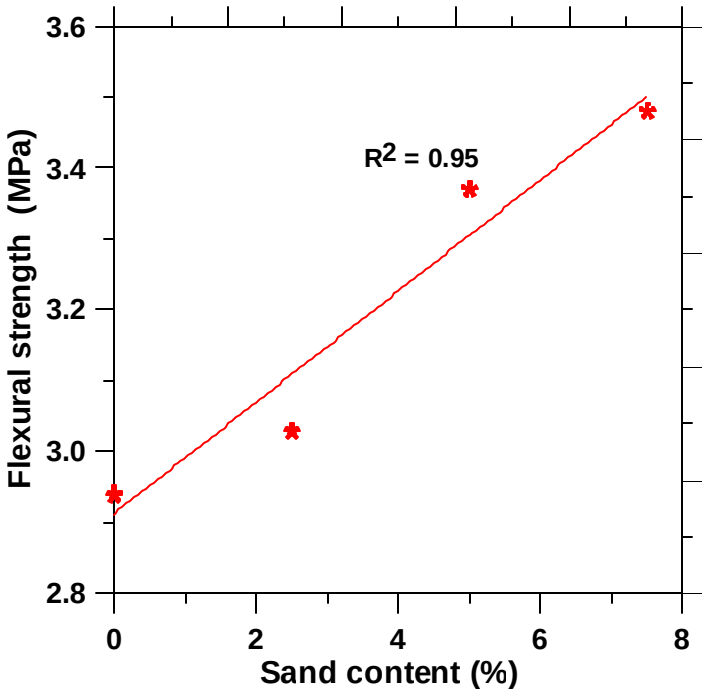

Figure 5.9 Influence of sand addition on flexural strength

The addition of silica fume also was carried out in EPC mixtures made using # 4 aggregates. Silica fume was added at either 6% or 12% by weight of cement. The flexural strengths were found to increase with increase in silica fume content, possibly due to the densification of the paste and strengthening of the paste phase as well as increased bond between the paste and aggregate. Figure 5.10 depicts this relationship.

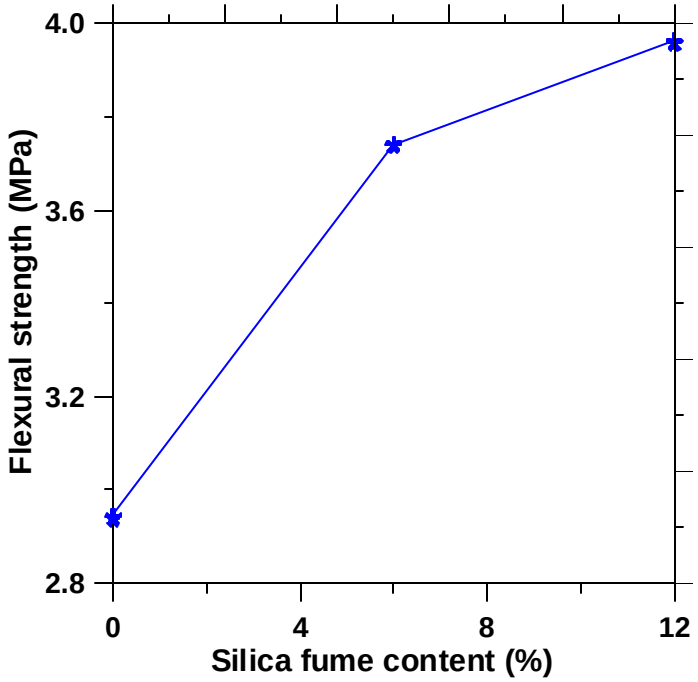

Figure 5.10 Influence of silica fume on flexural strength

5.5 Permeability of EPC

The hydraulic conductivity (K) of a porous material is determined by the arrangement of particles, pores, and their relative sizes. The intrinsic permeability (k) of a porous medium can be thought of as a measure of the frictional resistance to a single-phase fluid flowing through it. Therefore, the intrinsic permeability depends on the porosity, pore-size distribution, pore roughness, constrictions of the pore space, and the tortuosity and connectivity of the internal pore channels [de Lima and Sri Niwas, 2000]. The hydraulic conductivity can be related to intrinsic permeability as:

$$K = k\frac{rg}{m} \qquad 5.2$$

where ρ is the density of the fluid, g is the acceleration due to gravity, and μ is the dynamic viscosity of the fluid. For water, this equation can be simplified as:

$$K = k * 10^7 \text{ (in SI units)} \qquad 5.3$$

The hydraulic behavior of porous media is typically described using the Kozeny-Carman equation:

$$k = \frac{f^3}{F_s t^2 S_0^2 (1-f)^2} \qquad 5.4$$

where ϕ is the porosity, F_s is the generalized factor to account for different pore shapes, τ is the tortuosity, and S_0 is the specific surface area of pores.

5.5.1 Porosity-Permeability Relationship

Several studies have predicted the permeability (permeability here refers to intrinsic permeability) of porous media from the porosity. For example, it has been suggested that Darcy's law could be given a similar form as Archie's law [de Lima and Sri Niwas, 2000], to relate the permeability and porosity of rock systems:

$$k = a_1 f^{b_1} \qquad 5.5$$

where k is the intrinsic permeability (units of m^2), ϕ is the porosity, and a_1 and b_1 are constants. However, the predicted and measured permeabilities were observed not to correlate well since permeability is not a function of the porosity alone, rather connectivity and porosity are critical in understanding the permeability of the system.

For the EPC mixtures investigated in this study, the porosity-permeability relationship is shown in Figure 5.11. While permeability generally increases with an increase in porosity, there is no definitive relationship between these parameters. The reason for such poor correlations can be explained by the fact that porosity is a volumetric property of the material, whereas permeability is a parameter that defines the flow properties through the material that not only depends on the volumetric parameter but also on the distribution of the pore volume and its connectivity. In that sense, it is similar to the electrical conductivity, which was shown in the previous sections to have a dependence on the pore connectivity in addition to the porosity.

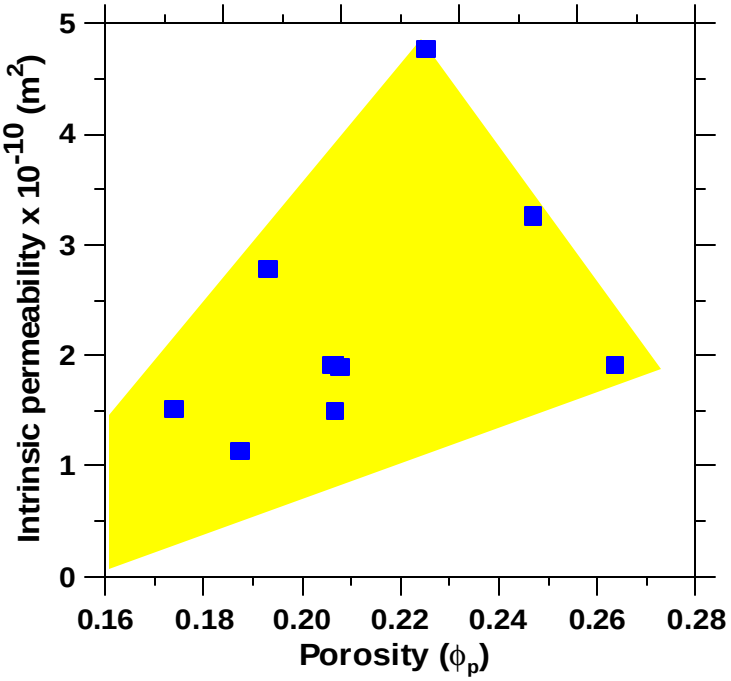

Figure 5.11 Porosity – permeability relationship – increasing permeability with porosity, but no definite trend

5.6 Summary

The influence of aggregate size, and blends on the pore sizes and porosity of EPC has been brought out in this chapter. Consequently, how these features dictate the fundamental mechanical properties (flexural strength), and transport properties (permeability) has been discussed. It was observed that increase in aggregate size resulted in increased pore sizes and porosity in EPC mixtures with both single sized aggregates and aggregate blends, and thus lower flexural strengths. The addition of sand and silica fume was found to increase the flexural strength.

The permeability of EPC mixtures were found to increase with porosity, though no definitive trends could be established. This can be attributed to the fact that permeability is not a function of porosity alone. Further discussions on this aspect can be found in Chapter 8.

CHAPTER 6: ACOUSTIC ABSORPTION OF EPC

6.1 General

This chapter reports the results of acoustic absorption studies on EPC carried out using the impedance tube described in Chapter 4. The acoustic absorption spectra (plot of acoustic absorption coefficient against frequency) for EPC made using both single sized aggregates as well as aggregate blends are provided. The reasons for variations in absorption coefficients with changes in aggregate size and proportion are brought out. The influence of addition of sand and silica fume on the acoustic absorption of EPC mixtures is explained, as is the influence of specimen thickness.

6.2 Influence of Aggregate Size and Gradation on Acoustic Absorption

The acoustic absorption spectra for EPC mixtures made with single sized aggregates as well as aggregate blends are presented in this section. The reasons for variations in maximum absorption coefficients are explained. The results shown here are for specimens having a length of 150 mm.

6.2.1 Single Sized Aggregate Mixtures

The absorption spectra of EPC with single sized aggregates (retained on 3/8", # 4, and # 8 sieves) are shown in Figure 6.1.

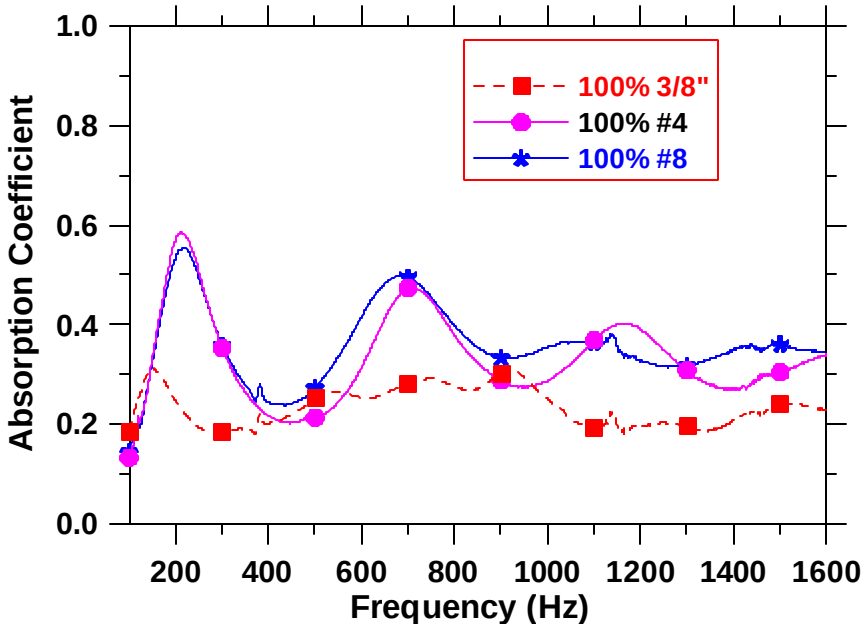

Figure 6.1 Acoustic absorption spectra of EPC made with single sized aggregates

The mixture with only 3/8" aggregates has a markedly lower absorption coefficient (~0.30) than the other two single sized aggregate mixtures. This can be explained by the fact that as the aggregate size increases, in a system devoid of sand, the pores tend to be larger. While the increased pore volume is beneficial (larger pore sizes enable sound to enter inside the material), a system with large size connected pores has lower tortuosity. The acoustic absorption is a function of total porosity as well as the tortuosity of the system, which increases the frictional losses. Therefore, EPC with 3/8" aggregates has a higher porosity but low frictional loss, thus leading to a markedly lower sound absorption. This implies that, finer, but well connected pores may be more

efficient in dissipating sound than larger pores. There is no discernible variation observed between mixtures with 100% # 4 and 100% # 8 aggregates (maximum α around 0.60), which is likely due to the existence of similar pore volumes and similar pore geometries in these mixtures.

6.2.2 Aggregate Blends

Binary blends (by weight) of the three aggregate sizes used were investigated for potential enhancement in acoustic behavior. The absorption spectra of EPC made using blend of # 4 and # 8 aggregates are shown in Figure 6.2. The # 4 aggregate is replaced in steps of 25% by the # 8 aggregate.

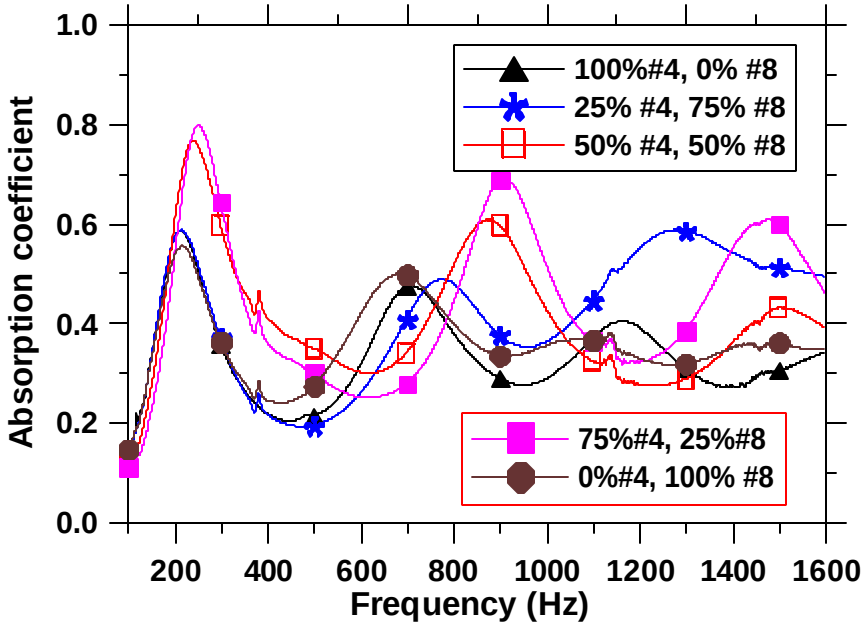

Figure 6.2 Acoustic absorption spectra of EPC made with blends of # 4 and # 8 aggregates

The blends with 75% # 4 (25% #8) and 50% # 4 (50% # 8) are found to be extremely effective in absorbing sound, with maximum absorption coefficients of approximately 0.80. Replacing larger aggregates (# 4) with smaller size ones (# 8) changes the characteristics of the pore structure. It can be noticed from Figure 5.2 of Chapter 5 that the characteristic pore sizes of those blends which are effective in absorption are in the same range (approximately 2.5 to 3.5 mm) and are all lower than that for the mixture with the larger size aggregate. For a given accessible porosity, a smaller pore size therefore appears to be more effective in increasing absorption. With further increase in the # 8 fraction (75%), the maximum absorption coefficient tends to approach that of EPC with single sized aggregates.

Blends of # 8 and # 4 aggregates with 3/8" aggregates were also evaluated for their acoustic absorption characteristics and are shown in Figures 6.3 and 6.4 respectively. For the # 8 and 3/8" blends, addition of 3/8" aggregates into the system with # 8 aggregates reduces the maximum absorption coefficient, since it is believed that the differences in aggregate sizes result in # 8 aggregates effectively filling the pore spaces created by 3/8" aggregates (characteristic pore size for mixtures with 3/8" aggregates is 4.76 mm whereas the size of # 8 aggregates range from 2.36-4.75 mm). Refining the pore size of EPC consisting of 3/8" aggregates with 50% # 4 aggregates results in only a marginal increase in the absorption coefficient as compared to that with # 4 aggregate even though the porosity is markedly increased in this case (see Figure 5.3). This can be attributed to the fact that the bulk of the porosity may due to the large sized pores that exist in the material, resulting in lesser frictional losses within the pore structure.

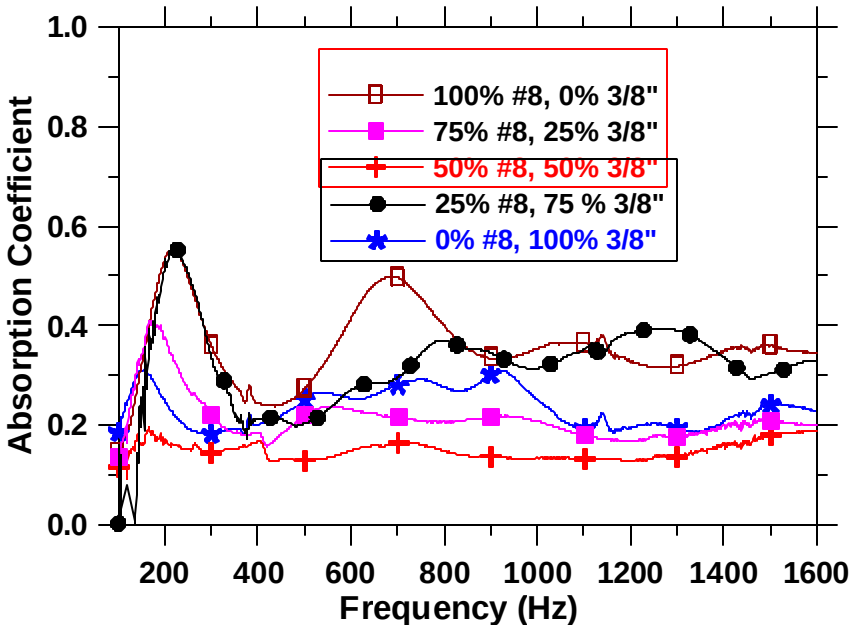

Figure 6.3 Acoustic absorption spectra of EPC made with blends of # 8 and 3/8" aggregates

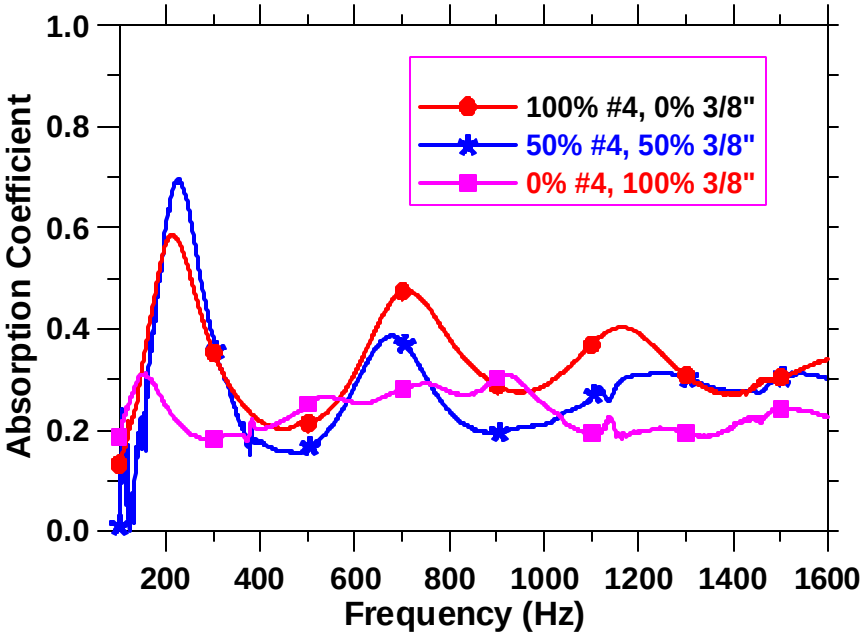

Figure 6.4 Acoustic absorption spectra of EPC made with blends of # 4 and 3/8" aggregates

In summary, a comparison of the single sized aggregate and blended systems shows that blending of different sized aggregates has a significant effect on the absorption coefficient of EPC. The blend of # 4 and # 8 aggregates is found to be a very promising option from this study. The use of 3/8" aggregates either by themselves or in blends does not seem to be effective, though systems with considerable porosity can be achieved. This leads to the conclusion that pore size, along with the porosity, is also a factor that has a significant impact on the acoustic absorption behavior of EPC. Though very large sized pores contribute to increased accessible porosity which would be preferred, they are not ideally suited for acoustic absorption since the viscous effects are not highly dominant with increased sizes. In general, it appears that certain optimal pore sizes exist that are more effective in improving the acoustic performance of EPC.

6.3 Influence of Sand and Silica Fume

The influence of the addition of sand and silica fume was studied on EPC made with only # 4 aggregates. The addition of sand is found to reduce the maximum absorption coefficients, as shown in Figure 6.5. This reduction in sound absorption can be described by the fact that the sand particles block access to the pores, resulting in an increase in sound reflection. Though the characteristic pore size is reduced with the addition of sand, the beneficial effect of pore refinement is negated to a certain degree by the reduction in connectivity of the pores. This shows that from the viewpoint of maximizing sound absorption, addition of sand in EPC mixtures is not a recommendable option.

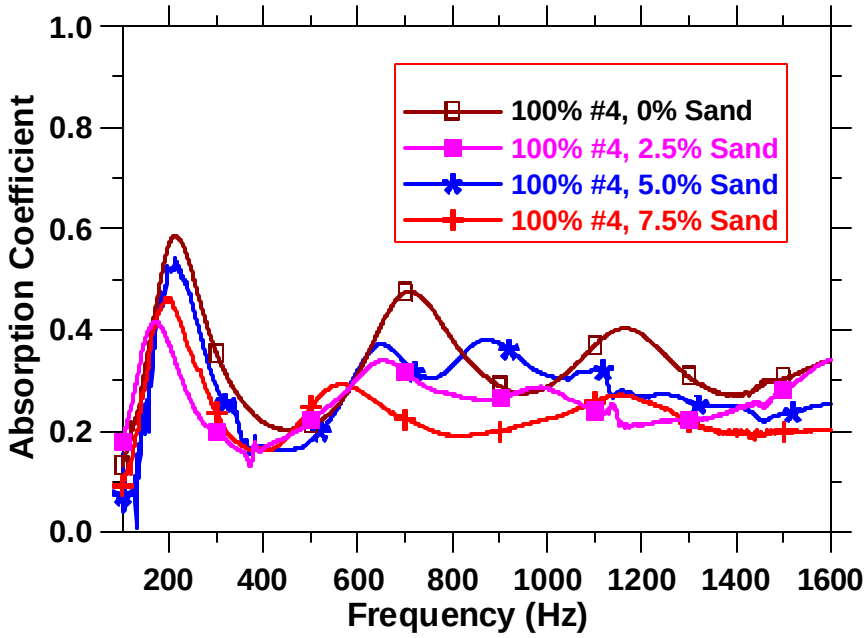

Figure 6.5 Influence of sand in acoustic absorption

The addition of 6 and 12% silica fume (by weight of cement) resulted in no significant changes in acoustic absorption, as is seen from Figure 6.6. This behavior is not unexpected since silica fume hardly changes the size of acoustically efficient pores. The use of silica fume primarily contributes to densification of cement paste and enhancement in bond, which results in an enhancement in flexural strength.

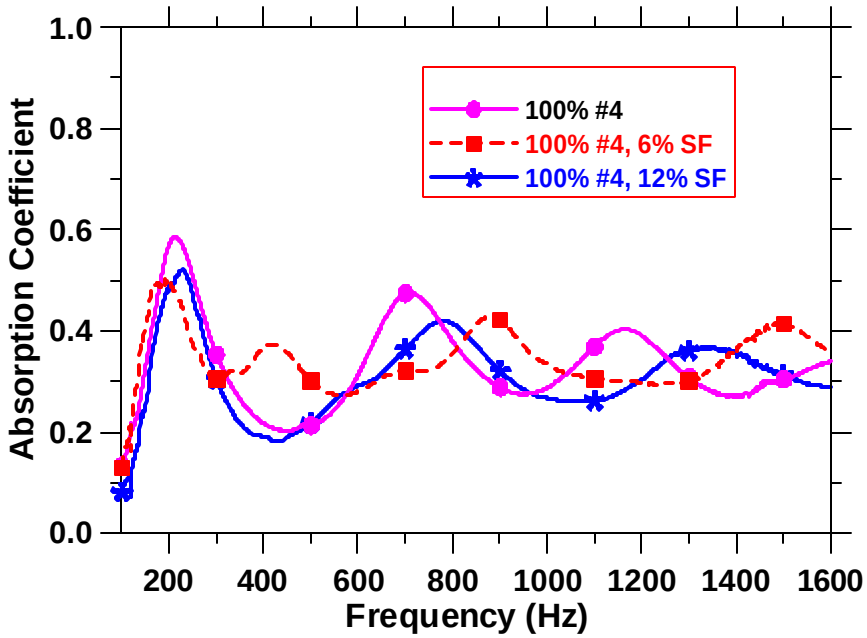

Figure 6.6 Influence of silica fume in acoustic absorption

6.4 Specimen Length Scales and Acoustic Absorption

Of particular significance in the acoustic absorption spectra are the magnitude and location of peak absorption values. The magnitude of the peak absorption coefficient is dependent on the mixture characteristics, whereas the frequency at which the absorption peaks occur is primarily dependent on the thickness of the specimen. Figure 6.7 shows the absorption spectra for an EPC mixture with a blend of 75% # 4 and 25% # 8 aggregates. It can be seen that for three specimens, as the thickness changes from 150 mm to 37.5 mm, the absorption spectra shifts as a function of the frequency. It can be shown that this characteristic can be effectively used to arrive at the thickness of

specimens (alternatively, the thickness of EPC pavements) so that attenuation of sound in the desired frequency range is obtained.

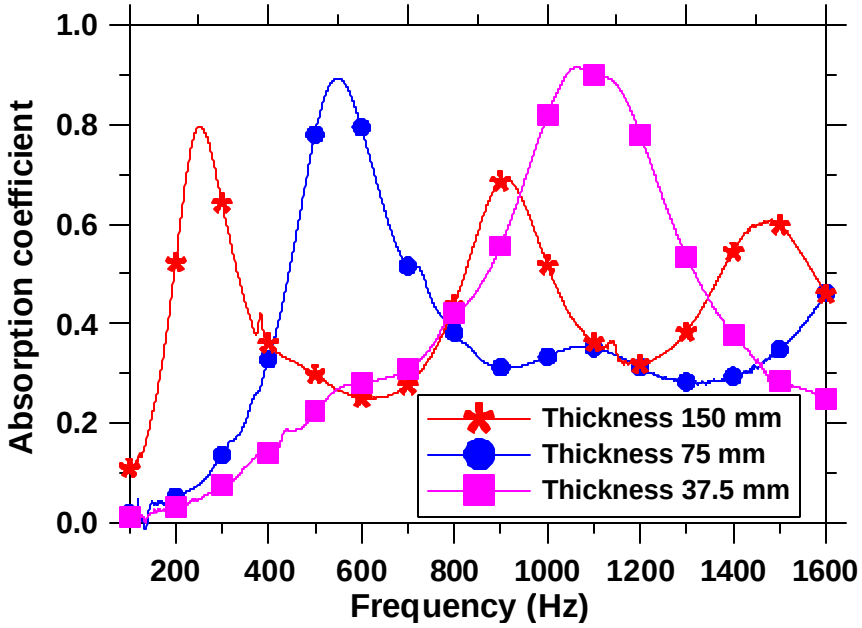

Figure 6.7 Influence of specimen thickness on frequency at peak absorption

For each of the absorption curves, the peak can be thought of as a function of wave speed in the particular medium and the specimen length. Because the speed of the wave in air is effectively a constant, the thickness of the sample must be changed, to shift the peaks. The peaks occur at frequencies that can be calculated according to the relationship [Zwikker and Kosten 1949]:

$$f_{peak} = \frac{nc}{4l} \qquad 6.1$$

where f_{peak} is the frequency at peak absorption, n is an odd integer number corresponding to the peak (1 for 1st peak, 3 for 2nd peak and so on), c is the effective speed of wave in the medium (343 m/s for air at 20^{o}C), and l is the thickness of the sample.

Since c and n are constants, the product of frequency and thickness of the sample should also be a constant. This implies that when the product of frequency and thickness is plotted against the absorption coefficient, the peaks must appear at the same frequency, irrespective of the specimen thickness. For illustrative purposes, this feature is shown in Figure 6.8 for the mixture of 75% # 4 and 25% # 8 aggregates. This plot shows that the product of frequency and the specimen thickness is a constant. This is advantageous in selecting the most acoustically efficient thickness of EPC overlays for pavements, based on the dominant frequency of sound to be attenuated.

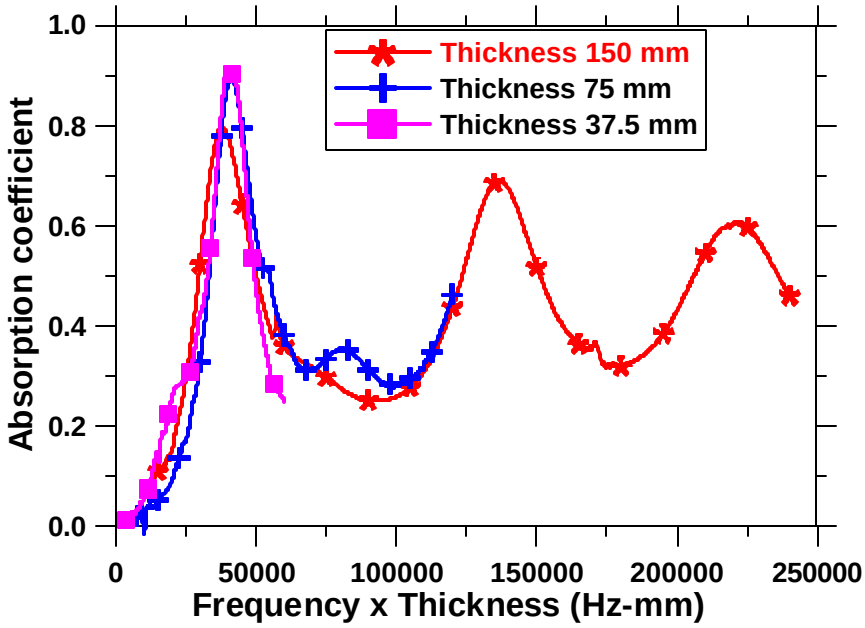

Figure 6.8 Illustration of Frequency x Thickness being constant irrespective of specimen thickness

For example, 800-1200 Hz is frequency range in which more of the objectionable highway noise falls. Hence, using a frequency of 1000 Hz and speed of sound in air as 343 m/s, the thickness of overlay required (1st absorption peak, hence n=1) can be calculated from Equation 6.1 as 8.6 cm (3.4 inches).

6.6 Summary

This chapter has dealt with detailed discussions on the acoustic absorption behavior of EPC. It was found that the acoustic absorption behavior is closely related to the porosity and pore size in the material. It appears that there is an optimal pore size depending on the mixture that maximizes sound absorption. Blending of aggregates, especially # 4 and # 8, is found to more effective than single sized aggregates. The addition of sand is found to be detrimental in acoustic absorption while silica fume does not significantly alter the absorption behavior. The frequency at the peak absorption is related to the thickness of the specimen. A procedure has been provided to calculate the optimal specimen thickness once the frequency range in which the most objectionable noise is generated, is known.

CHAPTER 7: MODELING THE EFFECTS OF PORE STRUCTURE CHARACTERISTICS IN ACOUSTIC ABSORPTION OF EPC

7.1 General

This chapter reports the studies conducted on modeling the acoustic absorption characteristics of EPC in relation with its pore structure. The details of the physical model used, and the accuracy with which it predicts the acoustic absorption behavior of EPC is explained. A parametric study that was conducted to ascertain the effects of pore structure parameters on acoustic absorption is also discussed.

7.2 Modeling the Acoustic Absorption of Porous Materials

EPC can be modeled as a "rigid-framed" porous material, where the sound propagation is governed by the effective density and effective bulk modulus of the fluid in the pore space. It is generally known that in rigid-framed porous materials, the acoustic absorption occurs primarily due to the viscous losses and thermo-elastic damping as the sound propagates through a large number of air cavities in the material [Wang and Lu 1999, Voronina 1999]. When an acoustic wave impacts a pervious surface, air is pushed into the pores, resulting in a partial reflection of the wave, and damping of the transmitted wave [Boutin et al. 1998]. Biot's theory has been used to model acoustic wave propagation in porous dissipative media for a long time. Delany and Bazley are

credited with the development of empirical power law relationships between the fundamental acoustical properties of porous materials, viz. the characteristic acoustic impedance and propagation constant, and the ratio of static flow resistivity to frequency. However, the low frequency predictions of these empirical relationships are stated to be unrealistic [Lu et al. 2000]. Non-linear, frequency dependent, complex expressions also have been derived to predict the acoustic performance of porous materials [Johnson 1987].

7.2.1 Different Modeling Approaches

Two major approaches have been used to model the acoustic characteristics of rigid framed porous materials [Francois and Michel 1993] – (i) phenomenological models, which consider the porous medium to be globally a compressible fluid where dissipations occur, and the equations for analysis are set up at a global scale (Delany-Bazley laws), and (ii) microstructural models, which consider the sound propagation in straight pores, and then accounting for the tortuosity with shape factors (Zwikker and Kosten 1949, Biot 1962). Kirchoff's theory provides a description of sound propagation in cylindrical tubes, taking into account the viscous and thermal effects, but does not account for non-circular cross sections [Allard 1993]. Several shape factors to extend the circular pore geometries to more complicated shapes have been suggested [Allard 1993, Stinson and Champoux 1992]. Both approaches describe the material in terms of its specific acoustic impedance and wave number. The concepts of acoustic mass, stiffness, and damping have been employed to arrive at non-dimensional expressions for characteristic impedance and wave number [Brennan and To 2001].

The foregoing discussion gives an insight into some of the common models used to describe the acoustic behavior of a porous material. This study uses physical modeling concepts of the pore system to predict the acoustic absorption of EPC. Toward this end, this work will utilize a modeling approach that was developed for highly porous metal matrix composites to quantify the sound absorption [Lu et al. 2000]. This model will be extended to consider lower pore volume materials. Numerical simulation will be compared with experimental observations to calibrate model parameters like porosity and pore size. For better material design, the acoustic absorption phenomenon has to be related to the material structure, i.e., the pore volume, pore size, and distribution. Hence, in this study, a microstructural approach will be used rather than a phenomenological approach since the aim is to relate the acoustic absorption behavior of EPC to the characteristics of its pore structure.

7.3 Numerical Simulation of the Acoustic Absorption Characteristics of EPC

This section deals with the simulation of the pore structure of EPC by an idealized model. An electro-acoustic analogy is used to model the acoustic absorption behavior. The comparison of the model predictions with the experimental values is also provided.

7.3.1 Physical Geometry of the Simulated Pore Structure

A typical cross section of EPC is shown in Figure 7.1. It could be seen that there are pores of varying sizes, and it is assumed that the pores are interconnected by apertures

of varying sizes, thereby alternatively compressing and expanding the acoustic waves to lose its energy.

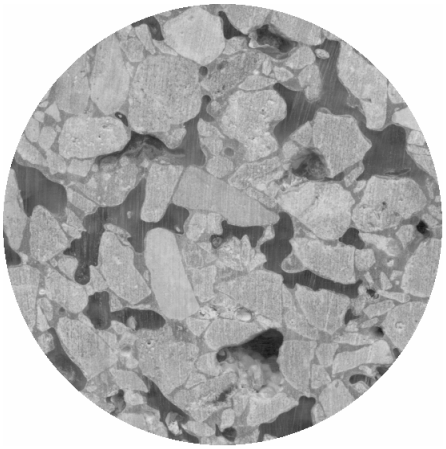

Figure 7.1 A typical cross-section of EPC

A model of the type shown in Figure 7.2 is believed to be a more adequate representation of the EPC system than one consisting of single sized openings. The models as described in Section 7.2 do not apply to materials where an abrupt change in cross section, as is believed to occur in EPC, happens.

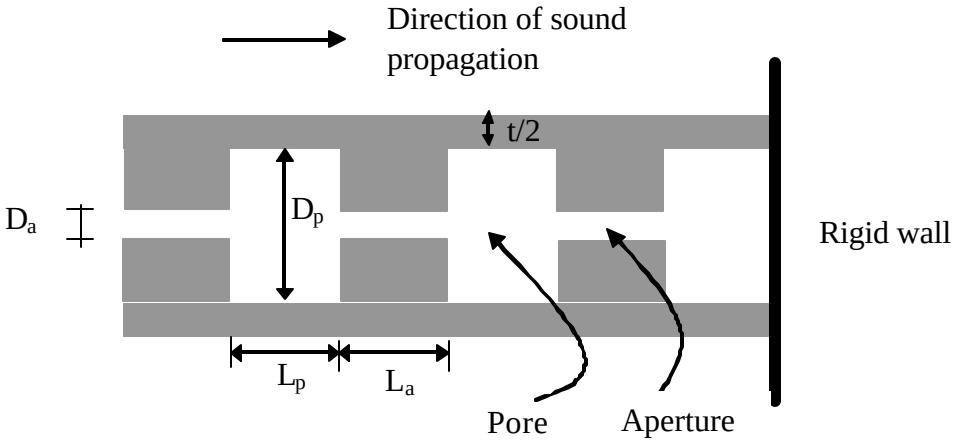

Figure 7.2 Pore-aperture model adopted to represent EPC

Based on the acoustic impedance of circular apertures and cylindrical cavities, the structure-property relationships for metallic foams with semi-open cellular structures have been developed [Lu et al. 2000].

The pore network is assumed to be a series of alternating cylinders with varying diameter. Each unit of the pore network consists of a pore and apertures entering the pore and leaving it, as shown in Figure 7.3. It can be argued that each of the units must exhibit the same porosity as the total system. The porosity (ϕ) can, therefore, be related to the length and diameter of the pore (L_p and D_p respectively), the length and diameter of the aperture (L_a and D_a respectively), and the wall thickness t as shown in Equation 7.1. The wall thickness t has been approximated as $D_p/2$ for the modeling efforts presented here. Further, the total length of the specimen is assumed to be an integer multiple of the sum of aperture length and pore length (this implies that the model in effect is an integer number of pore and pore aperture assemblies).

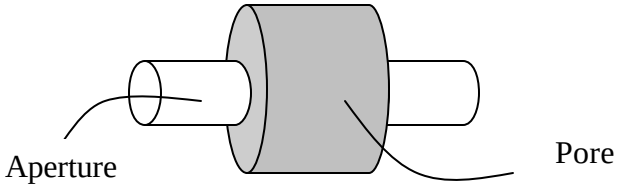

Figure 7.3 An individual cell of the pore-aperture network

$$f = \frac{(D_a{}^2 L_a + D_p^2 L_p)}{(L_a + L_p)(D_p + t)^2} \qquad 7.1$$

Further, it is assumed that the pores are arranged in a hexagonal array, and appropriate circular dimensions approximate these hexagons [Lu et al. 2000]. For a hexagonal prism of side D, and length L_p, if the volume of the hexagonal prism is set equal to a sphere of diameter D, it can be seen that $L_p = 0.806D$. Similarly, by setting the

area of a circle of diameter D_p, equal to the area of a hexagon with side D, $D_p = 0.909D$. From these, it could easily be deduced that the length of the pore $L_p \sim 0.90\ D_p$.

7.3.2 Structure Factor and its Influence in Acoustic Absorption

For porous materials with pores made up of an alternating sequence of cylinders (Figure 7.2), the structure factor or structure form factor (k_s) represents an important pore structure feature. k_s does not depend on the fluid inside the pores, but only on the geometry of the frame. The value of k_s is usually found to lie between 3 and 7, though it can have any value above 1 [Zwikker and Kosten 1949].

The physical significance of k_s can be explained as follows (Refer Fig. 7.4). Assume that there are lateral cavities located beside the main pores in a porous material. On application of a pressure gradient (a standing wave in an impedance tube, for instance), the air in the main pores move but in lateral cavities, it is largely at rest. This makes the air in lateral cavities act as if it were heavier than the air in the main pores by a factor k_s. Since the pressure gradient accelerates air in the main pores only, leaving those in cavities at rest, the porosity that is effective in acoustic absorption termed as the "acoustic porosity" is the ratio of measured porosity to the structure factor (ϕ/k_s). This property dictates the acoustic characteristics of the material.

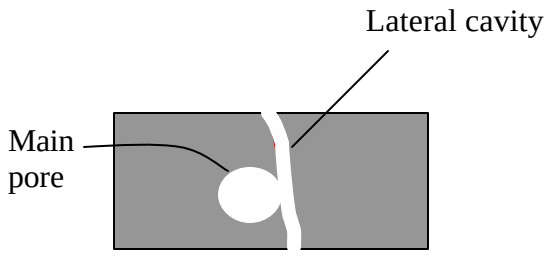

Figure 7.4 Concept of Structure Factor (Zwikker and Kosten 1949)

7.3.3 Determination of Structure Factor

In the determination of the structure factor, the pore network is considered to be an alternating sequence of cylinders of two different cross sections (Figure 7.2) [Allard 1993]. Assuming that ratio of velocities of both the sections is constant, k_s can be obtained as:

$$k_s = \frac{(L_a A_a + L_p A_p)(L_a A_p + L_p A_a)}{(L_a + L_p)^2 A_a A_p} \qquad 7.2$$

where L_a and L_p are the lengths of the aperture and the pore and A_a and A_p are the cross sectional areas of the aperture and pore respectively.

The value of D_p (diameter of the pore) can be obtained from image analysis as mentioned in Chapter 4. The length of pore, L_p was shown to be equal to 0.90 D_p in Section 7.3.1. This leaves two unknowns in the Equation 7.1 – D_a and L_a. In order to solve this, the following approach has been adopted: A value of D_p/D_a (say, 2) is initially assumed so that D_a becomes known. This gives a first estimate of L_a. The value of D_p/D_a is successively increased and corresponding L_a determined. A plot of D_p/D_a versus L_a is shown in Figure 7.5. The D_p/D_a value at which L_a tends to asymptotically approach a

constant value is chosen and based on this the aperture diameter D_a is calculated. The L_a corresponding to this D_p/D_a value is taken as the aperture length. The values of D_p, D_a, L_p and L_a for the mixtures investigated in this study, as calculated from the above procedure are shown in Table 7.1.

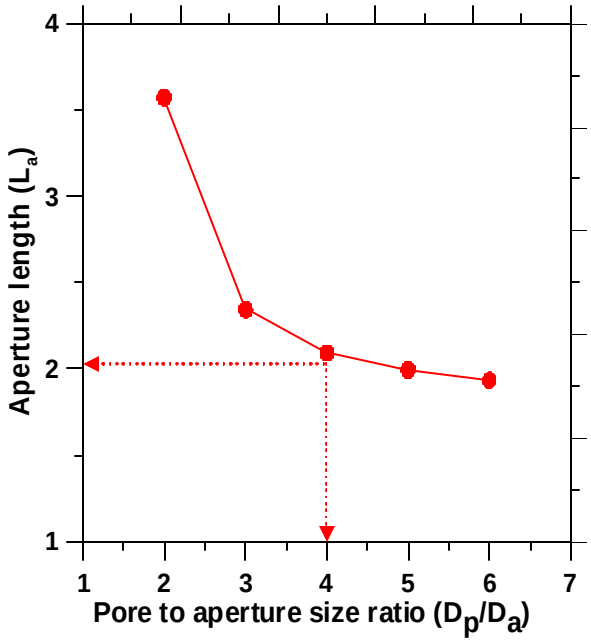

Figure 7.5 Determination of aperture diameter and length

Table 7.1 Estimated pore structure features of mixtures investigated

Mixture ID	% 3/8" aggregates	% # 4 aggregates	% # 8 aggregates	Pore Diameter (Dp) from image analysis, mm	Pore length (Lp) = 0.9Dp, mm	Optimal Dp/Da	Aperture diameter (Da),mm	Aperture length (La), mm
100 - #8	0	0	100	2.17	1.95	4	0.54	2.09
75-#8 - 25-#4	0	25	75	2.69	2.42	4	0.67	1.87
50-#8 - 50-#4	0	50	50	2.48	2.23	4	0.62	0.77
25-#8 - 75-#4	0	75	25	3.14	2.83	4	0.79	1.09
100 - #4	0	100	0	3.29	2.96	4	0.82	1.85
50-#8 - 50-3/8	50	0	50	3.04	2.74	7	0.43	1.74
100 - 3/8	100	0	0	4.77	4.29	8	0.60	1.78
50-#4 - 50-3/8	50	50	0	3.29	2.96	5	0.66	0.83

7.3.4 Acoustic Absorption and Structure Factor

The maximum acoustic absorption (α) for the EPC mixtures measured using the impedance tube is plotted against the structure factor (k_s) in Figure 7.6.

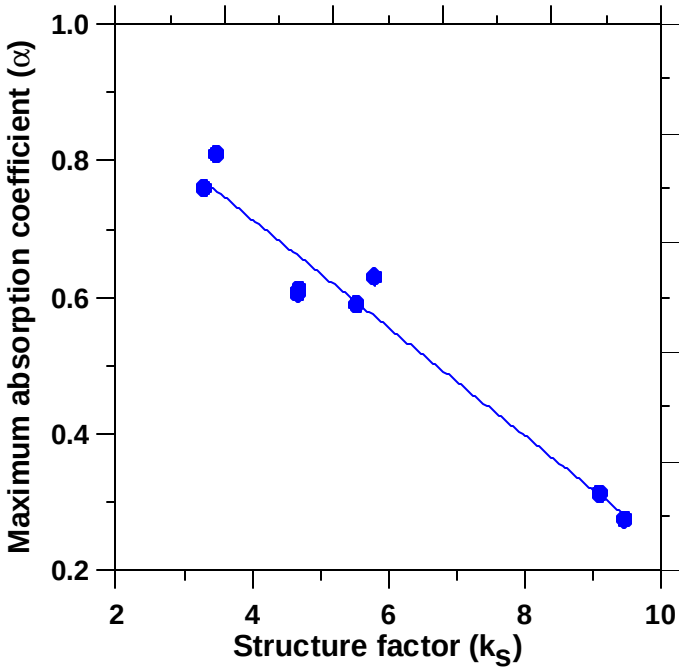

Figure 7.6 Variation of maximum acoustic absorption coefficient with structure factor

It can be seen that, with increase in structure factor, the maximum absorption coefficient decreases, and the trend is very linear. This can be explained as follows: Structure factor, by definition, is the ratio of the total pore volume to the volume of the main pores (i.e., the pores in which the air is accelerated by the pressure gradient), which is always greater than unity. The displacement of air through the porous medium is only possible through the main pores of the material. When the volume of the main pores decreases, structure factor increases, resulting in a reduction in "acoustic porosity" (ϕ/k_s), thereby reducing the maximum acoustic absorption.

7.3.5 Electro-Acoustic Analogy

The acoustic performance of the EPC system can be modeled using the principle of electro-acoustic analogy [Zwikker and Kosten 1949, Lu 2000]. The model is a series of resistors and inductors in parallel, as shown in Figure 7.7.

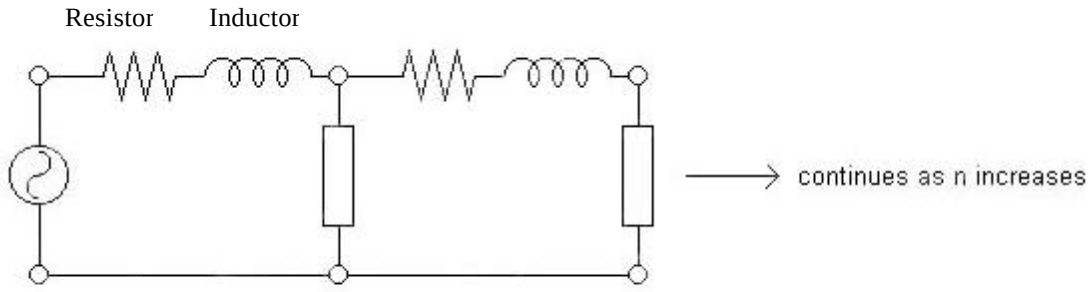

Figure 7.7 Electro-acoustic analogy for EPC – series of resistors and inductors in parallel

In this diagram, the resistors represent the real component and the inductors represent the imaginary component of the impedance of the apertures. The impedance of the air inside the pores are also modeled as resistors. The thermal effects are neglected in this study since it has been shown that the thermal effects do not have a large effect on the acoustic wave number of rigid framed porous materials [Brennan and To 2001]. The impedance of the air inside the pores (Z_D) is only a function of the pore diameter, and also varies with frequency. This can be calculated as follows:

$$Z_D = -ir_0 c_0 \cot\left(\frac{wD_p}{c_0}\right) \qquad 7.3$$

which can be simplified as:

$$Z_D = -ir_0 c_0^2 / wD_p \qquad 7.4$$

where ρ_0 is the density of air, c_0 is the speed of sound in air, ω is the angular frequency, and D_p is the diameter of the pore.

The impedance of the apertures, Z_o, is a sum of the real and imaginary components. Therefore, $Z_o = R_o + i M_o$, where R_o is the real component of impedance in the apertures and M_o is the imaginary component of impedance in the apertures. Due to a change in cross-section near the end of the aperture, there are also end effects that must be taken into consideration when calculating the impedance due to the apertures. This change in cross-section effectively lengthens the aperture, changing the value of impedance. These values are taken into consideration in the calculation of R_o and M_o.

Another term that has to be considered in the calculation of impedance is the acoustic Reynolds number (β) which is a dimensionless parameter related to the quotient of the stresses caused separately by sound pressure and viscosity [Wang and Lu 1999].

$$b = \frac{D_a}{2}\sqrt{\frac{w r_0}{h}} \qquad 7.5$$

ρ_0 is the density of air, ω is the angular frequency, and D_a is the diameter of the aperture, and η is the dynamic viscosity of air. $\beta<1$ implies the low frequency or very low aperture radius limit whereas $\beta>10$ is the high frequency or large aperture radius limit. An intermediate situation ($1<\beta<10$) is required for the case of EPC for the frequency range employed.

For $1<\beta<10$,

$$Z_o = \frac{32 h L_a}{D_a^{\,2}}\sqrt{(1+\frac{b^2}{32})} + i w r_o L_a (1+\frac{1}{\sqrt{9+\frac{b^2}{2}}}) \qquad 7.6$$

Z_o is the impedance of aperture, η is the dynamic viscosity of air, L_a is length of aperture, D_a is the diameter of aperture, β is the acoustic Reynolds number, ω is the angular frequency, and ρ_o is the density of air.

This case does not take into account the end effects of the aperture. For the real component of impedance, an additional factor has to be added to the length of the aperture, which is $(\beta D_a/4L_a)^{1/2}$. For the imaginary component, the factor is $0.85D_a/L_a$ [Stinson and Shaw 1985]. With end effects considered, for the case where β is between 1 and 10, the real and imaginary components are (using previously defined variables) [Lu et al. 2001]:

$$R_o = \frac{32hL_a}{D_a^{\,2}}\left(\sqrt{\left(1+\frac{b^{\,2}}{32}\right)}+\sqrt{\frac{bD_a}{4L_a}}\right) \qquad 7.7$$

$$M_o = wr_oL_a\left(1+\frac{1}{\sqrt{9+\frac{b^{\,2}}{2}}}+\frac{8D_a}{3pL_a}\right) \qquad 7.8$$

$$Z_o = \frac{32hL_a}{D_a^{\,2}}\left(\sqrt{\left(1+\frac{b^{\,2}}{32}\right)}+\sqrt{\frac{bD_a}{4L_a}}\right)+iwr_oL_a\left(1+\frac{1}{\sqrt{9+\frac{b^{\,2}}{2}}}+\frac{8D_a}{3pL_a}\right) \qquad 7.9$$

The theory so far has assumed a thickness of one cell (a pore and aperture combination). For the one-cell case, acoustic impedance of the system Z is given by:

$$Z = z_o + Z_D = R + iM \qquad 7.10$$

where Z_D is the impedance of air inside the pores, as given by Equations 7.3 and 7.4, R and M are the real and imaginary components of the impedance respectively, and z_0 is the relative specific impedance of apertures, given by

$$z_o = Z_o(D_f^{\,2}/D_a^{\,2}) \qquad 7.11$$

For the case where there is more that one cell along the length of the sample, the electro acoustic analogy must be applied to find the total impedance of the sample. For a series of n cells along the length of the sample, the impedance at each cell depth is given by the relationship:

$$Z_1 = z_0 + Z_D \qquad 7.12$$

$$Z_n = z_0 + \frac{1}{\frac{1}{Z_D} + \frac{1}{Z_{n-1}}} \qquad 7.13$$

where Z_n is the impedance of the system with n cells along the length of the sample, z_o is the relative impedance of apertures, Z_D is the impedance of air inside pores, and Z_{n-1} is the impedance with depth of (n-1) units. Using this value of impedance Z_n, the real and imaginary components can be used to calculate the absorption coefficient at each frequency (α) as:

$$a = \frac{\frac{4R}{r_o c_o}}{(1+\frac{R}{r_o c_o})^2 + (\frac{M}{r_o c_o})^2} \qquad 7.14$$

where R is the real component of Z_n, M is the imaginary coefficient of Z_n, ρ_o is the density of air, and c_o is the speed of sound in air.

It has been described earlier that the apparent air density is higher by a factor k_s since air displacement is possible only though a fraction ϕ/k_s of the pore space. To account for this effect, the air density ρ_o in the model has been modified by the multiplicative factor k_s.

7.3.6 Comparison with Experimental Measurements

The acoustic absorption spectra generated by the model described in the previous section are compared with the spectra obtained from impedance tube for selected mixtures, as shown in Figures 7.8, 7.9, and 7.10. The input parameters for the model are pore diameter (D_p), pore length (L_p), aperture diameter (D_a), aperture length (L_a), dynamic viscosity of air (η), density of air (ρ_o), and speed of sound in air (c_0). The pore feature characteristics (D_a, D_p, L_a, and L_p) are extracted as explained in Section 7.3.3. The dynamic viscosity of air is 1.82×10^{-5} kg/s-m, and the speed of sound in air is 344.2 m/s. The density of air is 1.2 kg/m^3, which is modified by multiplying with structure factor (k_s) so as to account for the air which is not effectively displaced in the lateral pores. Based on the pore and aperture lengths, and the length of the specimen, the number of cells (combination of pore and aperture) along the length of the sample is determined.

Figure 7.8 shows the experimentally determined as well as predicted acoustic absorption spectra for EPC mixture made with 100% # 4 aggregate, for specimen lengths of 150 mm and 75 mm. It can be seen that there is a good correlation between the measured and predicted values, and the absorption peaks match well. The frequencies of only up to 1000 Hz are shown in the figure (though measurements are made up to1600 Hz) since the first peaks of both the thickness considered appears with in that frequency range, and also the frequency of interest for tire-pavement interaction noise falls in that range. Also, this makes the comparison easier.

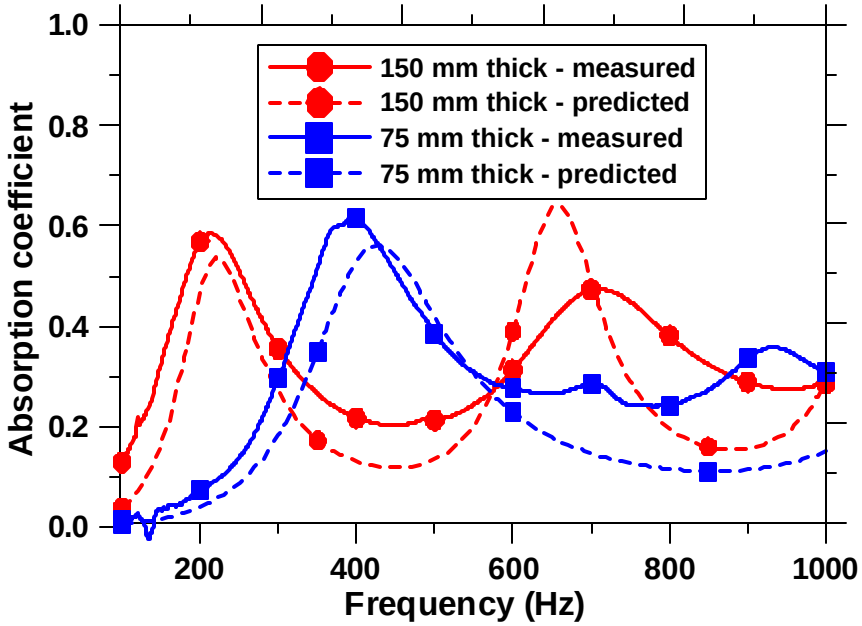

Figure 7.8 Measured and predicted acoustic absorption spectra for EPC with 100% # 4 aggregates

Similarly, the absorption spectra for EPC mixture with 100% 3/8" aggregate, for specimen lengths of 150 mm and 75 mm are shown in Figure 7.9, where as Figure 7.10 shows the spectra for EPC with a blend of 75% # 4 and 25% #8 aggregates. The predicted response matches the experimental observations closely. Considering the fact that the model largely idealizes the pore structure of EPC, the agreement between the model and experiment is quite remarkable.

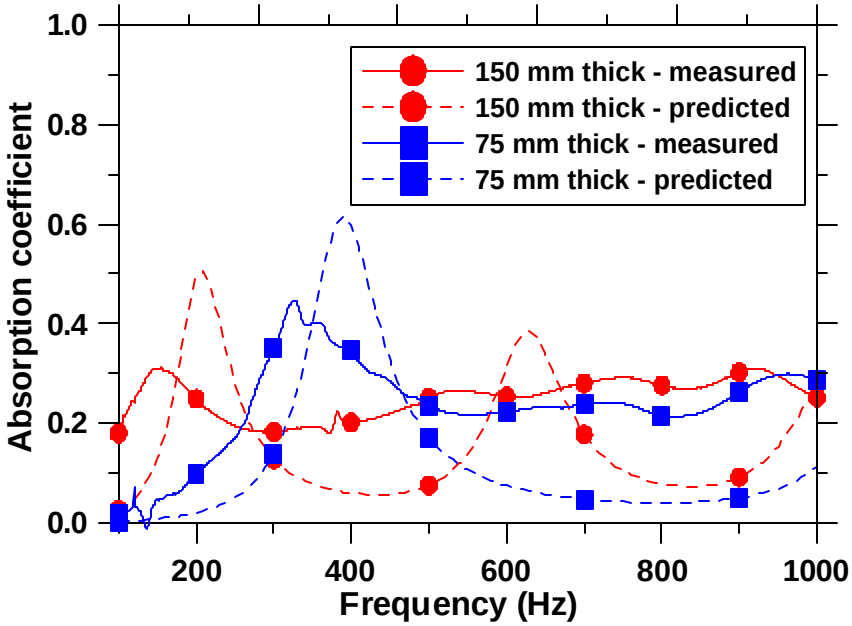

Figure 7.9 Measured and predicted acoustic absorption spectra for EPC with 100% 3/8" aggregates

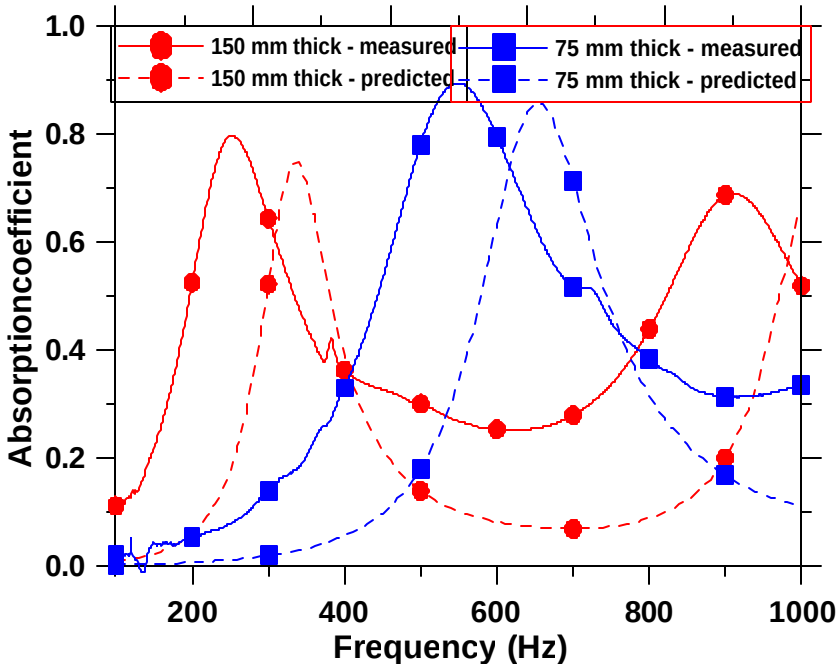

Figure 7.10 Measured and predicted acoustic absorption spectra for EPC with 75% # 4 and 25% # 8 aggregates

7.4 Parametric Study and Optimization of Pore Structure Features

To ascertain the applicability of the pore-aperture model in the acoustic absorption of EPC, and to separate the effects of various microstructural features on acoustic absorption, a parametric study was conducted. The reasonable agreement between the model predictions and the experimental measurements as shown in Figures 7.8, 7.9, and 7.10 indicates that a detailed parametric study could help in the design of EPC for acoustic absorption. The effect of pore size, pore aperture size, porosity, and specimen length (thickness) on the acoustic absorption behavior of EPC is elucidated in the following sections.

7.4.1 Effect of Varying Pore Sizes

To model the influence of varying pore sizes on acoustic absorption of EPC, a thickness of 100 mm, and a porosity of 0.25 is assumed. Pore sizes (D_p) of 2,3,4,5, and 10 mm were considered, maintaining the pore to aperture ratio (D_p/D_a) constant at 4. The pore length is fixed once the pore diameter is decided ($L_p \sim 0.9D_p$, from the model). The aperture length (L_a) can then be calculated from Equation 7.1. The structure factor (k_s) could then be determined from Equation 7.2. Based on the aperture length, pore length, and the thickness of EPC, the number of cells, n (pore and aperture combination) could be determined. The values of all these parameters are given in Table 7.2.

Table 7.2 Pore structure features – Effect of varying pore sizes

Pore Diameter (Dp) , mm	Pore length (Lp) = 0.9Dp, mm	Dp/Da	Aperture diameter (Da),mm	Aperture length (La), mm	No. of cells (n)
2.0	1.8	4	0.50	1.58	20
3.0	2.7	4	0.75	2.36	13
4.0	3.6	4	1.00	3.15	10
5.0	4.5	4	1.25	3.94	8
10.0	9.0	4	2.50	7.88	4

Figure 7.11 shows the plot of normal incidence absorption coefficient as a function of frequency for the pore sizes selected for this study.

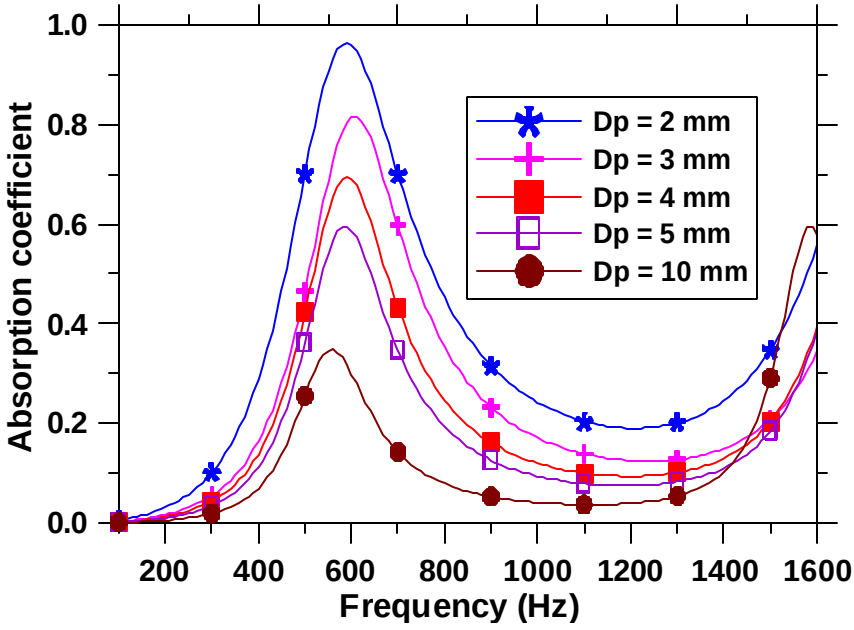

Figure 7.11 Variation of acoustic absorption with change in pore size

It can be noticed that an increase in pore size results in a reduction in the maximum absorption coefficient, though it does not change the frequency at which the maximum absorption occurs. It has been shown in Chapter 6 that an increase in pore size reduces the maximum absorption coefficient. This is because, for a system with large

sized pores, the frictional losses are low and a considerable portion of the acoustic waves that enter the pore system gets reflected back. It has also been shown that the pore sizes for the EPC systems could be related back to the aggregate sizes, and the proportion of each sizes in the mixture, in Chapter 5. This is a useful design tool since the aggregate sizes and their proportions could be selected based on the pore sizes that would maximize acoustic absorption.

7.4.2 Effect of Varying Aperture Sizes

In this case also, the porosity is maintained at 0.25, and a thickness of 100 mm is assumed. The pore size (D_p) is kept constant at 3 mm. Varying D_p/D_a values of 2,3,4, and 10 are chosen so that aperture sizes (D_a) are varied. The aperture length (L_a), number of cells (n), and the structure factor (k_s) are determined as explained in the previous section. Table 7.3 lists the values of the selected pore structure parameters.

Table 7.3 Pore structure features – Effect of varying aperture sizes

Pore Diameter (Dp) , mm	Pore length (Lp), mm	Dp/Da	Aperture diameter (D_a), mm	Aperture length (La), mm	No. of cells (n)
3.0	2.7	2	1.50	3.78	10
3.0	2.7	3	1.00	2.62	12
3.0	2.7	4	0.75	2.36	13
3.0	2.7	5	0.60	2.26	15
3.0	2.7	10	0.30	2.14	17

Figure 7.12 shows a plot of acoustic absorption as a function of frequency for varying pore to aperture size ratios chosen. For ease of interpretation, only the first peaks are plotted in this figure.

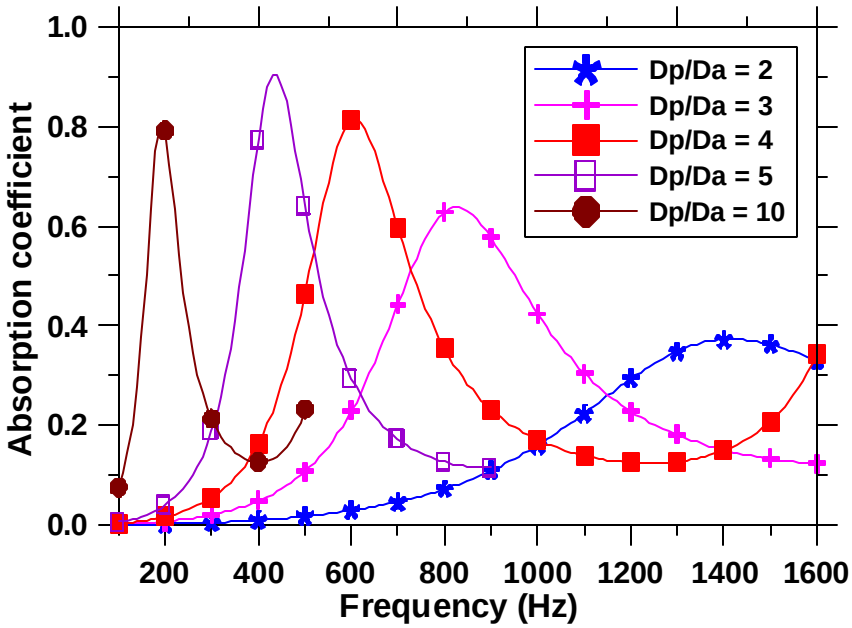

Figure 7.12 Variation of acoustic absorption with change in pore to aperture size ratios

It can be noticed that the maximum absorption coefficient increases with an increase in D_p/D_a values, until a D_p/D_a value of 5.0. For a D_p/D_a value of 10, the maximum absorption coefficient was found to decrease. The explanation for this observation is as follows: At very high values of D_p/D_a (smaller aperture sizes), the amount of air that can get into the pores is reduced, resulting in energy reflection at the surface, and consequently lower acoustic absorption. As D_p/D_a gets smaller (aperture sizes tend towards the pore sizes), there is less of a change in cross section that can lead to alternate compression and expansion of acoustic waves, resulting in a lower acoustic absorption. It can also be seen that the frequencies at peak absorption decrease with an increase in D_p/D_a, i.e., the absorption is enhanced in the low-frequency range.

Another representation of this effect is shown in Figure 7.13, where it can clearly be found that there is an optimal pore to aperture size ratio that maximizes acoustic absorption. For this model, to further simplify, the aperture length is kept constant at 5

mm, and D_p/D_a values of 3, 4, 5, 6, 9, 12, and 15 are chosen. Three pore sizes (D_p) of 2, 3, and 5 mm are also selected. The maximum absorption coefficient (α) predicted by the model is plotted against the pore to aperture size ratios. In this parametric study, the pore sizes chosen are close to those obtained for EPC mixtures investigated (2 to 5 mm), and the optimal pore to aperture size ratios vary from 4 to 7, which was also found true.

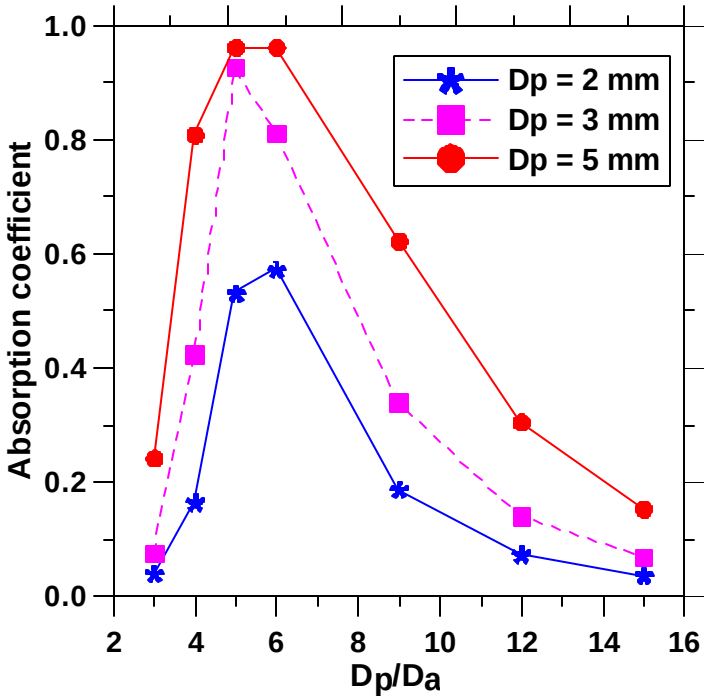

Figure 7.13 Variation of absorption coefficient with ratio of pore to aperture sizes for different pore sizes

7.4.3 Effect of Varying Porosities

The influence of porosity on acoustic absorption coefficient has been studied using a constant pore size (D_p) of 3 mm, and pore to aperture size ratio (D_p/D_a) of 4, with aperture length (L_a) and number of cells (n) calculated as described in previous sections. Five different porosities ranging from 0.15 to 0.35, at an interval of 0.05 are considered.

Table 7.4 gives the values of these parameters. Figure 7.14 shows the variation in absorption coefficient with frequency for different porosities.

Table 7.4 Pore structure features – Effect of varying aperture sizes

Porosity	Pore Diameter (Dp) , mm	Pore length (Lp), mm	Dp/Da	Aperture diameter (Da), mm	Aperture length (La), mm	No. of cells (n)
0.15	3.0	2.7	4	0.75	6.50	9
0.20	3.0	2.7	4	0.75	3.83	11
0.25	3.0	2.7	4	0.75	2.36	13
0.30	3.0	2.7	4	0.75	1.43	15
0.35	3.0	2.7	4	0.75	0.79	17

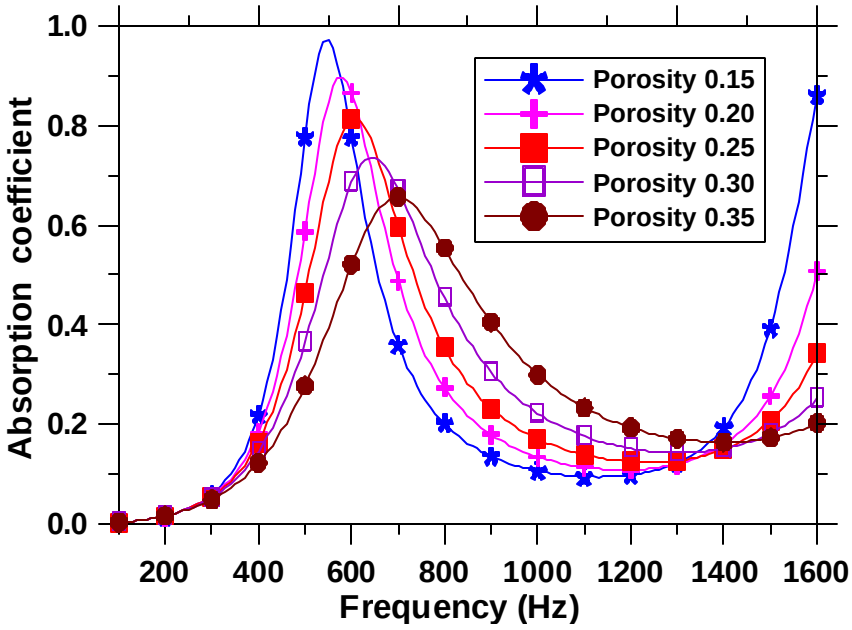

Figure 7.14 Variation of absorption coefficient with change in porosity

Increasing porosities slightly increases the frequencies at maximum absorption. It can also be observed that the maximum absorption coefficient decreases with increase in porosity, which may seem counter-intuitive. But, Table 7.4 shows that with increase in

porosity, for a constant pore diameter, the aperture length (L_a) decreases, and this is illustrated in Figure 7.15.

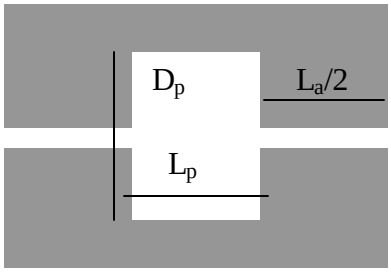

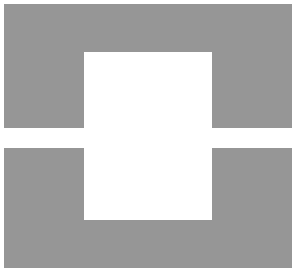

D_p = 3 mm, L_p = 2.7 mm, D_a = 0.75 mm
L_a = 5 mm, Porosity = **0.174**

D_p = 3 mm, L_p = 2.7 mm, D_a = 0.75 mm
L_a = 2.5 mm, Porosity = **0.244**

Figure 7.15 Illustration of variation in porosity with change in aperture length (L_a) for a single cell

It is in the apertures that the frictional losses occur, and hence reduced aperture length implies reduced absorption. If it is assumed that the aperture length remains constant, and the increase in porosity is achieved through increase in pore size, the same explanation as in Section 7.4.1 holds good. However, it should be noted that the porosity is influenced by the pore size, pore to aperture size ratio, and pore length, in addition to aperture length, and it is the synergetic effect of all these factors that dictate the effect of porosity in acoustic absorption.

7.4.4 Effect of Varying Specimen Thickness

The influence of varying specimen thickness on acoustic absorption is studied by using a pore size (D_p) of 3 mm, pore to aperture size ratio (D_p/D_a) of 4, porosity of 0.25, and an aperture length L_a determined as 2.36 mm. The number of cells required for a specimen thickness of 150 mm is 20, for a thickness of 75 mm, it is 10, and for a

thickness of 37.5 mm, 5. Figure 7.16 shows the variation in acoustic absorption with frequency for three different lengths as mentioned above, obtained from the model. Increasing the specimen thickness reduces the frequencies at the maximum absorption, as well as the spacing between the peaks. The same effect is observed in Figures 7.8 to 7.10 where the measured and predicted absorption coefficients are plotted for three different EPC mixtures.

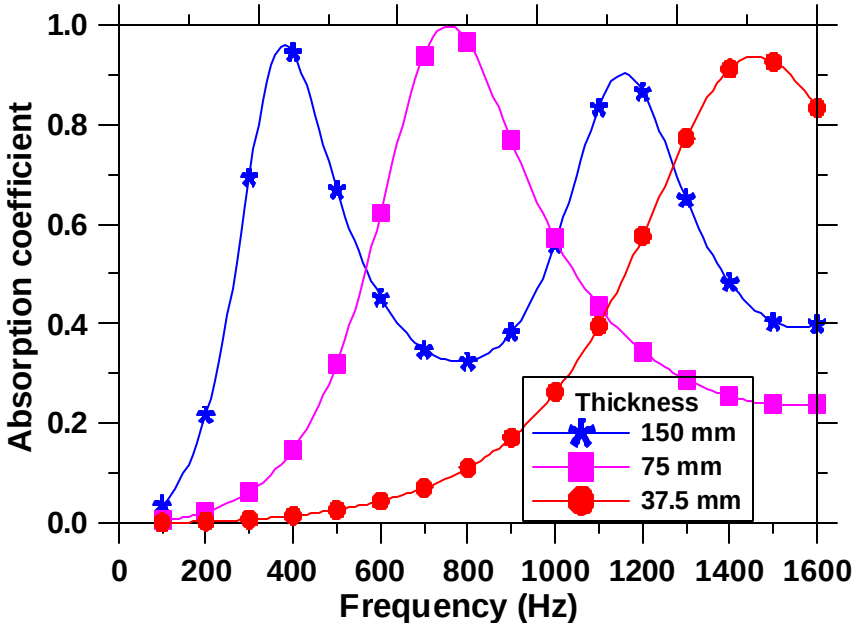

Figure 7.16 Variation of acoustic absorption coefficient with change in specimen thickness

7.5 Summary

This chapter has explained in detail the efforts undertaken to model the acoustic absorption behavior of EPC as a function of its pore structure characteristics. EPC has been modeled as a system consisting of alternate cylindrical pores and apertures. An electro-acoustic analogy, considering a series of resistors and inductors in parallel, which

is used to model the absorption behavior of semi-open metallic foams, has been employed to model the acoustic absorption of EPC. The concept of structure factor has been used to correct for the density of air in the pores. The maximum absorption coefficient was found to decrease with an increase in structure factor, and the relationship is linear. The model and the experiment match quite well, not withstanding the idealized nature of the pore system in the model. A detailed parametric study has been conducted to isolate the effects of pore size, aperture size, porosity and the specimen thickness on acoustic absorption.

CHAPTER 8: CHARACTERIZING EPC USING ELECTRICAL IMPEDANCE TO PREDICT ACOUSTIC AND HYDRAULIC PERFORMANCE

8.1 General

Characterization of the pore structure of EPC is significant in understanding the behavior of the material and to help design the material better for specific purposes. The most important feature that makes EPC acoustically absorbing is the amount and distribution of interconnected pores in the system, through which sound waves can pass and attenuate. The objective of this chapter is to develop test methods and assess the physical features of the pore system of EPC. Electrical property measurements (resistivity or conductivity) are being used increasingly to assess the physical properties of porous materials including the porosity and connectivity of the pore structure. Hydraulic conductivity also gives a detailed account of the distribution of pore connectivity. From these two parameters, it is expected that pertinent transport properties can be arrived at, that can give considerable information about the microstructure of the material. This feature can be used to design the material structure for acoustic absorption or water drainage.

8.2 Electrical Impedance Spectroscopy (EIS)

The use of Electrical Impedance Spectroscopy (EIS) to monitor and characterize cement-based systems has been in practice for some time now. This technique consists of applying an alternate voltage to a sample over a broad range of frequencies (μHz to MHz), in relatively quick time to collect electrical information. The resultant current and phase lag are then measured and used to compute the real and imaginary components of the impedance. A Nyquist plot represents the values, with the real component of the impedance (Z') plotted along the X-axis and imaginary component (Z") plotted along the Y-axis for each frequency investigated. A typical Nyquist plot consists of two arcs, as shown in Figure 8.1 – the bulk arc and the electrode arc. The two arcs meet at a point, where the imaginary component of the impedance is minimum, referred to as the bulk resistance (R_b) of the sample. The frequency corresponding to the bulk resistance is the cut-off frequency.

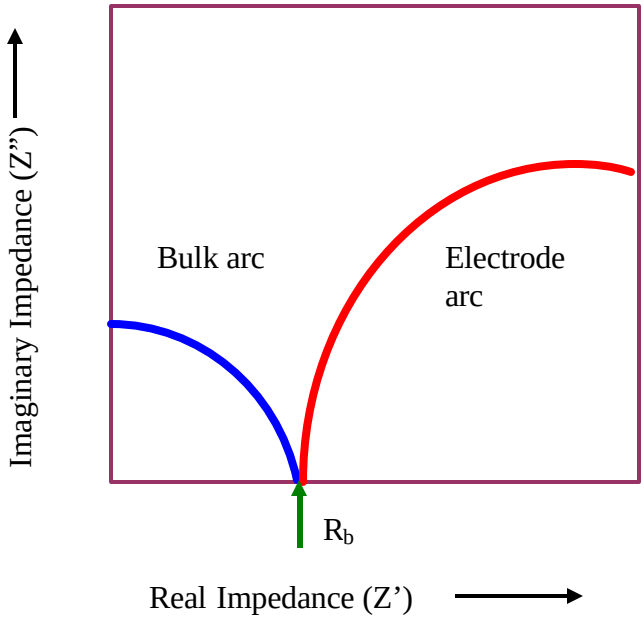

Figure 8.1 Typical Nyquist plot for EIS study

Several researchers have reported on the use of Electrical Impedance Spectroscopy (EIS) measurements in the study of cementitious materials [Christensen et al. 1994, Ford et al. 1995, Coverdale et al. 1995, Gu et al. 1993, Moss et al. 1996, Synder et al. 2000]. EIS has been used extensively to monitor hydration processes in cement-based materials [Christensen et al. 1994, Ford et al. 1995, Coverdale et al. 1995]. The principle behind this approach is that cement paste is electrically conductive by virtue of its interconnected pore network filled with pore solution, containing mobile ions. The changes in the pore structure as hydration proceeds are picked up by the changes in electrical resistance of the system, which in turn helps in microstructural characterization. In addition, normalized conductivity (ratio of the effective conductivity of the specimen to the pore solution conductivity) gives an indication of the connectedness and tortuosity of the pore space in the system, and is intimately related to the transport properties [Christensen 1993, Synder et al. 2000]. EIS has also been used in the determination of chloride diffusivity in concrete [Shi et al. 1999, Synder et al, 2000], characterization of conductive fiber reinforced composites [Garboczi et al. 2000, Torrents et al. 2001], and monitoring damage in cement composites during loading [Gu et al. 1993, Peled et al. 2001].

8.2.1 Electrical Conductivity Measurements using EIS

The electrical conductivity of EPC specimens were measured using the setup described in Section 4.5.7. Using the bulk resistance (R_b) obtained from the Nyquist plots, the effective electrical conductivity (σ_{eff}) of the sample is calculated as:

$$s_{eff} = \frac{l}{R_b A} \qquad 8.1$$

where l is the specimen length and A is the cross sectional area of the specimen.

8.3 Nyquist Plots of EPC

The Nyquist plots of EPC specimens made using single sized aggregates are given in Figure 8.2. NaCl solution of 3% concentration is used as the electrolyte.

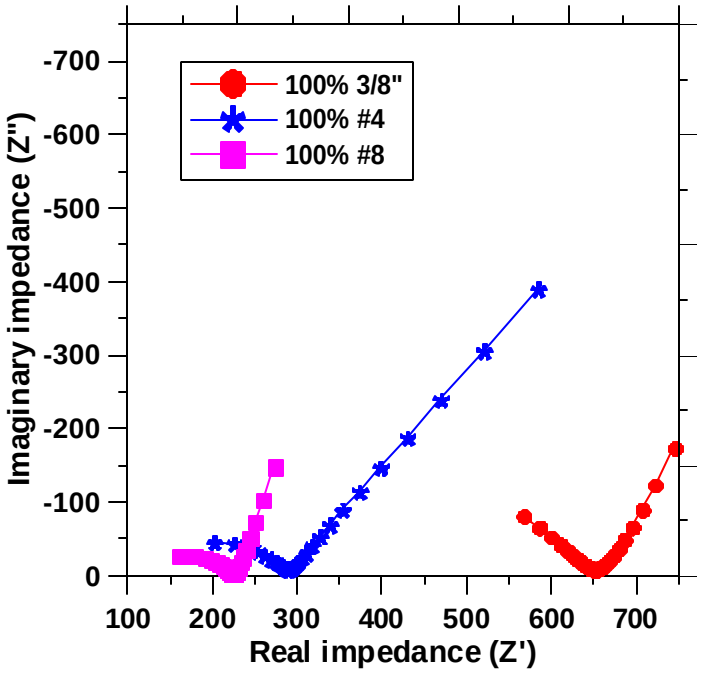

Figure 8.2 Nyquist plots of EPC made using single sized aggregates

This figure shows that the bulk resistance of mixtures made up of only # 4 or # 8 aggregates is relatively close to each other, whereas the one for EPC made with only 3/8" aggregates is much higher than the other two. It can therefore be inferred from these plots that the mixtures with # 4 and # 8 aggregates have a higher conductivity than the mixture with 3/8" aggregates. These observations agree well with Figure 6.1, which

shows that the acoustic absorption of EPC with # 4 and # 8 aggregates alone are similar, and much higher than the one with 3/8" aggregates alone.

Figure 8.3 shows the Nyquist plots of EPC mixtures made using a blend of # 4 and #8 aggregates.

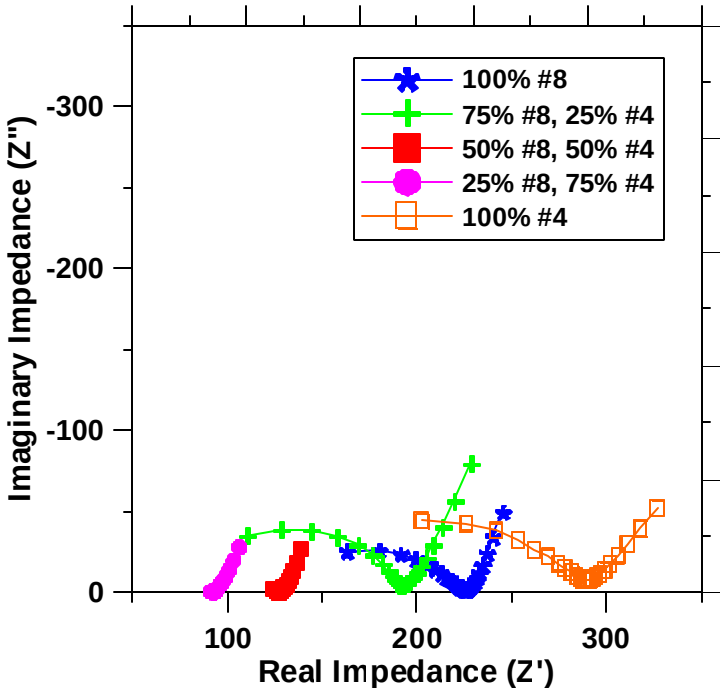

Figure 8.3 Nyquist plots of EPC made using blends of # 4 and # 8 aggregates

It can readily be noticed from this figure that the mixtures made using blends have a lower bulk resistance, and consequently higher conductivity than mixtures with single sized aggregates. This relates well to Figure 6.2, which shows that the mixtures with a proper blend of # 4 and # 8 aggregates perform better in acoustic absorption than one with single sized aggregates. This observation goes on to suggest that blending of aggregates creates a conducive pore structure for more efficient acoustic properties. This aspect is investigated further using EIS studies in the following sections.

8.4 Modeling the Electrical Conductivity of EPC

The effective electrical conductivity of a porous medium (σ_{eff}) with a conducting fluid phase depends on the electrical conductivities (σ_i), relative volumes (ϕ_i), and geometric distributions of each of the constituent phases. For a porous medium with a single conducting phase, Archie's law relates the overall conductivity of the material to that of a conducting medium present in the pores using Equation 8.2 [Wong et al. 1984, Glover et al. 2000, Chinh 2000, Bussian 1983, Roberts and Schwartz 1985, Christensen 1993, de Lima and Sri Niwas 2000]:

$$s_{eff} = Cs_0 f_0^m \qquad 8.2$$

where C is a constant (typically assumed to be 1.0), σ_0 is the conductivity of the conducting medium, ϕ_0 is the pore volume fraction, and *m* is the Archie's exponent.

The exponent m depends on the geometry of constituent particles and their arrangement [Jackson et al. 1978, Chinh 2000]. The values of m typically range from 1.5 to 4.0, with higher values indicating lower electrical connectivities of the phase [de Lima and Sharma 1990, Chinh 2000].

8.4.1 Conductivity – Porosity Relations: Single Phase Archie's Law

A plot of measured effective conductivities (σ_{eff}) and those predicted from Archie's law using Equation 8.2 for the EPC mixtures is provided in Figure 8.4. The three different symbols correspond to the three concentrations of the electrolyte used. As expected, the effective conductivity increases with the electrolyte conductivity. It can be

observed that the agreement between the measured and predicted conductivities is rather poor, indicating that the conventional form of Archie's law may not be the best representation of the electrical behavior of EPC system.

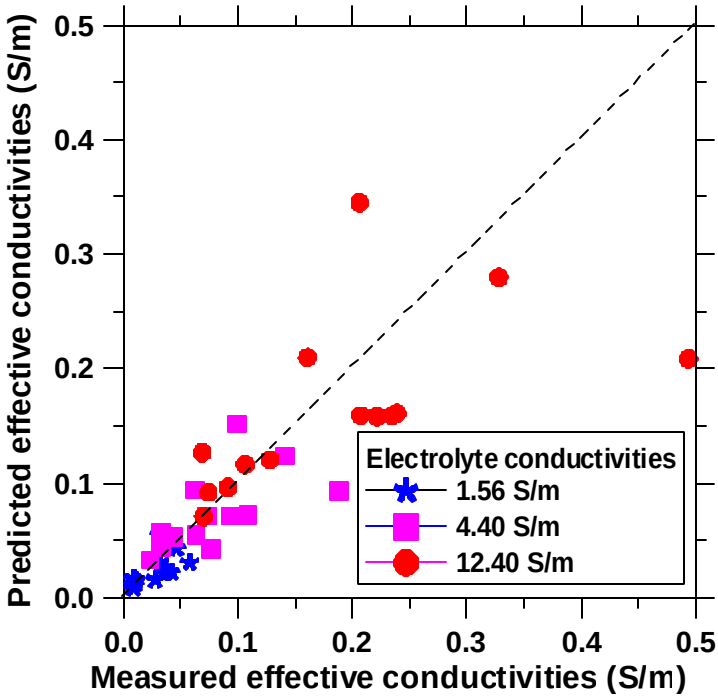

Figure 8.4 Predicted effective conductivities from conventional Archie's law plotted against measured effective conductivities

To prove this point further, Nyquist plots of EPC specimens proportioned using single sized aggregates (# 8, # 4, and 3/8") saturated with 3% NaCl electrolyte (conductivity 4.40 S/m) shown in Figure 8.2 are used. Though the pore volumes of these mixtures fall in a very narrow range (0.19-0.21), a significant variation in the bulk resistances (or conductivities) exists. If the Archie's law were to hold true, one would expect similar effective conductivities for these mixtures. The fair assumption in this case would be that the effective conductivity of the system is not only a function of the conductivity of the electrolyte in the pores and the porosity, but also on some other

component in the material structure of EPC. It is hypothesized that the matrix that coats the aggregates is also conductive, i.e., the assumption of a single conducting phase is no longer completely valid.

8.4.2 Multi-phase Conductivity Models for EPC

Based on the aforementioned observation, it is expected that the effective conductivity of EPC may be better predicted by considering the system to be a multi-phase medium, as illustrated in Figure 8.5.

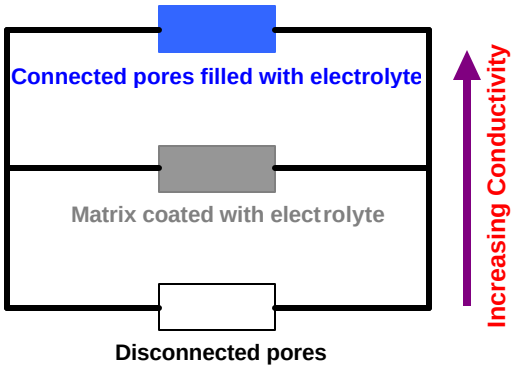

Figure 8.5 Dependence of conductivity on the different phases of EPC

The interconnected pore network filled with the electrolyte is the phase with the highest conductivity, followed by the matrix that coats the aggregates, and the disconnected pores. For the case of EPC, interconnected pore network refers to the network of large sized pores deliberately incorporated into the material for better acoustic and hydraulic performance. It is assumed that the matrix that coats the aggregates is homogeneous and continuous.

Three alternative versions of multi-phase models are considered: (i) a modified version of Archie's law, (ii) an equation of the Bruggeman-Hanay type, and (iii) a modified parallel model.

8.4.3 Modified Archie's Law

The conventional form of Archie's law does not account for a second conducting phase; therefore a modified version of Archie's law [Glover et al. 2000] is adopted to represent the conductivity of EPC.

The EPC system is considered as consisting of two-phases – the first phase being the large open porosity filled with an electrolyte – called pore phase (volume fraction ϕ_p and conductivity σ_p), and the second, the solid phase (volume fraction ϕ_s and conductivity σ_s). The total volume of the material is equivalent to the sum of the pore and solid fractions:

$$f_p + f_s = 1 \qquad 8.3$$

Using this approach, the modified Archie's law for a two-phase system takes the form: [Glover et al. 2000]

$$s_{eff} = s_p f_p^m + s_s f_s^{m'} \qquad 8.4$$

σ_p is the conductivity of the electrolyte in the pores, and σ_s is the conductivity of solid phase (in a water saturated condition). The exponents m and m' represents the degree of connectivity of the pore and solid phases respectively; a lower value indicating

better connectivity. The conductivity of the solid phase is derived from the fact that the matrix that coats the aggregates is continuous.

The effective conductivity of the composite, and the volume fraction of the pores (and hence the volume fraction of solids) can be directly measured. The conductivity of the electrolyte can be easily controlled. Therefore, the conductivity of the solid phase (σ_s), and the exponents *m* and *m'* are the only unknowns. Assuming that the conductivity of the solid phase and the exponents representing the degree of connectivity will remain constant for a particular mixture, three different electrolyte conductivities (σ_p) were used and the corresponding effective conductivities (σ_{eff}) were measured. This results in three variants of Equation 8.4, which can be solved simultaneously to give the values of σ_s, *m* and *m'*. σ_s remains almost the same (0.01-0.02 S/m) with varying electrolyte conductivity for various mixtures investigated. This is consistent with the idea that σ_s is necessarily a property of the "solid" matrix.

The relationship between the measured electrical conductivities and those predicted by modified Archie's law for all three electrolyte conductivities is shown in Figure 8.6. On comparison with Figure 8.4, it is immediately evident that the predictive capability is vastly improved by using modified Archie's law (the average deviation between the measured conductivities and those predicted by modified Archie's law is around 7%, whereas it is around 35% for conventional Archie's law). It also validates the assumption that the conductivity of EPC is dependent on more than just the characteristics of the pore phase alone.

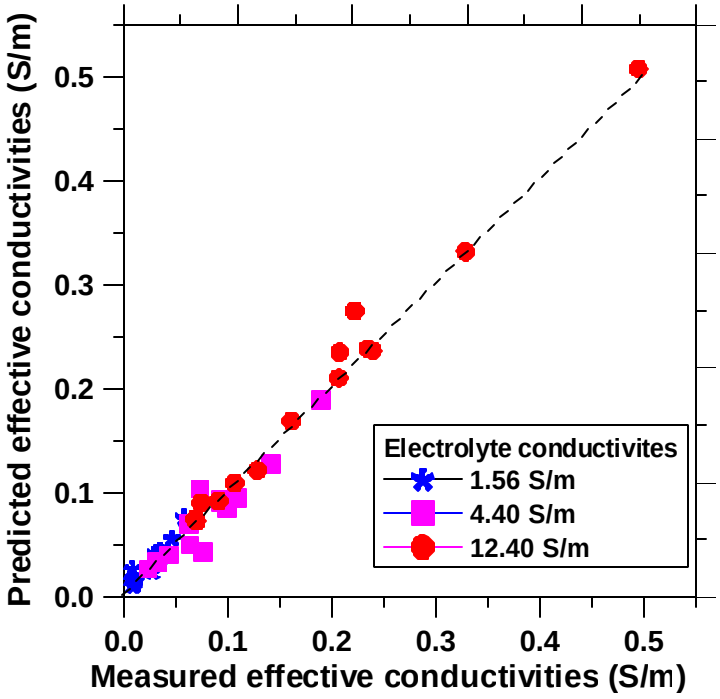

Figure 8.6 Predicted effective conductivities from modified Archie's law plotted against measured effective conductivities

It was also found from the solution of simultaneous equations to obtain σ_1, m and m', that the term m' is very small (0.03-0.10), rendering the value of $\phi_s^{m'}$ close to 1.0. Hence, the modified Archie's law can be simplified to:

$$s_{eff} = s_p f_p^m + s_s \qquad 8.5$$

Since σ_s is a constant irrespective of the conductivity of the electrolyte, the effective conductivity becomes less and less dependent on the matrix conductivity as the electrolyte conductivity is increased.

8.4.4 Bruggeman-Hanay Approach

The Bruggeman-Hanay equation has been used to relate the electrical properties of a heterogeneous mixture to the properties of individual components. For a granular material composed of conductive homogeneous particles of conductivity σ_s embedded in a medium of conductivity σ_p, the composite electrical conductivity σ_{eff} is given by [Bussian 1983] as:

$$s_{eff} = s_p f_p^m \left[\frac{1 - \frac{s_s}{s_p}}{1 - \frac{s_s}{s_{eff}}} \right]^m \qquad 8.6$$

where ϕ_p is the porosity and m is originally defined as a non-dimensional parameter that depends on the aspect ratio of the grains (equivalent to the Archie's exponent m). When $s_s \to 0$, Equation 8.6 reduces to Archie's law for a single conducting medium.

Assuming that conductivity of the composite is dominated by the pore fluid ($\sigma_p >> \sigma_s$), the equation can be simplified by a binomial expansion and retaining the first-order terms [Bussian 1983, de Lima and Sharma 1990] provides Equation 8.7:

$$s_{eff} \approx f_p^m \left[s_p + m\left(f_p^{-m} - 1 \right) s_s \right] \qquad 8.7$$

The advantage of such a relation as compared to the modified Archie's relation discussed in the previous section is that this equation contains only two unknowns (σ_s and m) as compared to three (σ_s, m and m') of modified Archie's equation.

The effective conductivities predicted from Equation 8.7 are plotted against the measured values in Figure 8.7 for all three electrolyte conductivities chosen for the study.

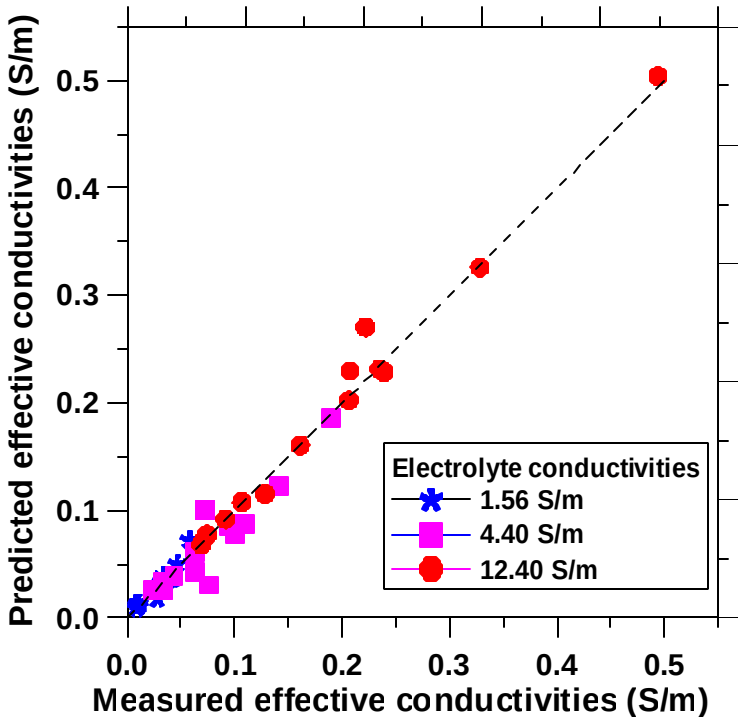

Figure 8.7 Predicted effective conductivities from Bruggeman-Hanay equation plotted against measured effective conductivities

The measured conductivities and those predicted using Bruggeman-Hanay equation are in good agreement (differing by about 9%), reiterating the significance of incorporating the matrix conductivity in effective conductivity predictions. Expanding the Equation 8.7 and neglecting very small magnitude terms also results in an expression that is equivalent to Equation 8.5.

8.4.5 Modified Parallel Model

The complex distributions of pore and solid phases in a porous material with different volume fractions of constituents and conductivities differing by orders of magnitude have been approximated by simpler models [Christensen et al. 1994, Glover et

al. 2000, Bussian 1983]. One such model is the parallel model where the effective conductivity is given by the arithmetic mean of the conductivities of each phase weighted by their respective volume fractions.

$$s_{eff} = s_p f_p + s_s f_s \qquad 8.8$$

where σ_{eff}, σ_p, σ_s, ϕ_p, and ϕ_s are the same as described in Section 8.4.3.

The first element represents the conductivity associated with the free electrolyte in the larger pores of EPC while the other represents the conductivity associated with the matrix coating the aggregates. The drawback of such a model is that this representation does not take into account the connectivity of the pore network. To counter this, the parallel model has been modified by including a connectivity factor (β) [Garboczi 1990]. The modified parallel model then becomes:

$$s_{eff} = s_p f_p b_p + s_s f_s b_s \qquad 8.9$$

where β_p and β_s are termed the connectivity factors, representing the connectivities of the pore and the solid phases respectively, much like the exponents *m* and *m'* in the modified Archie's law. The only difference between the exponents and the connectivity factors is that higher exponents imply decreased connectivity whereas an increase in the β factor implies increased connectivity. The modified normalized conductivity $(\frac{s_{eff} - s_s}{s_p})$, as well as β_p are the true measures of the pore structure of the material. The numerator is taken as $(\sigma_{eff}-\sigma_s)$ since the term $\sigma_s\phi_s\beta_s$ in Equation 8.9 is approximately equal to σ_s (i.e., solid connectivity factor $\beta_s \approx$ inverse of solid volume fraction ϕ_s, which is found true).

Equation 8.9 then becomes:

$$s_{eff} = s_p f_p b_p + s_s \qquad 8.10$$

From Equation 11, the pore phase connectivity is given by:

$$b_p = \frac{(s_{eff} - s_s)}{s_p}\frac{1}{f_p} = \frac{s^*_{eff}}{s_p}\frac{1}{f_p} \qquad 8.11$$

The term $(\sigma_{eff}-\sigma_s)$ is denoted as σ_{eff}^*.

8.4.6 Relationship between β_p and m

Equating the modified form of Archie's law (Equation 8.5) and the modified parallel law (Equation 8.10), the pore connectivity factor can be expressed as:

$$b_p = f_p^{m-1} \qquad 8.12$$

This equation gives a straightforward calculation of pore connectivity factor based on the pore volume fraction and the exponent *m* from modified Archie's law. Equation 8.11 gives the measured value of β_p from conductivities whereas Equation 8.12 is a derived value. The agreement between the calculated β_p from both equations is shown in Figure 8.8, indicating the validity of the exponent *m* calculated from modified Archie's law. This relationship also shows that Archie's exponent *m* can be used as a measure of the pore connectivity.

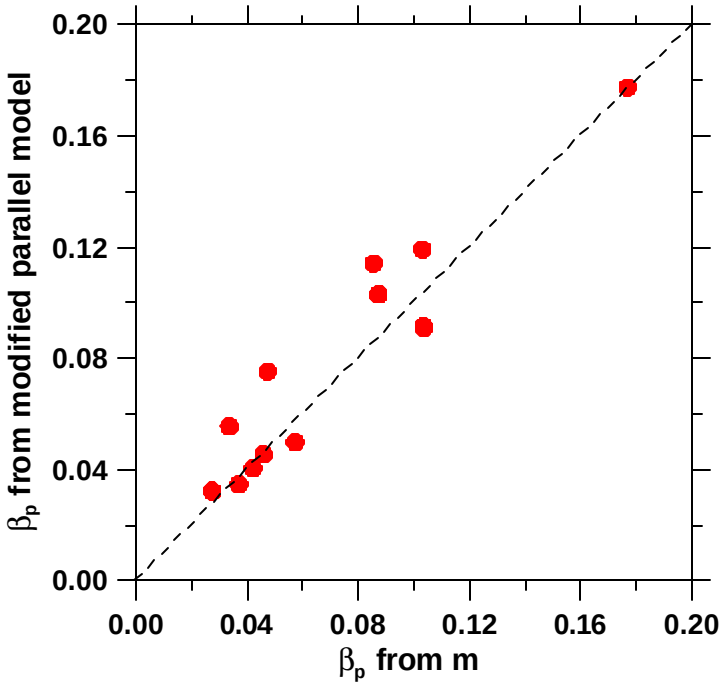

Figure 8.8 Relationship between pore connectivity factors calculated from modified Archie's exponent as well as from modified parallel model

8.4.7 Comparison between the Multi-Phase Models

The first two multi-phase models presented above are variants of the Archie's law, where the connectivity of the constituent phases are represented by the exponents. Modified Archie's law and Bruggeman-Hanay equation were found to deviate from the measured conductivities by 7 and 9% respectively, and as such there is no real reason to choose one model over the other. One advantage with using the Bruggeman-Hanay equation is that there are only two unknowns involved, therefore the use of electrolyte with two different concentrations is sufficient. The modified parallel model uses a multiplicative connectivity factor (β), an increase in which implies increased connectivity

of the corresponding phase. Due to the simplicity of the modified parallel model, it will be used further in this paper for assessing the acoustic performance, and the prediction of hydraulic conductivity of EPC mixtures.

8.4.8 Porosity and Pore Connectivity Factor

The relationship between the porosity (ϕ_p) and the pore phase connectivity factor (β_p) is shown in Figure 8.9. The plot shows that even when the pore volume fraction is similar, the pore connectivity can be quite different. It can be noticed that there exists no regular trend between these parameters though it would appear that the connectivity factor should increase with porosity. However, this behavior is not observed for all values of porosity. The data points that show a deviation from this trend are those containing 50% # 4 aggregates with either 50% 3/8" or 50% # 8 aggregates. The blends in both these cases are such that the smaller sized aggregates are not able to fill in the pore spaces between the larger sized aggregate, resulting in a higher overall porosity. However because of the arrangement of the particles, the connectivity factor of these mixtures is lower than some of the mixtures that have a lower porosity. This is further validated using acoustic absorption measurements in the following section.

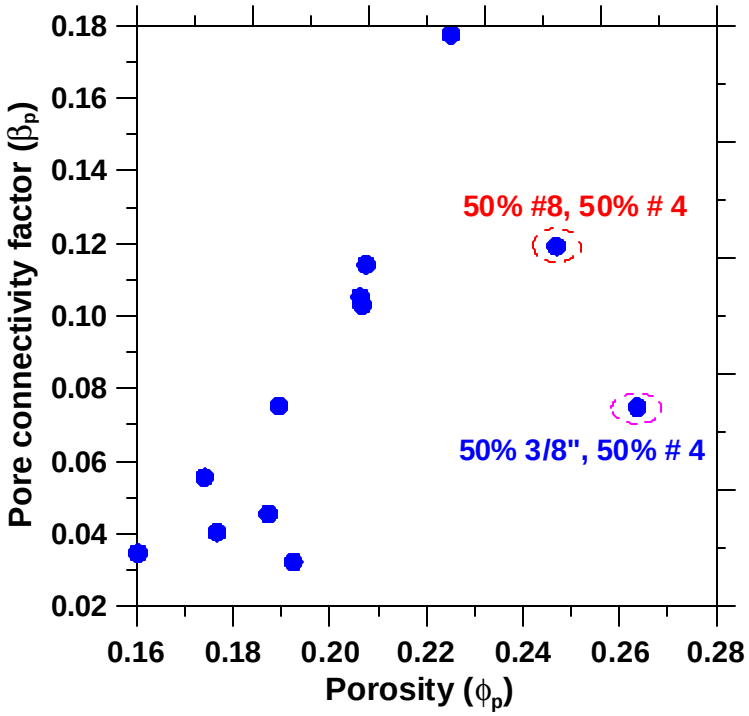

Figure 8.9 Relationship between porosity and pore connectivity factor calculated from modified parallel model

8.5 Porosity and its Relation to Acoustic Absorption

The acoustic absorption of EPC is related to the porosity, pore size, and the constrictions in the pore network through which acoustic energy can travel and attenuate inside the material. The acoustic absorption coefficient (α) is a measure of the ability of the material to absorb sound. Acoustic absorption spectra (variation of absorption coefficient with frequency) for various EPC mixtures were generated following the procedure described in Section 4.5. Typical acoustic absorption spectra for these materials can be found in Chapter 6.

It has been explained in the previous section that even when the pore volume fraction is same, its distribution can be different, and it significantly affects the conductivity, as well as the absorption coefficient. Thus, pore connectivity is an important pore feature that takes into account the constrictions in the pore space, which can be used to characterize the efficiency of EPC with respect to acoustic absorption. The relation between pore connectivity factor (β_p) and maximum acoustic absorption coefficient (α) for various EPC mixtures investigated in this study is shown in Figure 8.10. The maximum absorption coefficient increases with increasing pore connectivity and the relationship is relatively linear.

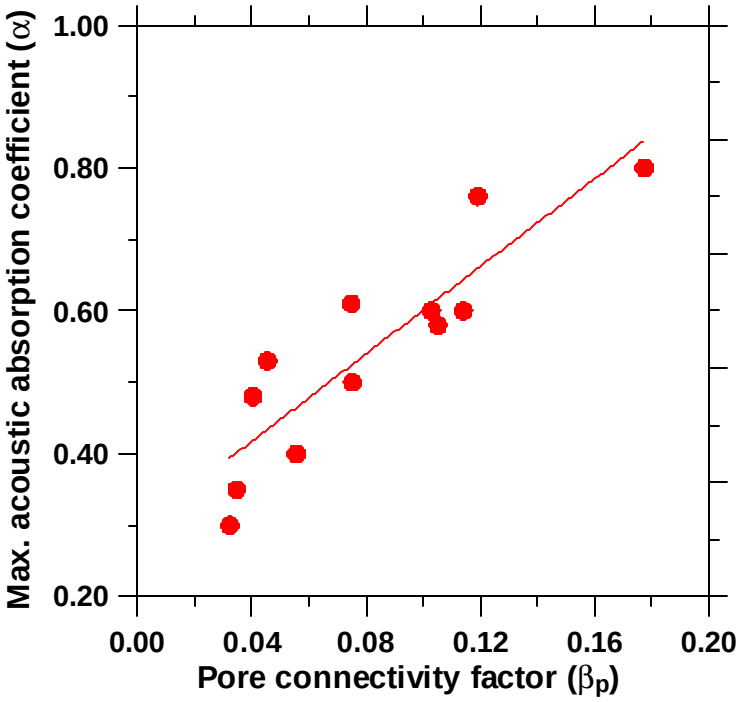

Figure 8.10 Relationship between pore connectivity factor and maximum acoustic absorption coefficient

8.6 Modeling the Hydraulic Conductivity of EPC from Electrical Measurements

This section deals with developing relations to predict the hydraulic conductivity (or permeability) of EPC from electrical conductivity measurements. It has been explained in Section 5.5 that there is no definitive relationship between porosity and permeability, though the permeability increases with increase in porosity. The reason for this is attributed to the fact that porosity is a volumetric property of the material, whereas permeability is a parameter that depends not only on the volumetric parameter but also on the distribution of the pore volume and its connectivity. The following discussion throws more light on this aspect.

8.6.1 Pore Structure Features and Permeability

The relationship between porosity and permeability was given by the Kozeny-Carman relation as shown in Equation 8.13.

$$k = \frac{f^3}{F_s t^2 S_0^2 (1-f)^2} \qquad 8.13$$

where ϕ is the porosity, F_s is the generalized factor to account for different pore shapes, τ is the tortuosity, and S_0 is the specific surface area of pores.

It can be shown that the tortuosity (τ) is equivalent to the inverse of connectivity ($\tau = 1/\beta_p$).

It can be seen from Equation 8.11 that $\beta_p\phi_p$ is equivalent to $\left[\frac{s^*_{eff}}{s_p}\right]$. Therefore, the term $\left[\frac{f_p}{t}\right]^2$ in Kozeny-Carman equation can be replaced by $\left[\frac{s^*_{eff}}{s_p}\right]^2$. Using this approach, Kozeny-Carman equation can be rewritten as:

$$k = \frac{1}{F_s S_0^2}\left[\frac{s^*_{eff}}{s_p}\right]^2\left(\frac{f_p}{(1-f_p)^2}\right) \qquad 8.14$$

Therefore, the intrinsic permeability k is equal to the product of a constant that describes the shape and specific surface area of pores, the square of modified normalized conductivity, and a function that accounts for the pore volume fraction.

The expression $\frac{1}{F_s S_0^2}\left[\frac{s^*_{eff}}{s_p}\right]^2$ is defined as hydraulic connectivity factor (β_H). As a result, the Kozeny-Carman equation is simplified as:

$$k = b_H\left(\frac{f_p}{(1-f_p)^2}\right) \qquad 8.15$$

The intrinsic permeability therefore is represented as a function of porosity (ϕ_p), and β_H. The hydraulic connectivity factor (β_H) can be thought of as a combination of parameters that describe the pore space volume and geometry in such a way that the intrinsic permeability is related to porosity and hydraulic connectivity factor. The experimentally determined relationship between k and β_H is shown in Figure 8.11.

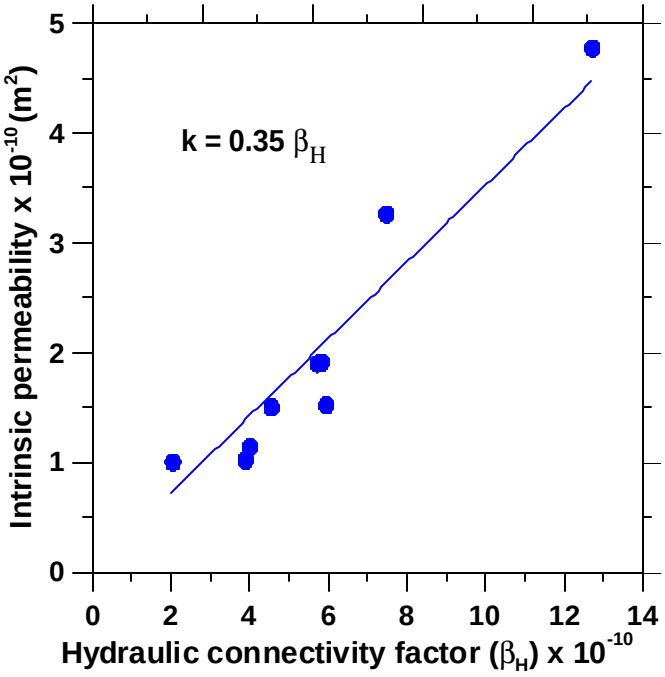

Figure 8.11 Relationship between hydraulic connectivity factor and intrinsic permeability

The hydraulic connectivity factor β_H offers a means of classifying EPC based on their hydraulic characteristics. The mixtures with similar β_H values exhibit similar permeability. The mixture with a low β_H value (i.e., 100% # 8 aggregates) has a small aggregate size. Therefore, the inter-particle pore sizes are also small and therefore its ability to sustain water flow is lower. Similarly, the mixture with 50% # 8 and 50% 3/8" aggregates also has a low β_H value since the smaller aggregates fill in between the larger particles, resulting in a reduced porosity and a reduced flow capacity. The mixtures with the highest β_H values either have a large porosity and pore size as with mixtures having 100% 3/8" aggregates or has a blend of aggregate sizes that helps to create a very continuous pore structure, as in mixtures with 75% #4 and 25% #8 aggregates.

8.6.2 Relating Electrical Conductivity and Intrinsic Permeability

Equation 8.14 shows that the intrinsic permeability is related to the square of the modified normalized conductivity. This is similar to the findings of Wong et al. [1984]. It should however be noted that some authors [Martys and Garboczi 1992] have expressed the intrinsic permeability as:

$$k = b' f_p l_c^2 \qquad 8.16$$

where β' is a factor that accounts for connectivity of the pores (similar to β_p), and l_c is a characteristic length.

Equation 8.16 can be restated in terms of normalized conductivity by substituting Equation 8.11 into it, to yield Equation 8.17.

$$k = \left[\frac{s^*_{eff}}{s_p}\right]\frac{b'}{b_p} l_c^2 \qquad 8.17$$

From this equation, it can be seen that permeability is directly proportional to the modified normalized conductivity.

As some authors relate permeability to the normalized conductivity [Martys and Garboczi 1992, Katz and Thompson 1986] while others relate permeability to the square of the normalized conductivity (Equation 8.14, Wong et al. 1984), the modified normalized electrical conductivity as well as its square are plotted against the intrinsic permeability in Figures 8.12 and 8.13 respectively. The plots show that there is no significant statistical difference between the two, but as Equation 8.14 can be easily derived from the Kozeny-Carman equation, it is suggested that the permeability of EPC should be taken as being related to the square of the electrical conductivity.

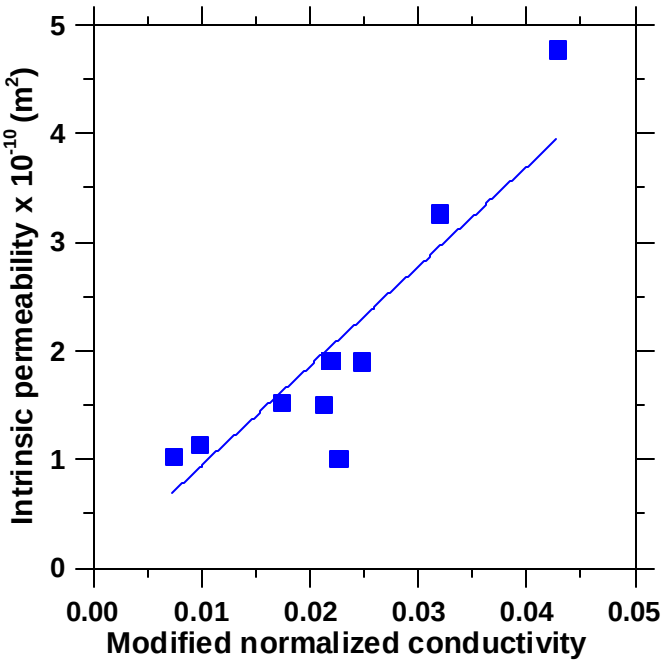

Figure 8.12 Relationship between intrinsic permeability and modified normalized conductivity

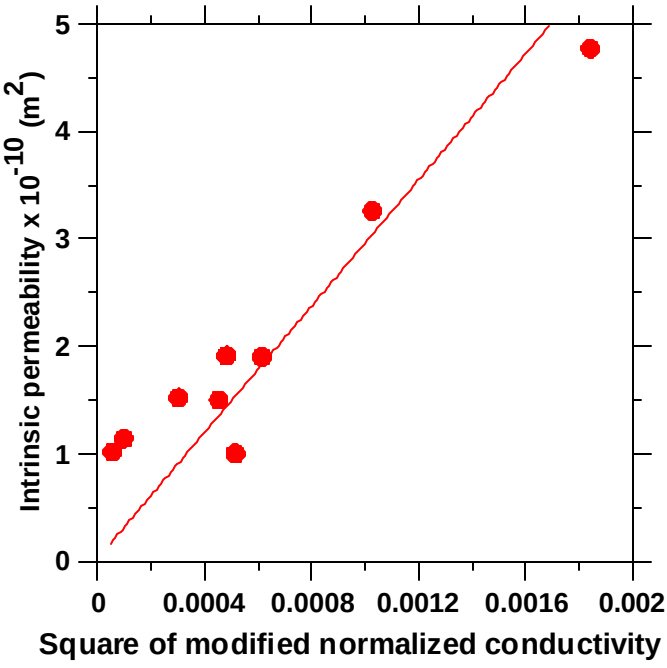

Figure 8.13 Relationship between intrinsic permeability and square of modified normalized conductivity

8.7 Acoustic Absorption and Intrinsic Permeability

Table 8.1 is a concise representation of the electrical, hydraulic, and acoustic properties of EPC mixtures investigated in this study.

Table 8.1 Electrical, hydraulic, and acoustic properties of EPC mixtures investigated

Mixture ID	Pore solution conduct-ivity (S/m)	Measured conduct-ivity (S/m)	Solid phase conduct-ivity (S/m)	Predicted conductivity (modified Archie's law) S/m	Predicted conductivity (B-H equation) S/m	Pore connectivity factor (β_p)	Hydraulic connectivity factor (β_H) x 10^{-10}	Maximum acoustic absorption coefficient (α)
100 - #8	1.56	0.0369	0.0151	0.0429	0.0359	0.1029	4.567	0.61
	4.40	0.0936		0.0941	0.0872			
	12.40	0.2346		0.2384	0.2315			
75-#8 - 25-#4	1.56	0.0421	0.0168	0.0442	0.0364	0.1141	5.743	0.59
	4.40	0.1090		0.0946	0.0867			
	12.40	0.2388		0.2365	0.2286			
50-#8 - 50-#4	1.56	0.0464	0.0166	0.0559	0.0504	0.1192	7.489	0.76
	4.40	0.1410		0.1281	0.1226			
	12.40	0.3281		0.3316	0.3261			
25-#8 - 75-#4	1.56	0.0579	0.0143	0.0758	0.0727	0.1774	12.731	0.81
	4.40	0.1888		0.1888	0.1857			
	12.40	0.4939		0.5071	0.5040			
100 - #4	1.56	0.0346	0.0101	0.0432	0.0390	0.0915	5.833	0.61
	4.40	0.0965		0.1038	0.0996			
	12.40	0.2599		0.2746	0.2704			
75-#8 - 25-3/8	1.56	0.0324	0.0155	0.0347	0.0261	0.0498	5.456	0.42
	4.40	0.0626		0.0699	0.0613			
	12.40	0.1609		0.1691	0.1605			
50-#8 - 50-3/8	1.56	0.0280	0.0103	0.0242	0.0177	0.0752	3.325	0.28
	4.40	0.0636		0.0497	0.0432			
	12.40	0.1281		0.1216	0.1150			
25-#8 - 75-3/8	1.56	0.0087	0.0177	0.0267	0.0140	0.0555	5.955	0.56
	4.40	0.0765		0.0434	0.0432			
	12.40	0.0743		0.0902	0.0774			
100 - 3/8	1.56	0.0089	0.0095	0.0177	0.0107	0.0323	9.373	0.31
	4.40	0.0325		0.0327	0.0306			
	12.40	0.0689		0.0751	0.0681			
50-#4 - 50-3/8	1.56	0.0310	0.0173	0.0414	0.0334	0.0748	4.211	0.63
	4.40	0.0998		0.0856	0.0258			
	12.40	0.2065		0.2102	0.2023			
97.5 - #4 2.5 sand	1.56	0.0111	0.0027	0.0161	0.0144	0.0455	5.833	0.52
	4.40	0.0435		0.0406	0.0388			
	12.40	0.1066		0.1094	0.1077			
95 - #4 5 sand	1.56	0.0103	0.0018	0.0133	0.0118	0.0404	4.019	0.44
	4.40	0.0326		0.0343	0.0327			
	12.40	0.0914		0.0934	0.0919			
92.5 - #4 7.5 sand	1.56	0.0089	0.0022	0.0111	0.0095	0.0347	3.898	0.40
	4.40	0.0236		0.0272	0.0256			
	12.40	0.0700		0.0726	0.0710			

Examining the hydraulic connectivity factor (β_H) and the maximum acoustic absorption (α) values from Table 8.1, it is rather difficult to obtain a direct relationship between the acoustic absorption and intrinsic permeability (Recall $k \propto \beta_H$). For instance, the mixture with 100% 3/8" aggregates exhibited the lowest acoustic absorption characteristics, but has a higher permeability. The reason for this behavior can be described as follows: when the material has very large sized pores and fairly large apertures to connect the pores (i.e., lesser pore constrictions), drainage of water will be rapid, and the permeability will be high. But sound waves can easily pass through these channels without losing much energy because the pore structure does not force them to alternatively compress and expand, resulting in a lower acoustic absorption. The mixture with 100% # 8 aggregates, on the other hand, has a lower pore size and is hydraulically inefficient, resulting in a lower β_H value. But the ratio of pore and aperture sizes for this mixture is in the acoustically efficient range, resulting in a higher acoustic absorption coefficient. Alternatively, there are instances of aggregate blends like 75% # 4 and 25% # 8 where the pore and aperture sizes created by the aggregate blending are very effective in increasing permeability as well as acoustic absorption. This is an evidence of the fact that there exists an optimal range of pore sizes and connectivity that make the material both hydraulically and acoustically efficient.

8.8 Summary

This chapter focused on developing methodologies to extract the pore structure features of EPC from electrical conductivity measurements. The need for a multi-phase conductivity model has been brought out, and the relationships between porosity, pore connectivity, and electrical conductivity has been arrived at. From these, it is evident that a combination of pore structure features – porosity that can be directly measured, and pore connectivity factor determined through electrical conductivity experiments - form a powerful tool to characterize the pore structure of EPC and ascertain its efficiency in acoustic absorption. Both electrical and hydraulic conductivities are related to the pore volume and pore space distribution in the material, though in different length scales. The larger pores in the material and its connectivity are important for hydraulic conductivity while the matrix that coats the aggregates is significant to electrical conductivity.

CHAPTER 9: FREEZE-THAW DURABILITY OF EPC

9.1 General

The previous chapters were devoted to developing mixture proportions and understanding the physical, mechanical, and acoustic properties of EPC. However, if such a new material has to be used successfully in the field, an in-depth evaluation of its durability characteristics is absolutely vital. This chapter explains the freeze-thaw durability of EPC. For a material designed for use in pavements, durability against alternate cycles of freezing and thawing is extremely important.

In this study, selected EPC mixtures were subjected to two different kinds of freeze-thaw cycles. In the first method, the prismatic specimens (75 mm x 75 mm x 375 mm) were subjected to rapid freezing and thawing under water, in a freeze-thaw machine, as per ASTM C 666 Procedure A. Each 24 hour period incorporated 5-6 cycles of freezing and hawing. In the second method, prismatic specimens of the same size as mentioned above were subjected to slow freezing and thawing in a controlled temperature chamber, subjecting the specimens to one freeze-thaw cycle every 24 hours.

9.2 EPC Mixtures Studied

The EPC mixtures selected for freeze-thaw durability were representative from a large matrix of mixtures given in Chapter 4. EPC mixtures with all the three single sized

aggregates (# 8, # 4, and 3/8") were chosen, whereas from the blended mixtures, EPC with 50% # 4 and 50% # 8 aggregates was chosen. The selected mixtures encompass a wide range of porosity, and pore sizes. In addition, an EPC mixture with 100% # 4 aggregates was prepared that incorporated an air entraining agent at 0.05% by weight of cement. This was required to study the influence of air entrainment on the freeze-thaw response of EPC.

9.3 Rapid Freezing and Thawing

This section describes the response of EPC specimens under rapid freeze-thaw conditions as per ASTM C 666. The response of both single sized and blended aggregate mixtures, as well as the influence of the addition of air entraining agent are discussed.

9.3.1 Single Sized Aggregate Mixtures

Figure 9.1 shows the variation in relative dynamic modulus with increasing number of freeze-thaw cycles for EPC made with single sized aggregates. It can be noticed from the figure that the mixture with # 8 (2.36 mm) aggregates show a larger reduction in relative dynamic modulus than mixtures with # 4 (4.75 mm) and 3/8" (9.5 mm) aggregates. Since the aggregate size of the # 8 mixture is small, the specific surface area is large, requiring more paste to coat the aggregates than the mixtures with # 4 or 3/8" aggregates. These mixtures are not air entrained, and therefore freezing and thawing results in damage of the paste, consequently reducing the relative dynamic modulus.

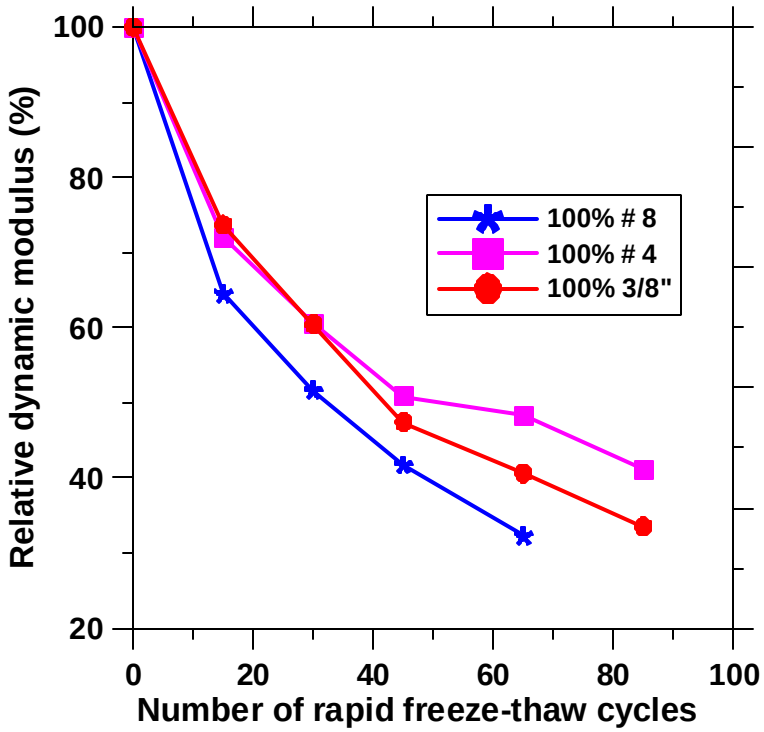

Figure 9.1 Drop in relative dynamic modulus with number of rapid freeze-thaw cycles for single sized EPC mixtures

Also, the characteristic pore sizes in mixtures with # 8 aggregates are smaller than those in mixtures with # 4 or 3/8" aggregates. Freezing of water and thawing of ice induces more stresses in pores of smaller sizes. This also could be a reason for the reduced relative modulus of EPC mixtures with # 8 aggregates as compared to the other mixtures that have larger pore sizes.

9.3.2 Blended Aggregate Mixtures

The reduction in relative dynamic moduli for a mixture with a blend of 50% # 4 and 50% # 8 aggregates is shown in Figure 9.2. Also shown in this figure are similar plots for mono sized aggregates that make up this blend. The response for the blended mixture lies very close to that of mixture with # 4 aggregates.

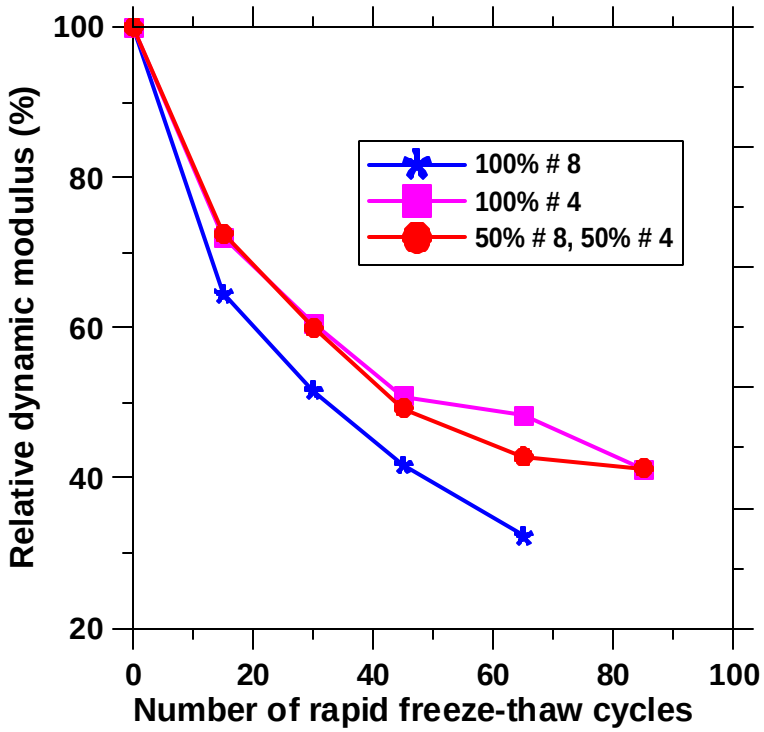

Figure 9.2 Comparison of drop in relative dynamic modulus between blended and single sized aggregate mixtures

Comparison of this with Figure 9.1 brings out certain features of the pore network of EPC that is significant in freezing and thawing response. Small pores induce larger stresses under freezing and thawing as explained earlier, and there seems to exist a threshold pore size between 2 mm (characteristic pore size of mixtures with # 8 aggregates) and 3 mm (characteristic pore size of mixtures with # 4 aggregates), below which the freezing of water and thawing of ice exerts enough stress to damage the material structure more than it does when pores of larger sizes are present.

9.3.3 Air Entrained and Non-Air Entrained Mixtures

EPC mixtures with # 4 aggregates were prepared by incorporating an air entraining agent to understand the influence of air entrainment on mixes with high porosities. Figure 9.3 depicts the variation in relative dynamic modulus for both non-air entrained and air entrained mixtures.

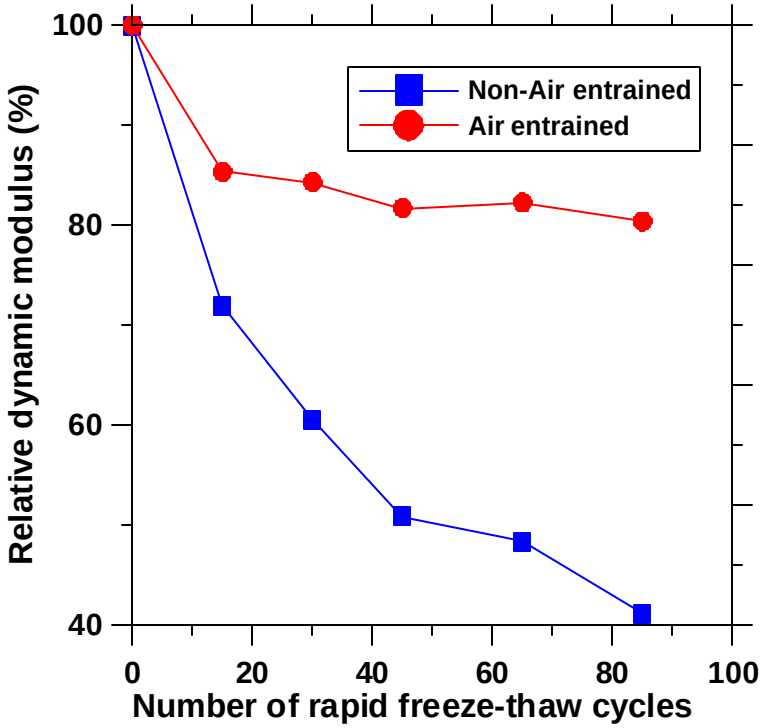

Figure 9.3 Relative dynamic moduli for non-air entrained and air entrained EPC made with # 4 aggregates

It can be seen that entraining small microscopic air bubbles is effective even when the material contains a large open porosity and pores of large sizes. Air entrainment prevents the paste from damaging, which the large pores cannot accomplish.

9.4 Slow Freezing and Thawing

In addition to the rapid freezing and thawing tests, slow freezing and thawing (one cycle per day) tests were also carried out on selected EPC mixtures, which are described in this section.

9.4.1 Single Sized Aggregate Mixtures

The variation in relative dynamic modulus with number of slow freeze-thaw cycles for EPC mixtures with single sized aggregates is shown in Figure 9.4. As was observed in the case of rapid freezing and thawing, in this case also, the mixture with 100% # 8 aggregates suffers the highest modulus loss.

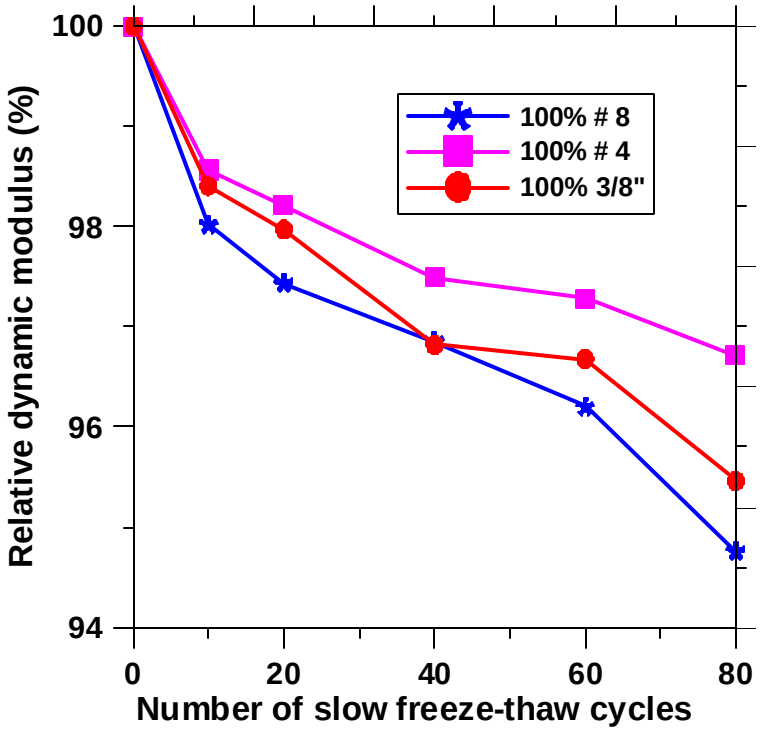

Figure 9.4 Drop in relative dynamic modulus with number of slow freeze-thaw cycles for single sized EPC mixtures

However, the drop in relative modulus as compared to the specimens subjected to rapid freezing and thawing is very small. After 80 cycles of slow freezing and thawing, the relative dynamic modulus remains between 95% and 97% for these mixtures.

9.4.2 Blended Aggregate Mixtures

Figure 9.5 shows the reduction in relative dynamic moduli with number of slow freezing and thawing cycles for EPC mixtures made up of 100% # 8, 100% # 4, and 50% # 4 and 50% # 8 aggregates. After 80 cycles, the relative dynamic modulus of the blended mixture lies in between those for mixtures 100% # 4 and # 8 aggregates.

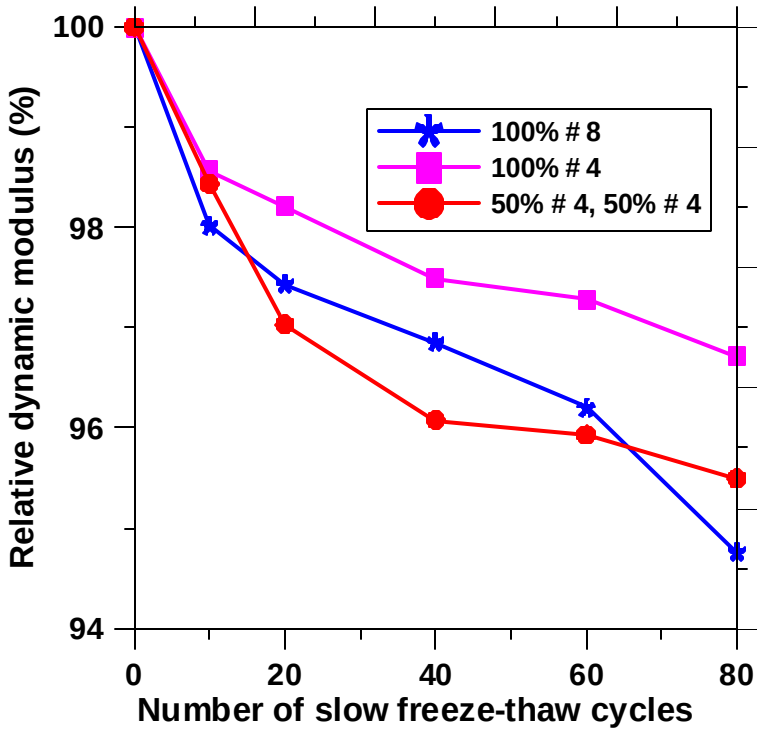

Figure 9.5 Comparison of drop in relative dynamic modulus between blended and single sized aggregate mixtures

9.5 Influence of Freezing Rate on the Response of EPC

Two rates of freezing and thawing were used in this study – rapid freezing and thawing in a Freeze-Thaw machine conforming to ASTM C 666 where the specimens are subjected to 5 to 6 cycles of freezing and thawing in 24 hours, and slow freezing and thawing in a controlled environmental chamber where the specimens are subjected to one freezing and thawing cycle every 24 hours. The rate of freezing and thawing significantly influences the degree of damage induced in the specimen [Powers 1945, Natesaiyer and Hover 1992].

Figure 9.6 depicts the comparison of relative dynamic modulus between mixtures subjected to rapid and slow freezing and thawing. Comparisons are made for EPC mixtures consisting of 100% # 4 and 100% # 8 aggregates.

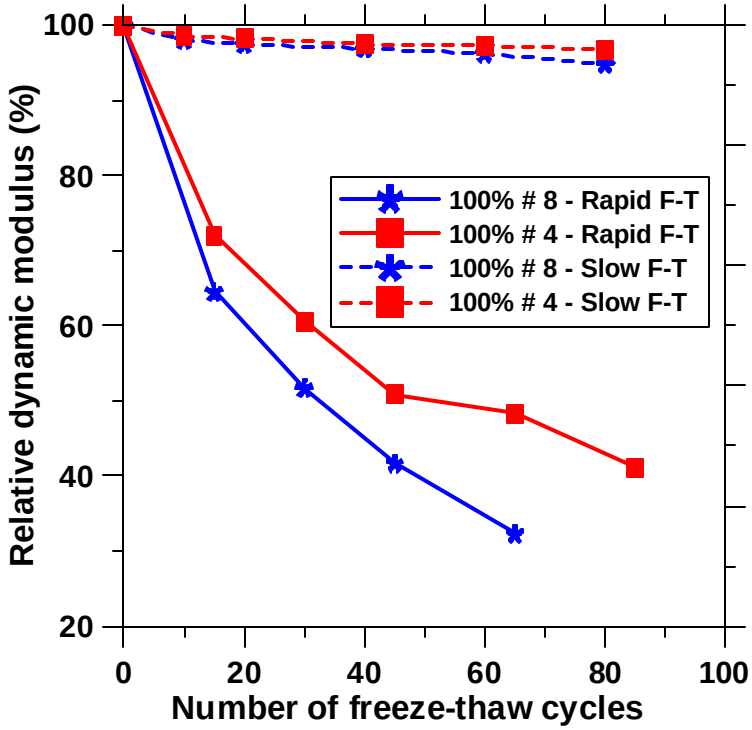

Figure 9.6 Comparison of relative dynamic modulus for EPC mixtures subjected to rapid and slow freezing and thawing

It can be observed from this figure that the specimens subjected to rapid freezing and thawing suffers extensive damage as compared to specimens subjected to slow freezing and thawing. The relative modulus of the specimens undergoing rapid freeze-thaw drops to around 40-50% at the end of 45 cycles whereas for those undergoing slow freeze-thaw, the dynamic modulus drops to only around 95%. It has been reported that slower rates of freezing produces reduced freeze-thaw damage. Rapid freezing conditions probably induce movement of water, while slow freezing conditions are more likely to induce the movement of ice [Powers 1953].

9.6 Summary

The impact of cyclic freezing and thawing on EPC was studied. It was found that EPC mixtures with smaller sized aggregates suffer more damage than those with larger aggregate sizes because of the presence of more paste in the former. The relative dynamic modulus for all mixtures after 80 cycles of rapid freezing and thawing drops to around 35-40%. However, in practice, because of the interconnected void system, drainage of water will be effective, and it is expected that EPC will never be completely saturated. Hence the actual performance could be superior to what was observed in the laboratory. Air entrainment was found to be an efficient way to protect the paste in EPC. The freezing rate has a significant influence on the relative dynamic modulus. When subjected to rapid freezing and thawing, the modulus loss was much more drastic than when subjected to slow freezing and thawing. Further experimentation is required to completely understand the performance of EPC in alternate freezing and thawing, and to develop means to increase the freeze-thaw resistance.

CHAPTER 10: TESTING OF EPC SLABS IN TPTA

10.1 General

Three EPC slabs were tested in the Tire-Pavement Test Apparatus (TPTA) to understand their influence in noise reduction. The TPTA at Purdue University's Ray W. Herrick Laboratories, was built to provide a facility for the fundamental study of tire/pavement noise generation mechanisms [Bernhard et al., 2003]. The facility has the capability to utilize realistic pavement samples and tire loading conditions in a controlled environment. The TPTA facility has been designed for the efficient investigation of the effect of variables, such as pavement type/texture or tire design and loading conditions, on tire/pavement noise generation.

10.2 Details of TPTA

The TPTA, which is shown in Figure 10.1(a) and (b), consists of a stationary drum that is 3.7 m in diameter. Pavement segments, which are approximately 20 cm deep, are mounted on the surface of the drum. Thus, the outer diameter of the pavement samples is greater than 4 m. The TPTA has two rotating arms. The tires are mounted on the end of these arms and can be loaded to a maximum of 4.45 kN using a screw jack system. The rotating assembly is driven by a DC motor, gearbox, and belt drive system. The drive system is mounted inside the stationary drum. The TPTA is located in a hemi-

anechoic chamber. This chamber also provides for the control for temperature and humidity.

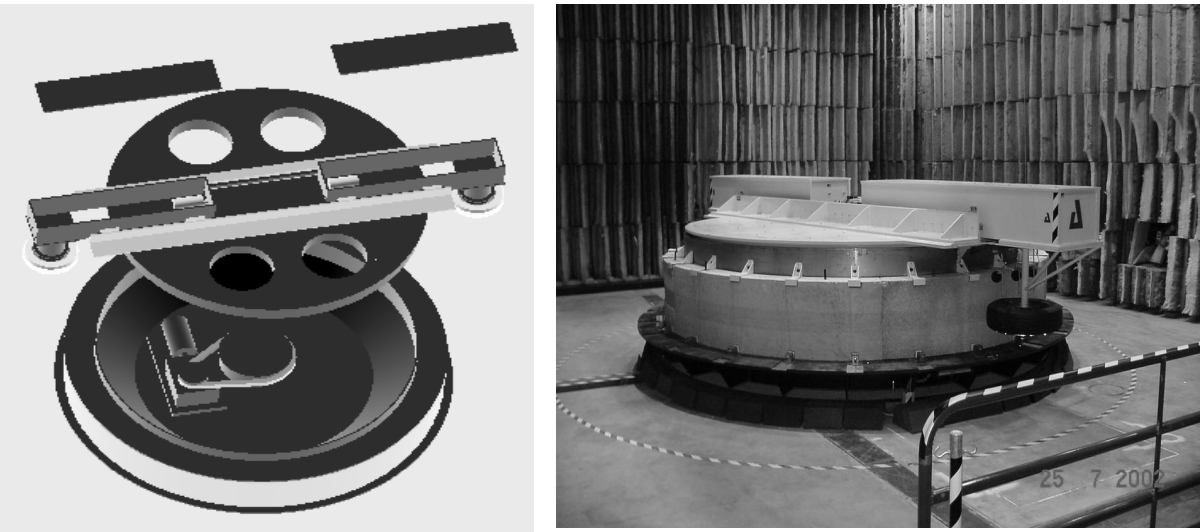

(a) (b)

Figure 10.1 (a) Exploded view of TPTA, (b) TPTA with a treaded tire on the near arm

Figure 10.2 shows a closer view of the TPTA with the pavement sections.

Figure 10.2 A closer view of the TPTA with the pavement sections

10.3 Specimen Preparation

The EPC specimens for testing in the TPTA were prepared on curved molds, as shown in Figure 10.3. The curvature of the molds and the dimensions were chosen in such a way that six specimens could accurately fit on the TPTA forming a continuous ring on which the tire can move. The design details, and the fabrication of the molds are explained in detail in another report [Olek et al. 2003].

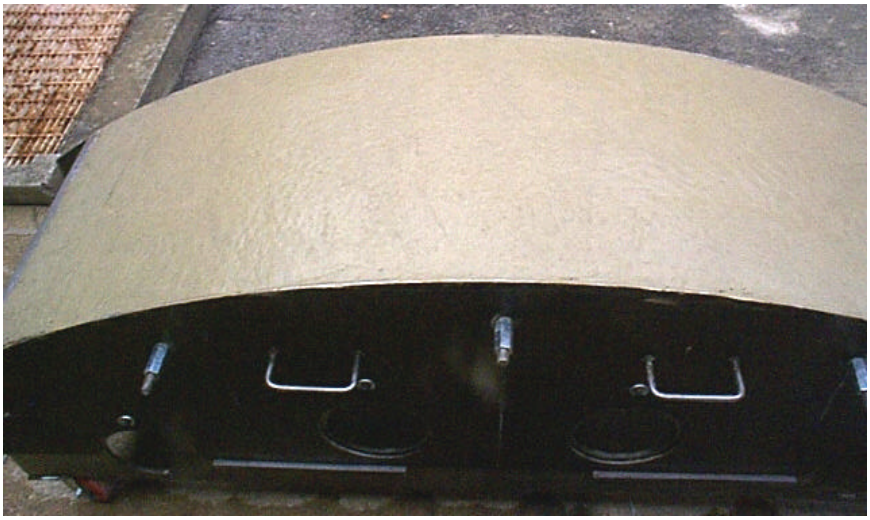

Figure 10.3 Mold filled with concrete

The molds were filled to the desired depth (depending on the thickness of porous layer required) using conventional concrete supplied by a ready-mix concrete manufacturer. The mixture contained 564 lb/cu.yd of cement, and was proportioned to be delivered with a slump of 1.5 to 2 inches. The curved shape of the molds forced this stringent limits on the slump, as otherwise the concrete would flow towards the ends of the molds, rendering the smooth leveling and finishing operation impossible. The concrete was filled to the desired level on the molds, and screeded off so as to obtain a level surface for the placement of EPC.

Two different EPC mixtures were prepared for this study. The first was using 100% # 4 aggregates, and the second had a blend of 75% # 4 and 25% # 3. The mixture proportions are the same as given in Table 4.2 of Chapter 4. For the mixture with 100% # 4 aggregates, specimens with two different thicknesses – 1 inch and 2 inch were made whereas for the blended aggregate specimen, only 2 inch thick specimen was made. In the further analyses, "porous 1", and "porous 3" indicate the specimens made with 100% # 4 aggregate with 1 inch and 2 inches thickness respectively, whereas "porous 2" indicates the mixture made with blended aggregates. Figure 10.4 shows a closer view of one of the EPC overlaid specimens. The surface appearances of these specimens are shown in Figure 10.5.

Figure 10.4 A closer look at an EPC specimen

(a) (b)

Figure 10.5 Surface appearances of EPC (a) 100% # 4 aggregates, and (b) 75% # 4, 25% # 8 aggregates

10.4 Testing Procedure

This study examined the noise radiated by the tire/pavement interaction due to a treaded and a tread-less tire passing over various Portland Cement Concrete samples. The treaded tire is a production General Ameri*G4S P205/65R15. The concrete samples had varying degrees of texturing and or porosity. Acoustical measurements were conducted at 10, 20 and 30 mph for each of the tires with a normal loading of 600 lbs. (approximately equivalent to a 1 ton vehicle).

10.4.1 Microphone Placement

The test tires were mounted to one of the TPTA arms and surrounded by an array of five microphones as shown in Figure 10.6. Three of the microphones, Bruel and Kjaer Type 4188-A-021, were placed according to the Close Proximity Method (CPX) draft

standard (ISO/CD 11819-2). The CPX microphone locations are referred to throughout this report as CPX Lead microphone and CPX Trail microphone to denote the CPX microphones traveling at the leading edge, center and trailing edge of the tire, respectively. These CPX microphones were the only microphones used for data collection for this report.

Figure 10.6 Five microphone array that travels with the tire

10.4.2 Data Acquisition

The data measured by the microphone array was analyzed with Bruel & Kjaer PULSE Noise and Vibration Analysis Type 7700 software. The PULSE system was configured as a narrow band Fourier analyzer. Linear frequency averaging was used with 100 averages. Triggering for each average was accomplished via a magnetic proximity probe mounted on the moving arm. This probe sensed a stationary magnet mounted at the position at which acoustical measurements were to be initiated for a given pavement surface. The average was updated once per revolution of the TPTA arm such that a

complete measurement encompassed 100 revolutions. The microphone locations were measured simultaneously during testing.

10.4.3 Data Reduction

The A-weighted auto-spectra of the acoustical signals measured at each of the microphones were calculated in real time. The auto-spectra were calculated from 0 to 5000 Hz with a resolution of 400 lines. For this report, 1/3rd octave band spectra were calculated from the narrow band spectra using EXCEL. To achieve this, narrow band spectral data was imported into EXCEL. This A-weighted narrow band data was then assigned to appropriate 1/3rd octave bands using a brick wall filter design. The data in these bands was summed to synthesize A-weighted, 1/3rd octave band spectra.

10.5 Test Results

The collected data for the treaded and tread-less tires at 30 mph over the six PCC samples are shown in Figures 10.7 to 10.10. These figures contain the A-weighted, 1/3rd octave band spectra for the various cases studied. These figures are representative of the various operating speeds measured [Bernhard et al., 2003].

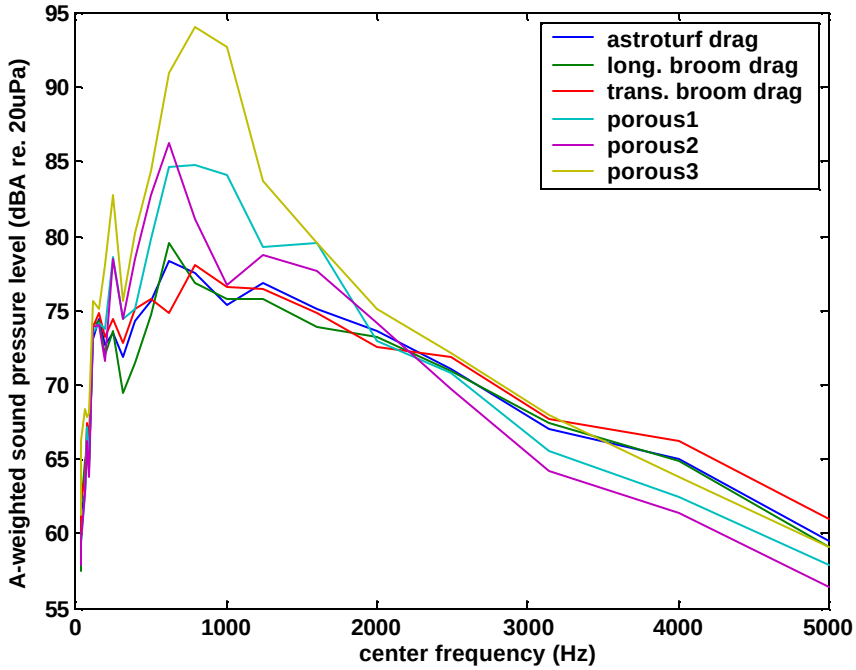

Figure 10.7 A-weighted, 1/3rd octave noise spectra for the tread-less tire over all pavements at 30mph at CPX Lead Microphone

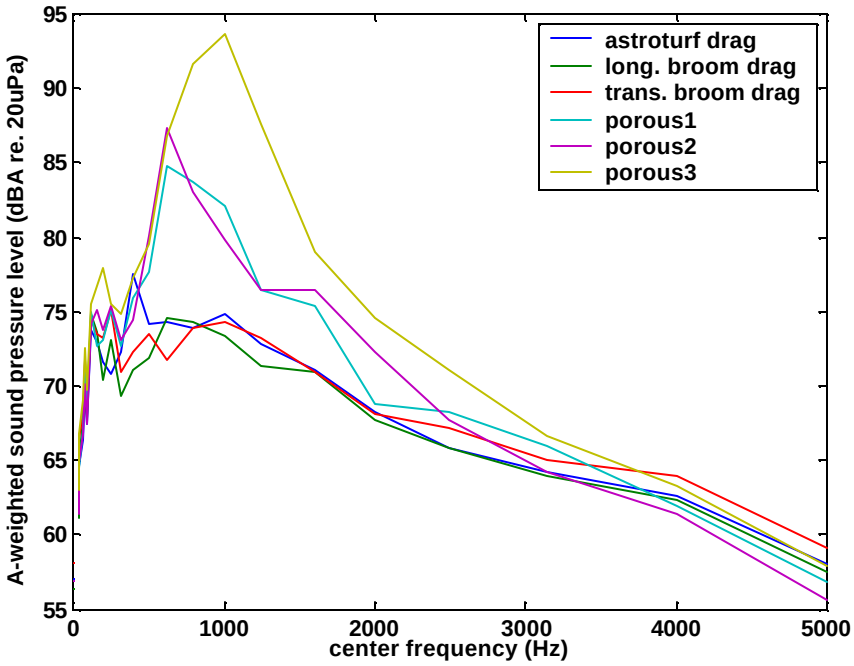

Figure 10.8 A-weighted, 1/3rd octave noise spectra for the tread-less tire over all pavements at 30mph at CPX Trail Microphone

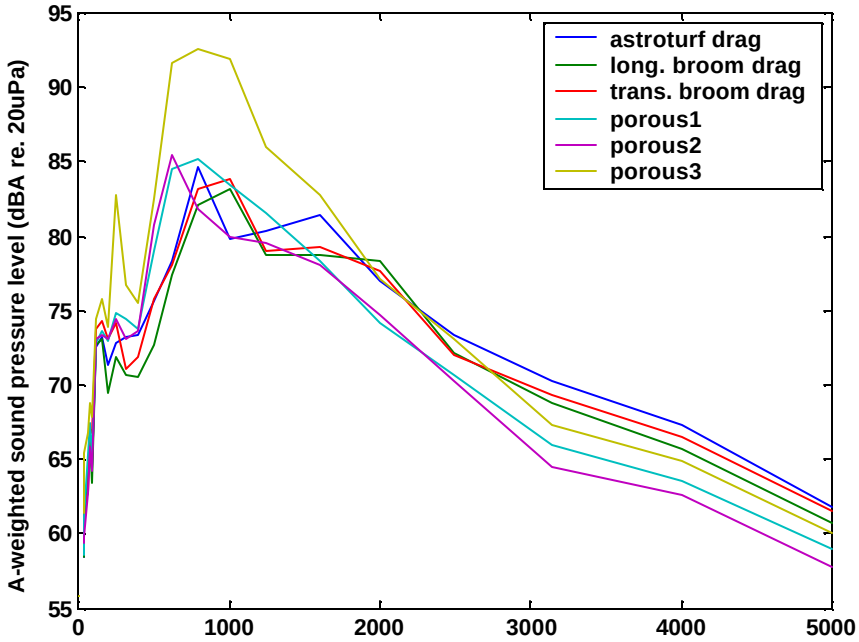

Figure 10.9 A-weighted, 1/3rd octave noise spectra for the treaded tire over all pavements at 30mph at CPX Lead Microphone

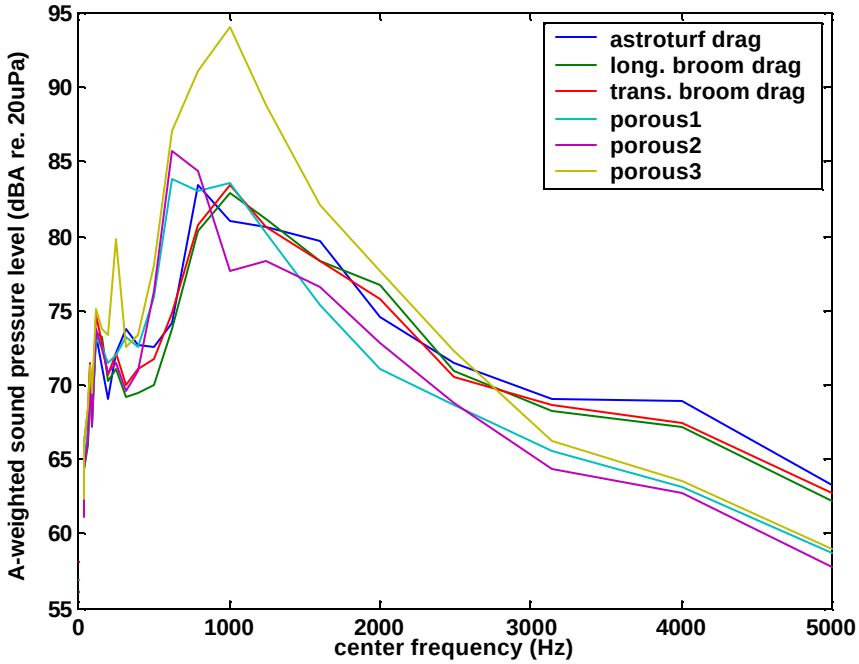

Figure 10.10 A-weighted, 1/3rd octave noise spectra for the treaded tire over all pavements at 30mph at CPX Trail Microphone

10.6 Conclusions

For the case of the treaded tire, increased texture / porosity lead to increased noise levels below approximately 1000 Hz and decreased noise levels above approximately 1000 Hz. The preliminary explanation for this behavior is that the increased texture / porosity produces increased mechanical excitation and interaction between the tire and pavement which appears to dominate the noise generation at low frequencies, below approximately 1000-1500 Hz. At frequencies above approximately 1000-1500 Hz, it appears that air pumping mechanisms are dominant and that these mechanisms are relieved by increased texture depth and porosity leading to decreased high frequency noise levels. It should be noted that this case involves a production treaded tire and represents a realistic case of tire-`pavement noise generation.

These trends are also evident for the case of the tread-less tire; however the frequency range in which the texture/porosity switches from increasing noise to decreasing noise occurs at approximately 2500 Hz.

It should be noted that the spectra produced by sample "Porous 3" are higher in the low frequency range than other samples in all measured cases. This sample was cast such that the surface aggregates in contact with the tire was randomly oriented such that the contact surface was quite irregular and rough. This contrasts "porous 1" and "porous 2" where the surface aggregates are well aligned such that the surface in contact with the tire is relatively flat.

CHAPTER 11: SUMMARY AND CONCLUSIONS

11.1 Summary

The main goal of this research work has been to develop porous Portland cement concrete that has noise reduction capabilities for use in pavements. The mechanisms by which enhanced porosity concrete (EPC) can reduce sound were studied to obtain a fundamental understanding of how the material should be tailored for noise reduction purposes. Several aggregate sizes and gradations were used to develop mixtures incorporating a sufficient amount of useful porosity to absorb sound. The influence of aggregate sizes, blends of aggregates, and gap grading on the pore structure features (pore volume, and pore size), mechanical properties (flexural strength), water transport (permeability), and acoustic absorption were examined in great detail. Experimental methods based on image analysis were devised to evaluate the porosity and pore size. A falling head permeameter was designed and fabricated to evaluate the water transport properties of EPC. Normal incidence acoustic absorption was measured using an impedance tube. Physical concepts based on the propagation of acoustic waves in porous media were used to model the acoustic absorption behavior of EPC. A microstructural model that takes into account the pore structure features to predict acoustic absorption at different frequencies was developed.

In order to better understand the behavior of EPC in both acoustic and hydraulic performance, the pore structure of EPC was characterized using Electrical Impedance Spectroscopy (EIS). Using a pore connectivity factor developed from this study, the acoustic absorption could be related to the pore structure features. The ranges of pore features that are efficient in acoustic absorption were found to be different from those for hydraulic conductivity (permeability). A hydraulic connectivity factor was developed to take this aspect into account. It was found that using a single measured electrical characteristic, the acoustic and hydraulic performance of EPC could be predicted.

11.2 Conclusions

The salient conclusions drawn from this research study are listed in this section. The findings pertaining to each subsection are listed separately.

11.2.1 Properties and Pore Structure Features

1. Pore size, along with accessible porosity is instrumental in determining the acoustic characteristic of EPC. The median pore sizes increase with increasing aggregate size.
2. An increase in aggregate size results in a reduction in the flexural strength of EPC, due to the increased total porosity and pore size.
3. Blending aggregates of different sizes typically results in a higher accessible porosity in the mixtures as compared to the mixtures made using single sized

aggregates. The blended aggregate system resulted in an increased acoustic absorption in most cases.

4. The permeability of EPC mixtures were found to increase with porosity, though no definitive trends could be established. This can be attributed to the fact that permeability is not a function of porosity alone.

11.2.2 Acoustic Absorption Behavior and Modeling

5. Acoustic absorption behavior is closely related to the porosity and pore size in the material. It appears that there is an optimal pore size depending on the mixture that maximizes sound absorption. Blending of aggregates, especially # 4 and # 8, is found to more effective than single sized aggregates. The addition of sand is found to be detrimental in acoustic absorption while silica fume does not significantly alter the absorption behavior. In both cases, the flexural strength is improved.

6. The frequency at the peak absorption is related to the thickness of the specimen. A procedure is provided to calculate the optimal specimen thickness once the optimal frequency range is known.

7. A simple shape specific model is developed for EPC, which can explain the variation in absorption behavior using pore and aperture geometry. The idealized model for EPC consists of pores, and apertures connecting the pores. This model is found to adequately describe the acoustic behavior of the EPC system.

8. The concept of structure factor has been employed to correct for the density of air in the pores, in the prediction of acoustic absorption. An algorithm to determine

the aperture length from the pore diameter and length has been developed, which can be used in the calculation of structure factor. The maximum absorption coefficient decreases with increase in structure factor, and the relationship is linear.

9. An electro-acoustic analogy, considering a series of resistors and inductors in parallel has been employed to model the acoustic absorption of EPC. The model assumes the real component of impedance of aperture as a resistor, and the imaginary component as an inductor. The air inside the pores is modeled as resistors.

10. A detailed parametric study has been conducted to isolate the effects of pore size, aperture size, porosity and the specimen thickness on acoustic absorption. An increase in pore size is found to reduce the maximum absorption coefficient while it was observed that there is an optimum pore to aperture size ratio that maximizes acoustic absorption. The acoustic absorption was enhanced in the low frequency range by increasing the pore to aperture size ratio. It was observed that increasing the porosity by keeping the aperture length constant results in a reduced maximum acoustic absorption. Increasing the thickness of the specimen results in maximum absorption peaks being shifted to lower frequencies.

11.2.3 Characterization and Prediction of Acoustic and Hydraulic Properties

11. Electrical conductivity studies can be used to characterize the pore structure of EPC.

12. A single conducting phase model (i.e., like Archie's law) showed a 35% average error in predicting effective conductivities of EPC. To improve the accuracy of prediction, models with two conducting phases were evaluated. A modified version of Archie's law, an equation of the Bruggeman-Hanay type, and a modified parallel law incorporating a connectivity factor were found to adequately describe the electrical conductivity of EPC system, with similar errors of 7-10%.

13. The pore connectivity factor (β_P) and the acoustic absorption coefficient (α) are linearly related. By using the pore connectivity factor β_P determined through electrical conductivity experiments, the pore structure of EPC could be characterized and its efficiency in acoustic absorption can be ascertained.

14. Porosity or electrical conductivity alone are inadequate descriptors of the hydraulic flow characteristics of the EPC system. The Kozeny-Carman equation has been modified to use a hydraulic connectivity factor (β_H), which is observed to be proportional to the product of square of modified normalized electrical conductivity and a function of porosity. Therefore β_H can be used as an index to classify the EPC systems based on their permeability. Mixtures having similar values of β_H exhibit similar permeabilities irrespective of their porosities.

15. The pore features that result in efficient hydraulic and acoustic performance are different. The electrical conductivity can be used to obtain the pore connectivity which can provide a measure of the acoustic effectiveness of the material. The product of electrical conductivity and a function of the total porosity are needed to describe the intrinsic permeability. It was discussed that the features of an

acoustically efficient material (pore constriction and pore connectivity or tortuosity) are not the same as a hydraulically efficient material (open porosity and lesser pore constriction). Though these two parameters may seem to be inversely related, it was found that there are certain mixtures (blended aggregates) in which the effective pore sizes and pore connectivity created by blending the aggregates result in a system that is effective both acoustically and hydraulically.

11.2.4 Freezing and Thawing

16. EPC mixtures prepared with smaller sized aggregates (# 8) suffer more damage in cyclic freezing and thawing than mixtures with large sized aggregates (# 4 or 3/8"). This is true for both rapid and slow freezing and thawing. This could probably be because of the fact that the paste content is higher in small sized aggregate mixtures. Also, characteristic pore sizes are smaller in mixtures with smaller aggregate sizes, leading to larger stresses.
17. It was found that entraining small air bubbles in the paste is a good means of improving the freeze-thaw resistance of EPC even when the material consists of deliberately incorporated pores of large sizes. More research in this direction is needed.
18. The freezing rate has a considerable impact on the dynamic modulus drop in EPC specimens. Mixtures subjected to rapid freezing and thawing undergo damage at a much faster rate than those subjected to slow freezing and thawing. For instance, after 45 cycles of rapid freezing and thawing, the relative modulus of

most mixtures studied drops to around 40% whereas after 80 cycles of slow freezing and thawing, the modulus drops to only around 95%.

11.2.4 TPTA Testing

19. TPTA tests show that the EPC pavements reduce the tire-pavement interaction noise above around 1000 Hz, where as there is an increase in noise levels below 1000 Hz.

20. Increased porosity produces increased mechanical excitation and interaction between the tire and pavement, which dominates the noise generation at low frequencies, below approximately 1000-1500 Hz. At frequencies above approximately 1000-1500 Hz, it appears that air pumping mechanisms are dominant and that these mechanisms are relieved by increased porosity leading to decreased high frequency noise levels.

LIST OF REFERENCES

Allard, J. F., "Propagation of sound in porous media – modeling sound absorbing materials", Elsevier Applied Science, 1993.

ASTM C 192-00, "Standard method of making and curing concrete test specimens in the laboratory", American Society of Testing and Materials, Pennsylvania, 2000.

ASTM C 78-02, "Standard method for flexural strength of concrete (using simple beam with third point loading)", American Society of Testing and Materials, Pennsylvania, 2002.

ASTM E 1050-98, "Standard test method for impedance and absorption of acoustic materials using a tube, two microphones and a digital frequency analysis system", American Society of Testing and Materials, Pennsylvania, 1998.

Bernhard, R. J., "The state of the art of quiet highways", Presentation at the 88th Purdue Road School, March 2002.

Bernhard, R.J., Personal communication, 2003

Bernhard, R.J., Thornton, W.D., and Baumann, J., "The effects of varying tire cap ply, sidewall filler height, and pavement texture on tire-pavement noise generation", Final Research Report No. SQDH 2003-1, The Institute of Safe, Quiet, and Durable Highways, 2003.

Biot, M.A., "Generalized theory of acoustic propagation in porous dissipative media", Journal of the Acoustic Society of America, Vol. 34, 1962, pp. 1254-1264.

Boutin,C., Royer,P., and Auriault, J.L., "Acoustic absorption of porous surfacing with dual porosity", International Journal of Solids and Structures Vol. 35, No. 34-35, 1998, pp. 4709-4737.

Brennan, M.J., and To, W.M., “Acoustic properties of rigid frame porous materials – an engineering perspective”, Applied Acoustics, Vol. 62, 2001, pp. 793-811.

BRITE/EURAM project BE 3415 “Surface properties of concrete roads in accordance with traffic safety and reduction of noise”, November 1994.

Bussian, A.E., “Electrical conductance in a porous medium”, Geophysics, Vol. 48, No.9, 1983, pp. 1258-1268.

Chinh, P.D., “Electrical properties of sedimentary rocks having interconnected water-saturated pore spaces”, Geophysics, Vol. 65, No. 4, 2000, pp. 1093-1097.

Christensen, B.J., “Microstructure studies of hydrating Portland cement based materials using impedance spectroscopy”, Ph.D Thesis, Northwestern University, 1993.

Christensen, B.J., Coverdale, R.T., Olson, R.A., Ford, S.J., Garboczi, E.J., Jennings, H.M., and Mason, T.O., “Impedance spectroscopy of hydrating cement based materials: Measurement, interpretation and application”, Journal of American Ceramic Society, Vol. 77, 1994, pp. 2789-2804.

Christory, J. P., Pipien, G., Soudieu, B., and Chauchot, J., “The road and the environment – a marriage of convenience: Thick porous pavements”, Proceedings of the Fifth International Conference on Concrete Pavement and Rehabilitation, Purdue University, Indiana, 1993, Vol.2, pp. 107-124.

Coverdale, R.T., Christensen, B.J., Jennings, H.M., Mason, T.O., Bentz, D.P., Garboczi, E.J., “Interpretation of impedance spectroscopy via computer modeling – Part I Bulk conductivity and offset resistance”, Vol. 30, 1995, pp. 71-719.

de Larrard, F., “Concrete mixture proportioning – a scientific approach”, Modern Concrete Technology Series 9, E & FN Spon, New York, 1999.

de Lima, O.A.L., and Sharma, M.M., “A grain conductivity approach to shaly sandstones”, Geophysics, Vol. 55, No.10, 1990, pp. 1347-1356.

de Lima, O.A.L., and Sri Niwas., "Estimation of hydraulic parameters of shaly sandstone aquifers from geoelectrical measurements", Journal of Hydrology, Vol. 235, 2000, pp. 12-26.

Descornet, G., "Low-noise road surface techniques and materials", Proceedings of Inter Noise 2000, Nice, France, August 2000.

Descornet, G., Faure, B., Hamet, J.F., Kestemont, X., Luminari, M., Quaresma, L., and Sandulli, D., "Traffic noises and road surfaces: State of the art", SIRRUS project, Belgian Road Research Center, Brussels, March 2000.

Descornet, G., Fuchs, F., and Buys, R., "Noise reducing concrete pavements", Proceedings of the Fifth International Conference on Concrete Pavement and Rehabilitation, Purdue University, Indiana, 1993, Vol.2, pp. 93-98

Ford, S.J., Mason, T.O., Christensen, B.J., Coverdale, R.T., and Jennings, H.M., "Electrode configurations and impedance spectra of cement pastes", Journal of Materials Science, Vol. 30, 1995, pp. 1217-1224.

Francois, H. J., and Michel, B., "Acoustical characteristics of porous pavements: A new phenomenological model", Proceedings of Inter Noise 93, Leuven, Belgium, August 1993, pp. 641-646.

Francois, H.J., and Michel, B., 'Acoustical characteristics of porous pavements: A new phenomenological model', Proceedings of Inter Noise 93, (Leuven, Belgium, 1993), 641-646.

Garboczi, E.J., "Permeability, diffusivity and microstructural parameters: A critical review", Cement and Concrete Research, Vol. 20, 1990, pp. 591-601.

Gerharz, B., "Pavements on the base of polymer-modified drainage concrete", Colloids and Surfaces A: Physicochemical and Engineering Aspects, Vol. 152, 1999, pp 205-209.

Glover, P.W.J., Hole, M.J., and Pous, J., “A modified Archie’s law for two conducting phases”, Earth and Planetary Science Letters, Vol. 180, 2000, pp. 369-383.

Gu, P., Xu, Z., Xie, P., and Beaudoin, J.J., “Application of A.C. impedance techniques in studies of porous cementitious materials – (I) Influence of solid phase and pore solution on high frequency resistance” , Cement and Concrete Research, Vol. 23, 1993, pp. 531-540.

Iwase, T., “Acoustic properties of porous pavement with double layers and its reduction effects for road traffic noise”, Proceedings of Inter Noise 2000, Nice, France, August 2000.

Jackson, P.D., Smith, D.T., and Stanford, P.N., “Resistivity-porosity-particle shape relationships for marine sands”, Geophysics, Vol. 43, No.6, 1978, pp. 1250-1268.

Johnson, D.L., Koplik, J., and Dashen, R., “Theory of dynamic permeability and tortuosity in fluid saturated porous media”, Journal of Fluid Mechanics, Vol. 176, 1987, pp. 379-402.

Katz, A.J., and Thompson, A.H., “Quantitative prediction of permeability in porous rock”, Physical Review B, Vol. 34, 11, 1986, pp. 8179-8181.

Kuemmel, D.A., Jaeckel, J.R., Satanovsky, A., Shober, S.F., and Schmiedlin, R.B., “Impacts related to pavement texture selection”, Final Report WI/SPR-06-96, Marquette University, Milwaukee, Wisconsin, 1997.

Lu, T. J., Chen, F., and He, D., “Sound absorption of cellular metals with semi open cells”, Journal of the Acoustic Society of America, Vol. 108, No.4, 2000, pp. 1697-1709.

Martys, N., and Garboczi, E.J., “Length scales relating to the fluid permeability and electrical conductivity in random two-dimensional model porous media”, Physical Review B, Vol. 46, No. 10, 1992, pp. 6080-6090.

McCarter, W.J., Starrs, G., Chrisp, T.M., “Electrical conductivity, diffusion, and permeability of Portland cement-based mortars”, Cement and Concrete Research, Vol.30, 2000, pp. 1395-1400.

Moss, G.M., Christensen, B.J., Mason, T.O., and Jennings, H.M., “Microstructural analysis of young cement pastes using impedance spectroscopy during pore solution exchange”, Advanced Cement Based Materials, Vol. 4, 1996, pp. 68-75.

Natesaiyer, K.C., and Hover, K.C., “The protected paste volume of air entrained cement paste – Part I”, Journal of Materials in Civil Engineering, Vol.4, No.2, pp. 166-184.

Nelson, P. M., “Designing porous road surfaces to reduce traffic noise”, TRL Annual Review, Transportation Research Laboratories, UK, 1994.

Nelson, P. M., and Phillips, S. M., “Quieter road surfaces”, TRL Annual Review, Transportation Research Laboratories, UK, 1994.

Nissoux, J-L., Gnagne, C., Marzin, J., Lefebvre, J-P., and Pipien, G., “A pervious cement concrete wearing course below 73 dB(A)”, Proceedings of the Fifth International Conference on Concrete Pavement and Rehabilitation, Purdue University, Indiana, 1993, Vol.2, pp. 269-284.

Olek, J., Bolton, J.S., and Bernhard, R.J., “Fundamentals of tire-road interaction noise”, Progress Report - December 2001, submitted to The Institute of Safe, Quiet, and Durable Highways.

Onstenk, E., Aguado, A., Eickschen, E., and Josa A., “Laboratory study of porous concrete for its use as top layer of concrete pavements”, Proceedings of the Fifth International Conference on Concrete Pavement and Rehabilitation, Purdue University, Indiana, 1993, Vol.2, pp. 125-139.

Permanent International Association Road Congresses (PIARC), “Report of the Technical Committee on Concrete Roads, Marrakesh, 1991.

Philips, S. M., Parry, A. R., and Ferne, B. W., “Monitoring the safety and environmental performance of road surfaces”, TRL Annual Review, Transportation Research Laboratories, UK, 1994.

Powers, T.C., “Basic considerations pertaining to freezing and thawing tests”, Proceedings of the American Society for Testing and Materials, 1955, Vol. 55, pp. 1132-1155.

Roberts, J.N., and Schwartz, L.M., “Grain consolidation and electrical conductivity in porous media”, Physical Review B, Vol. 31, No.9, 1985, pp. 5990-5997.

Sandberg, U., and Ejsmont, J. A., “Tyre / Road noise reference book”, Informex, Kisa, Sweden, 2002.

Stinson, M.R., and Champoux, Y., “Propagation of sound and the assignment of shape factors in model porous materials having simple pore geometries”, Journal of the Acoustic Society of America, Vol. 91, 1992, pp. 685-695.

Stinson, M.R., and Shaw, E.A.G., “Acoustic impedance of small, circular orifices in thin plates”, Journal of the Acoustic Society of America, Vol. 77, 1985, pp. 2039-2042.

Synder, K.A., Ferraris, C., Martys, N.S., and Garboczi, E.J., “Using impedance spectroscopy to assess the viability of rapid chloride test for determining chloride conductivity”, Journal of Research of the National Institute of Standards and Technology, Vol. 105, No. 4, 2000, pp. 497-509.

Voronina, N., “An empirical model for rigid frame porous materials with low porosity”, Applied Acoustics, Vol. 58, 1999, pp. 295-304.

Wang, X., and Lu, T. J., “Optimized acoustic properties of cellular solids”, Journal of the Acoustic Society of America, Vol. 106, No.2, 1999, pp. 756-765.

Wayson, R.L., “NCHRP Synthesis 268 - Relationship between pavement surface texture and highway traffic noise”, Transportation Research Board, National Academy Press, Washington D.C, 1998.

Weiss, W.J., and Olek, J, “Development of quiet and durable porous cement concrete paving materials”, Proposal No. 571-1284-0007, Institute of Safe, Quiet, and durable highways, Purdue University, 2001.

Whittington, H.W., McCarter, J., Forde, M.C., “The conduction of electricity through concrete”, Magazine of Concrete Research, Vol. 33, No.114, 1981, pp. 48-60.

Wong, P., Koplik, J., and Tomanic, J.P., “Conductivity and permeability of rocks”, Physical Review B, Vol. 30, No.11, 1984, pp. 6606-6614.

Yang, J., and Jiang, G., “Experimental study on properties of pervious concrete pavement materials”, Cement and Concrete Research, Vol. 33, 2003, pp. 381-386.

Zwikker, C., and Kosten, C. W., “Sound absorbing materials”. Elsevier Publishing Company Inc., 1949.

LIST OF PUBLICATIONS

Marolf, A., Neithalath, N., Sell, E., Wegner, K., Weiss, W.J., and Olek, J., "Influence of aggregate size and gradation on the acoustic absorption of Enhanced Porosity Concrete", Accepted for publication in ACI Materials Journal

Neithalath, N., Weiss, W.J., and Olek, J., "Characterizing Enhanced Porosity Concrete using electrical impedance to predict electrical and hydraulic performance", under review, Cement and Concrete Research

Neithalath, N., Marolf, A., Weiss, W.J, and Olek, J., "Modeling the effects of pore structure characteristics in the acoustic absorption of Enhanced Porosity Concrete", under review, Concrete Science and Engineering

Neithalath, N., Weiss, W.J., and Olek, J., "Acoustically efficient concretes through engineered pore structure", Presented at the ACI Spring Convention, Vancouver, March 2003, and under review for ACI Special Publication.

Neithalath, N., Weiss, W.J., and Olek, J., "Enhanced Porosity Concrete: Electrical Impedance, Acoustic Absorption, and Hydraulic Permeability", Presented at the ACI Fall Convention, Boston, September 2003.

Neithalath, N., Weiss, W.J., and Olek, J., "Pervious concrete pavements to reduce tire-pavement interaction noise", Presented at the ACI Fall Convention, Boston, September 2003.